UNCLASSIFIED

AD 406 320

DEFENSE DOCUMENTATION CENTER

FOR

SCIENTIFIC AND TECHNICAL INFORMATION

CAMERON STATION, ALEXANDRIA, VIRGINIA

UNCLASSIFIED

63-3-6

(1)

MODEL STUDIES OF THE VLF PAC ANTENNA

Seal-1

U. S. NAVY

VLF-COMMFACPAC

NBy 37636

12 April 1963

HNCD

A JOINT VENTURE

Los Angeles, California

Holmes & Narver, Inc.
Continental Electronics Manufacturing Company
DECO Electronics, Inc.

ENCL (1) TO BUSHIPS SER 694E-349

DEPARTMENT OF THE NAVY
BUREAU OF SHIPS
WASHINGTON 25, D. C.

IN REPLY REFER TO
Ser 694E-349

18 JUN1963

UNCLASSIFIED
Downgraded to

when enclosure(s) is/are detached

Address All Replies to Chief, Bureau of Ships

TO: Defense Documentation Center (TISIA), Arlington Hall Station, Arlington, Virginia

VIA:

THE MATERIAL ITEMIZED BELOW, OR ON ATTACHED LIST, IS FORWARDED AS INDICATED:

	Forwarded per your request
X	*For information and retention*
	On loan and to be returned to the Bureau of Ships
	Return of loaned material
	For use in connection with
	Partial fulfillment of order - Balance will be forwarded when available
	SECRET AND TOP SECRET - THE ATTACHED RECEIPT, OPNAV 5511-10 MUST BE SIGNED AND RETURNED TO THE BUREAU OF SHIPS IMMEDIATELY.

Encl: (1) MODEL STUDIES OF THE VLF FAC ANTENNA (NBy 37636, 12 April 1963)

Copy to:
BuDocks
(Mr. Himoe) less encl (1)

NAVSHIPS 4669 (4-56)

H41916

MODEL STUDIES OF THE VLF PAC ANTENNA

U. S. NAVY

VLF-COMMFACPAC,

NBy 37636

12 April 1963

HNCD

A JOINT VENTURE

Los Angeles, California

Holmes & Narver, Inc.
Continental Electronics Manufacturing Company
DECO Electronics, Inc.

CONTENTS

Page

Appendices

ILLUSTRATIONS

TABLES

SYMBOLS (MKS Units or as Specified)

Electrical Symbols:

E_i = Incident electric field strength (volts/meter)

E_s = Gradient at conductor surface (kv/mm)

H_i = Incident magnetic field strength (amps/meter)

V_b = Base voltage of antenna (volts)

V_t = Top hat voltage (kv)

I_o = Antenna base current (amps)

Antenna Parameters:

h_o = Effective height (feet or meters)

f_o = Resonant frequency (kc)

R_o = Radiation resistance (ohms)

C_o = Effective antenna capacitance (μf)

C_b = Near-base capacitance (μf)

C_s = Static antenna capacitance (μf) = $C_o + C_b$

L_o = Effective antenna inductance (μh)

Z_b, X_b = Antenna base impedance, reactance (ohms)

bw_o = Bandwidth of theoretical lossless antenna (cycles)

$\underline{a}$ = Aspect ratio (tower height/top hat span)

$\underline{s}$ = Similitude scaling factor to be applied to all dimensions

Range Calibration:

K_1 = Ratio of monitor base voltage to the field incident on the model = (V_m / E_i)

h = Physical height of thin monopole used in range calibration

V_m = Base voltage of E-field monitor antenna (volts)

1. INTRODUCTION

This report presents information developed in the scale model study of the high-power, very-low-frequency (vlf) transmitting antenna for the U. S. Navy VLF Communication Facility, Pacific. The study is an integral part of the final design effort under Contract NBy 37636 between the U. S. Navy Bureau of Yards and Docks and the Joint Venture firm of Holmes & Narver, Inc., Continental Electronics Manufacturing Company, and DECO Electronics, Inc. (HNCD).

The basic configuration of the antenna system under study was chosen in the Preliminary Engineering Report (PER) phase of the project. This phase was carried out by the Joint Venture firm of Developmental Engineering Corporation (later, DECO Electronics, Inc.) and Holmes & Narver, Inc., under Bureau of Yards and Docks Contract NBy 37598. Supplement 1 of the PER, Single Modified Cutler Antenna and VLF Antenn Comparison, presented the recommended configuration based on cost and performance data for a single-element antenna approximately 28 percent larger than the Cutler-type element. Further studies carried out under Change Order F of Contract NBy 37598 provided cost-trade information relating to the aspect ratio (relation of top hat spans and tower heights) and structural alternatives such as halyard slope, cantilever length, etc.

From considerations based on the PER, an initial choice of major antenna dimensions was established. The purpose of the model study described in this report is to present a detailed summary of the electrical performance data derived from a 1:100 scale model of the initial antenna and of the subsequent modifications leading to a final design.

2. TEST PROCEDURES

2.1 Model Range

The model range used in this study is a modified version of the one used in the PER modeling program. (See Appendix E of PER.) An increase in the size of the antenna over that of the Appendix E studies required an extension of the ground plane (as shown in Figure 2-1). To increase the accuracy of effective height measurements, it was necessary to install an E-field monitor consisting of a short monopole off the south end of the range. However, because of scheduling considerations, the resonant frequency tests were performed before the E-field monitor was calibrated. These earlier tests employed the H-field monitor used in the PER test series.

2.2 Equipment

Except for the E-field monitor and current distribution probe, the equipment used in this work was identical to that used in the PER modeling.

2.2.1 Effective Height Measurements

Figure 2-2 is a block diagram of the equipment used in the effective height measurements. The figure illustrates the use of the E-field monitor employed in most of the work. However, some early work in this study used the H-field monitor (RCA type WX-2C Field Intensity Meter) as described in the PER. In using the E-field monitor, the same receiver-voltmeter combination was employed to indicate both the incident field (as indicated by the monitor base voltage) and the base voltage of the vlf antenna model under test. Both the monitor and the test antennas were terminated in low-input-capacitance cathode followers to reduce loading effects. In either case, the

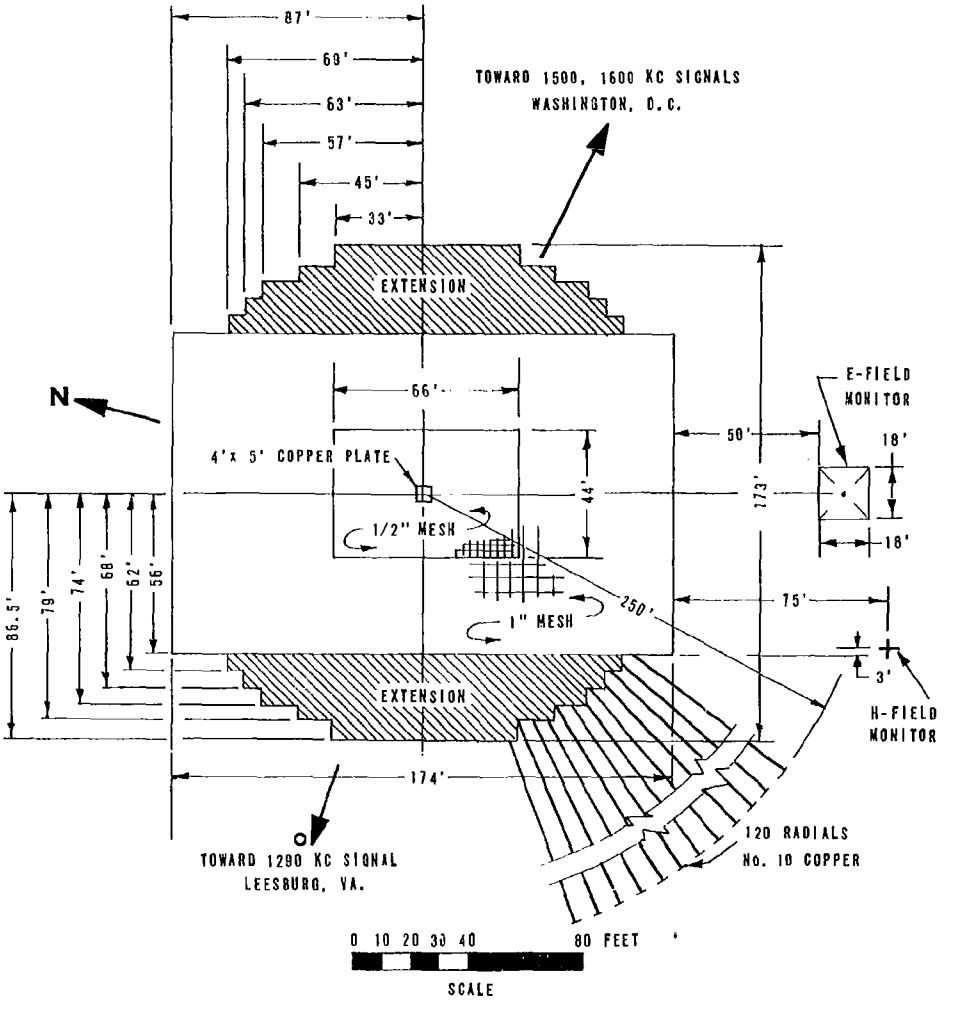

Figure 2-1 VLF MODEL RANGE

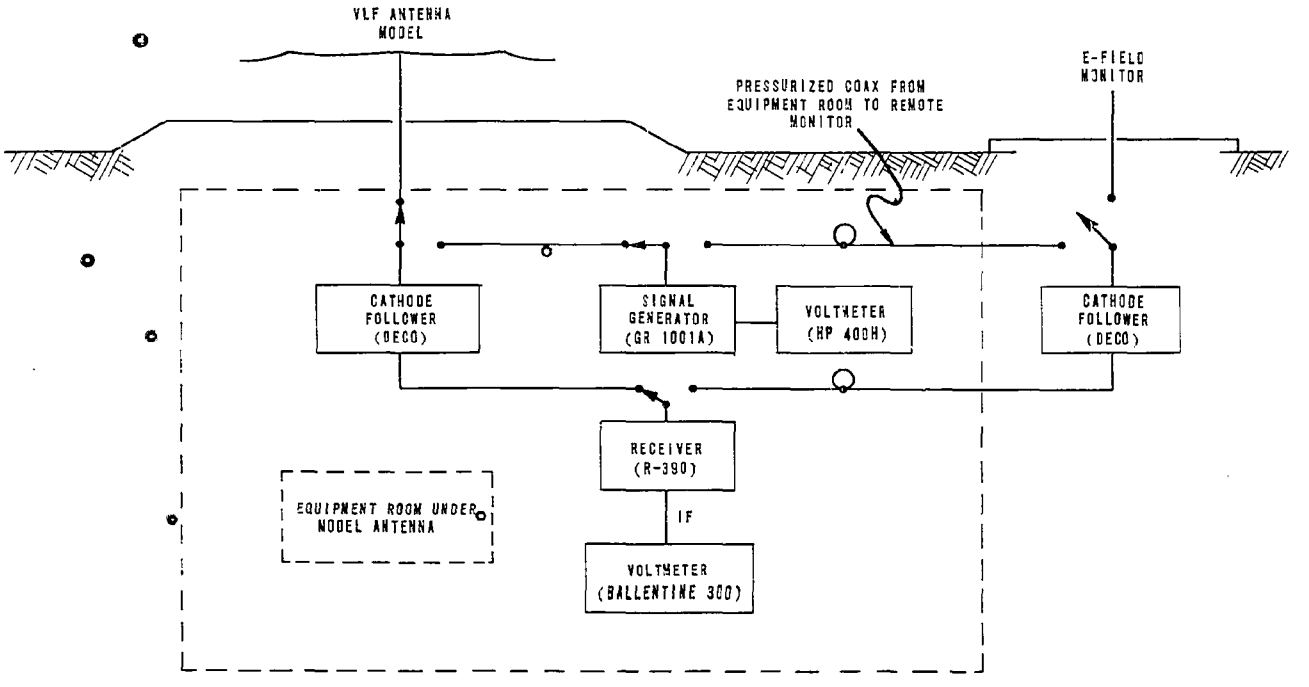

Figure 2-2 EQUIPMENT BLOCK DIAGRAM FOR EFFECTIVE HEIGHT MEASUREMENTS

measurement consisted of tuning the receiver (R-390) to the local broadcast station (WAGE, 1290 kc) and observing a reference voltage on a vacuum tube voltmeter (Ballantine 300) monitoring the receiver i-f output during a period of no modulation. Then, the signal generator (GR 1001A) output was substituted for the antenna at the cathode follower and adjusted to give the same reference indication in each case. The actual recorded voltage was indicated by a calibrated rf voltmeter (HP 400H) across the signal generator output.

This technique uses the same procedure for measuring both the incident field and the base voltage of the antenna under test, thus assuring the same degree of accuracy in both measurements.

2.2.2 Static Capacitance Measurements

Measurements of static capacitance were accomplished with the equipment arrangement shown in Figure 2-3. Static capacitance is defined as the apparent capacitance at the antenna terminals as the frequency approaches zero. It is sufficient that the test frequency not be greater than a few percent of the resonant frequency for the purpose of measurement. In this case, resonance occurred near 3.0 mc, and static capacitance was measured at 30 kc (i.e., 1 percent of resonant frequency). The actual measurement involved a high-Q, parallel resonant circuit employing a high-Q work coil, and a precision variable capacitor (GR 722). The antenna was connected in such a way that its capacitance appeared in parallel with this circuit. The variable capacitor was then adjusted to bring the circuit to resonance as indicated on the rf voltmeter. The capacitor setting at resonance was recorded. Then the antenna was removed from the circuit and the capacitor again adjusted to restore resonance. The difference between the two capacitor settings was determined to give the static capacitance of the antenna.

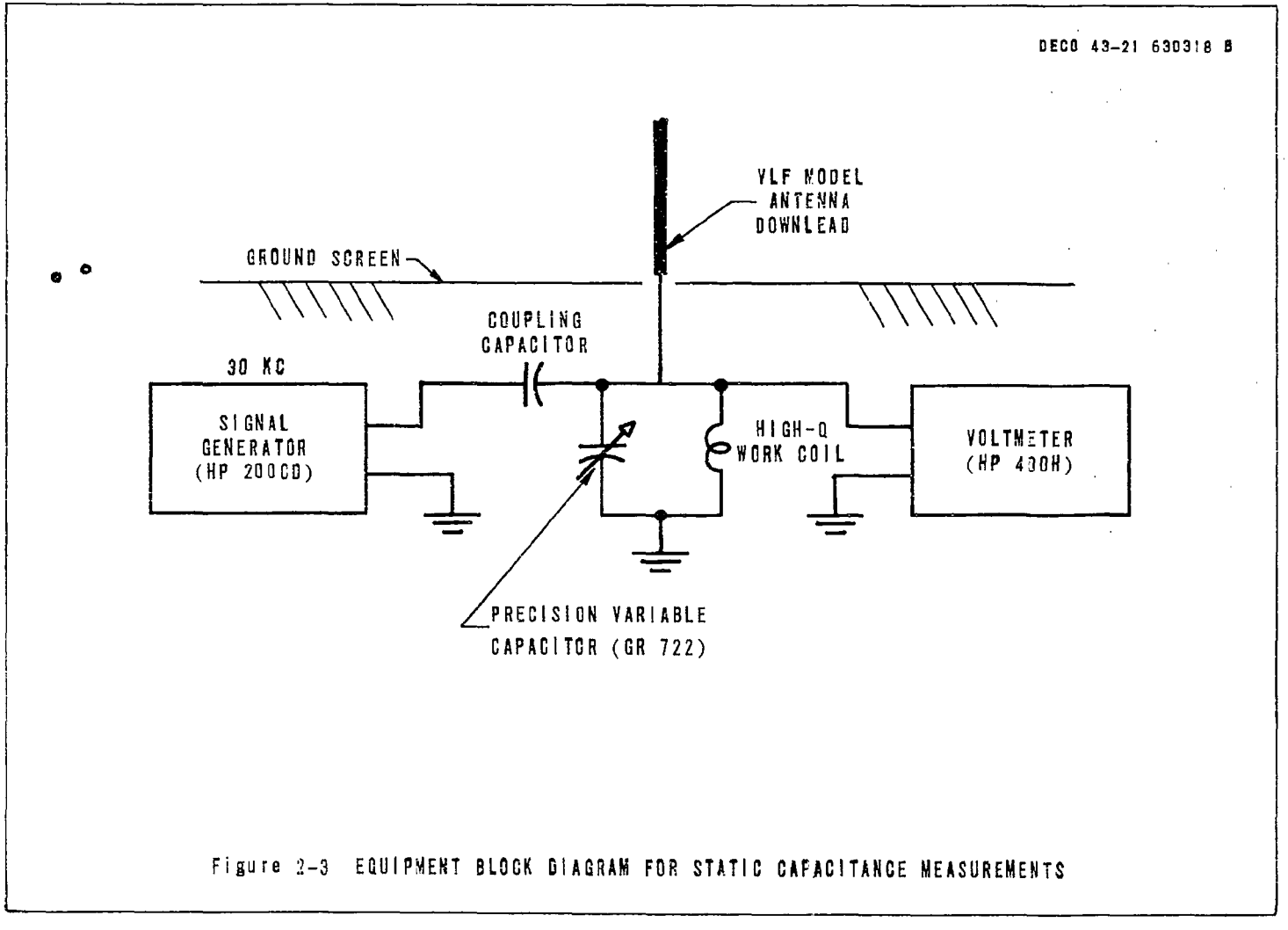

Figure 2-3 EQUIPMENT BLOCK DIAGRAM FOR STATIC CAPACITANCE MEASUREMENTS

It should be noted that the static capacitance measurement does not indicate the distribution of capacitance within the circuit. It is convenient to consider the top hat as the main capacitor element. However, a significant portion (5 to 10 percent) of the static capacitance results from the downleads and appears to act on the ground side of the antenna inductance. This effect cannot be seen without complete impedance data over a wide frequency range, including the region around resonance.

2.2.3 Base Impedance Measurements

Base impedance measurements between approximately 1 and 4 mc were obtained with the equipment shown in Figure 2-4. The measuring instrument used was a radio-frequency impedance bridge (GR 1606A). A signal generator (GR 1001A) provided the drive signal, and a receiver (R-390) with a voltmeter (Ballantine 300) monitoring the i-f output provided the null indication. Frequency calibration was established by comparison with WWV and at intermediate frequencies by use of an electronic counter (HP 524).

The measurement point for base impedance was at an opening in the model Transmitter/Helix Building floor just below the bushings. A short vertical lead provided the path from floor to bushing. Later, measurements were made directly at the bushing entrance point to determine the inductance of the inserted lead, using the top of the corridor dividing wall as the ground return terminal.

Resonant frequency was established by repeated impedance measurements in the region of resonance.

2.2.4 Current Distribution Measurements

The distribution of current over the antenna (top hat and downleads) was accomplished with the use of a small, electrostatically

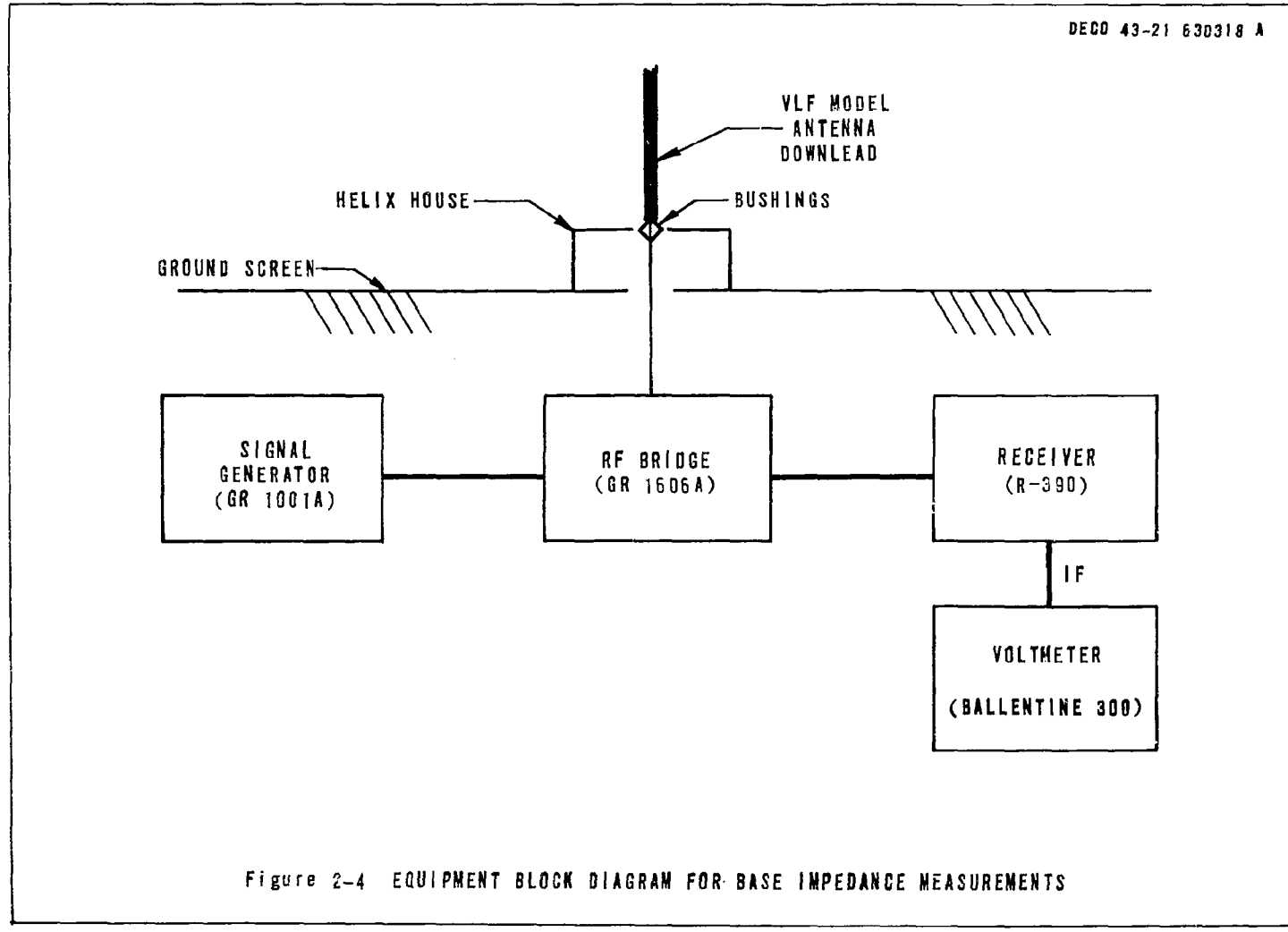

Figure 2-4 EQUIPMENT BLOCK DIAGRAM FOR BASE IMPEDANCE MEASUREMENTS

shielded oscillator positioned along the various conductors as shown in Figure 2-5. The oscillator probe consisted of a self-contained 1560 kc crystal-controlled transistor oscillator with a small coupling toroid, all (except for a small break in the toroid shield) encompassed by an electrostatic shield. This device, loosely coupled to the antenna conductor under test, was passed along each conductor, and the receiver (R-390) i-f output was monitored with an rf voltmeter (HP 400H). Before and after each conductor test, the probe was coupled to the bus at the bushing entrace point for a reference reading.

To establish proper operation of the probe oscillator, a short, thin monopole was constructed, and current distribution measurements were made using the probe. Since the current distribution on such an antenna is well known (i.e., linear), it is possible to obtain a good check on the probe performance.

2.2.5 Field Distribution Measurements

In the area over and around the Transmitter/Helix Building (T/HB), both E- and H-field measurements were made on the antenna model. These measurements were made with small probes (loop for magnetic field, capacitor for electric field) connected through coaxial cables to a sensitive receiver (Stoddart NM-20B). This type of measurement requires careful orientation and positioning of the sensing device and adequate shielding to avoid stray pick-up. The receiver provides an indication of only relative magnitude, and the data must be normalized to a known reference value. Two types of reference, or calibration, were used:

(a) The magnetic field probe positioned at the conducting surface of the Transmitter/Helix Building (T/HB) or nearby ground screen,

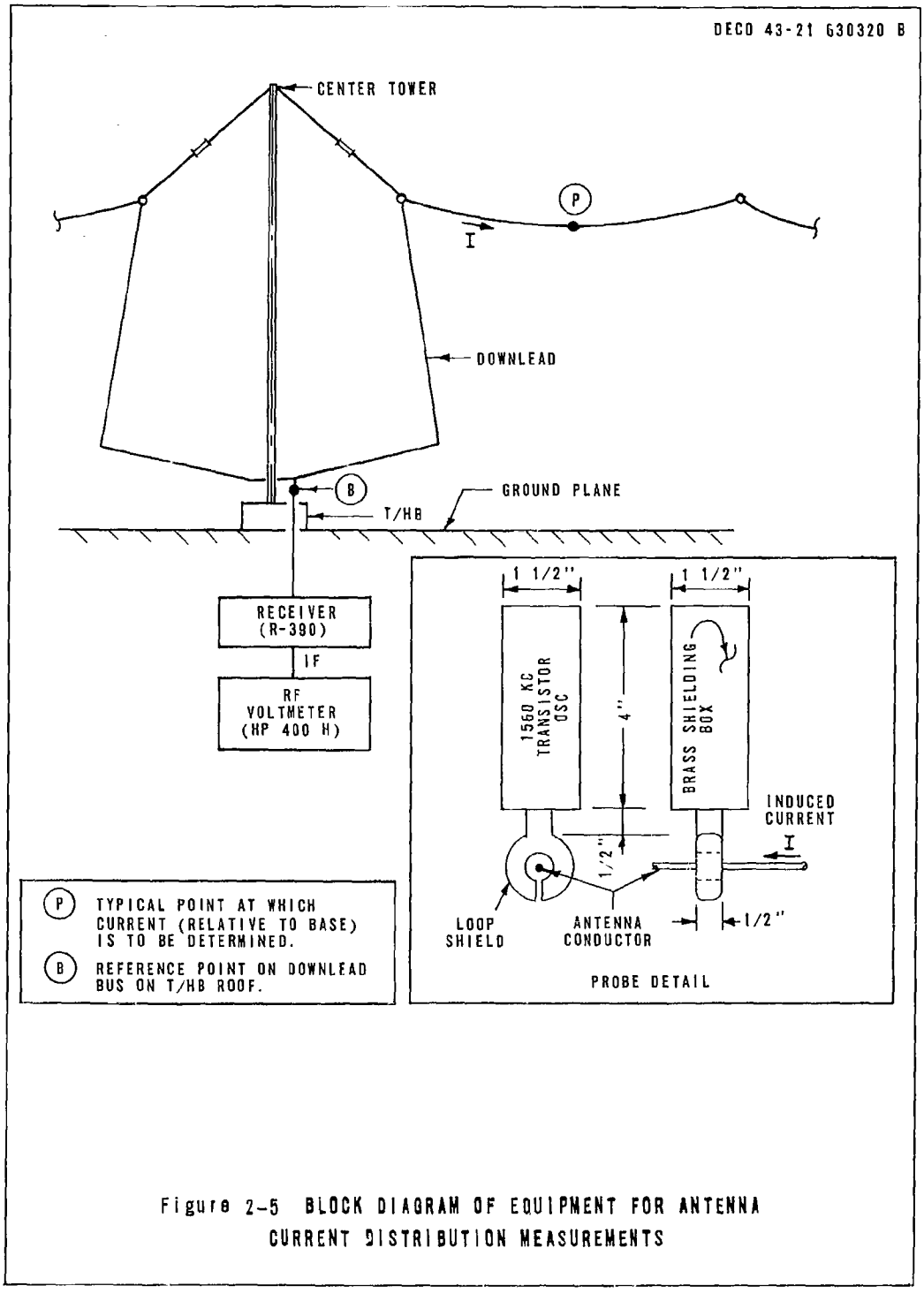

Figure 2-5 BLOCK DIAGRAM OF EQUIPMENT FOR ANTENNA CURRENT DISTRIBUTION MEASUREMENTS

measures the tangential H-field component. At the surface, this component is identically equal to the surface current density. Calibration consisted of measuring the relative tangential H-field (i.e., surface current density) at several points a short distance from the bushing entrance point. Integrating the radial current density around a path enclosing the bushing entrance yields the total base current. Other readings were then referenced to this value.

(b) The capacitive E-field probe was calibrated by positioning a short distance apart two metal sheets, large with respect to the 1-inch probe, and providing rf excitation at the test frequency. For large plates closely spaced, the field is uniform over most of the interior and is equal to the ratio of the impressed voltage to the separation. This calibration yields a proportionality constant which, when the actual base current of the antenna model is measured, allows each relative E-field reading to be referenced to an absolute value.

2.2.6 Corona Study

Qualitative data on the distribution of charge on the antenna was obtained by applying high voltage (up to approximately 60 kv), 60-cycle excitation to the model at night and photographically recording the occurrence of corona by means of long exposures. These photographs, taken at progressively higher voltages, show the critical regions where corona first appears, and can be correlated with indirect methods of gradient analysis (i.e., current distribution). Since the critical gradient for corona formation is a non-linear function of the radius of curvature, the direct scaling of corona onset voltage is not possible (see Appendix E). However, the capability of directly observing the entire antenna (or a characteristic part such as one panel) at corona onset is highly useful in confirming the indications of the alternate method.

2.3 Scale Model Factors

For all of the model work, a scale factor of 1:100 was employed. To convert to full-scale data, the model data is multiplied by the appropriate scaling factor below:

Parameter	Scaling Factor
• Effective Height (and all other distances)	100
• Capacitance	100
• Inductance	100
• Frequency	0.01
• Radiation Resistance	1 (at scale frequency)
• Base Impedance	1 (at scale frequency)

To model the ohmic component of the resistance, it would be necessary to scale all conductivities 100 times greater than the full-scale values. Since this is obviously impossible, no attempt was made to use base resistance data from the model.

2.4 Calibration

The purpose of the model range is to provide a relatively large, smooth, highly conducting plane over which the incident radio-frequency field propagates unperturbed by discontinuities and reflections. In practice, this can only be approximated because some variations in the surface characteristics still remain which cause small variations of the incident field over the area of interest (i.e., the region around the test antenna, including the monitor antenna which measures the incident field). Therefore, it is necessary to perform calibration measurements to determine the relation between the incident field at the monitor and at the test antenna.

Effective height measurements were accomplished by comparing the open-circuit base voltage V_b with the incident field strength E_i at the model:

$$h_o = V_b / E_i \quad \text{meters} . \tag{2-1}$$

Since the incident field at the model is not necessarily equal to that at the monitor but in all cases is directly proportional, the effective height may be expressed as

$$h_o = K_1 V_b / V_m \quad \text{meters} , \tag{2-2}$$

where V_m = monitor base voltage, and K_1 = range calibration constant.

The determination of the range calibration constant K_1 in Equation 2-2 was made using several short, thin monopoles of known effective height. For a thin monopole, the effective height (h_o) is simply related to the physical height h by

$$h_o = h/2 . \tag{2-3}$$

Depending on the thickness of the monopole and on the near-base or insulator capacitance, the actual effective height may depart from half the physical height by as much as several percent. However, by a proper choice of diameter and base insulator configuration, the difference between Equation 2-3 and the actual effective height may be reduced to a fraction of a percent.

For the calibration tests seven monopoles were employed. A specially tapered 3-meter monopole was constructed to have uniform capacitance per unit length,as suggested by Schelkunoff.[1] In theory,

---

[1] Schelkunoff, S. A., and H. T. Friis. Antennas, Theory and Practice. New York, Wiley. 1952. P 318, Figure 10.9.

this element has an effective height equal to exactly half of its physical height. However, some uncertainty about the near-base capacitance led to the use of cylindrical monopoles of various lengths all utilizing the same base configuration. Since the same near-base capacitance was present in each monopole of this calibration series, an empirical determination of this parameter was possible through the correlation of the measured effective height data.

Table 2-1 summarizes the range calibration data. The effective heights shown are the assumed values of one-half the physical heights. The ratio of monitor voltage V_m to base voltage V_b corrected for near-base capacitance loading effects is as shown in the table at 1290 kc for all test monopoles.

TABLE 2-1

Summary of Calibration Data

Element Length (feet)	Element Diameter (inches)	Effective Height (meters)	V_m / V_b	Range Constant (K_1)
9.85	tapered	1.5010	.6724	1.0093
9.85	1/4	1.5010	.7143	1.0722
9.00	1-1/8	1.3716	.7656	1.0501
12.00	1-1/8	1.8290	.5690	1.0407
15.00	1-1/8	2.2860	.4621	1.0564
18.00	1-1/8	2.7432	.3823	1.0487
21.00	1-1/8	3.2004	.3286	1.0517
			average constant =	1.0470

Since the ratio V_b / V_m is theoretically a linear function of the effective height h_0, the last five monopoles (1-1/8 inch diameter) were treated by the least-squares method to fit a line to the data. This analysis yielded $K_1 = 1.055$. This value was used as the calibration constant in the 1290-kc measurement of effective height rather than the average value because more data was available to evaluate the influence of voltmeter (cathode follower) and near-base capacitance.

3. RESONANT FREQUENCY TESTS

An analysis of construction costs carried out under the PER phase indicated that radiation system performance (primarily the antenna bandwidth) could be improved without increasing the cost by altering the aspect ratio and the similitude scale factor of the antenna. Specifically, it was determined that reducing tower heights and increasing top hat spans would result in greater bandwidth for the same cost. The performance characteristics of various aspect ratios* and similitude scale factors** were determined from a model study carried out under Change Order F of the PER.

The model study indicated, however, that the self-resonant frequency of the antenna for the near-optimum combinations of aspect ratio and similitude scale factor was marginally close to the 30-kc upper operating limit specified for antenna performance. This included some reduction in resonant frequency because of residual inductance in the tuning and coupling circuitry at the high end of the frequency range. Since it was not considered economically feasible to use series capacitive tuning to provide for operation above natural resonance, the U. S. Navy directed that this method not be used. Therefore, other means were sought to extend the operating range with inductive tuning. The method used to solve this problem was the reduction of the aggregate downlead inductance by altering the configuration or by employing more parallel conductors.

---

* Aspect ratio a is defined as the ratio of outer tower height to maximum top hat span, normalized to the 1.28-Cutler dimensions.

** Similitude scale factor s relates all linear dimensions to the 1.28-Cutler design for unity aspect ratio.

Since the selection of final antenna dimensions had not been concluded, the resonant frequency study was carried out on a 1:100 scale model of the 1.28-Cutler configuration.

3.1 Techniques

To increase the resonant frequency, several downlead configurations were suggested which would alter the effective radius of the aggregate downlead path (consisting of six identical cages or groups) with the possibility of reducing the inductance. Since the downlead "bundle" was roughly 700 feet in diameter and only 900 feet in length, simple analytical approximations based on long, thin conductors did not produce accurate quantitative results. However, for such simple structures the inductance is proportional to the logarithm of the length-to-diameter ratio. Therefore, it was expected that increasing the effective diameter of the downlead bundle would result in the desired increase in resonant frequency. However, it became apparent that the structural problems associated with increasing the center tower-downlead truss separation were formidable. For this reason several configurations were tested which employed a variety of truss and hinge point locations as well as various numbers of downlead conductors.

3.2 Description of Tests

Figure 3-1 is an elevation view of a typical downlead configuration. Since the resonant frequency tests were undertaken at the start of the final design contract and prior to the determination of the first Transmitter/Helix Building configuration, the Helix Building design of the PER was used for these tests; this version employed three bushing entrance points each of which fed two adjacent panels. The dimensions lettered (A), (B), and (C) in Figure 3-1 are those which were varied and found to influence the resonant frequency.

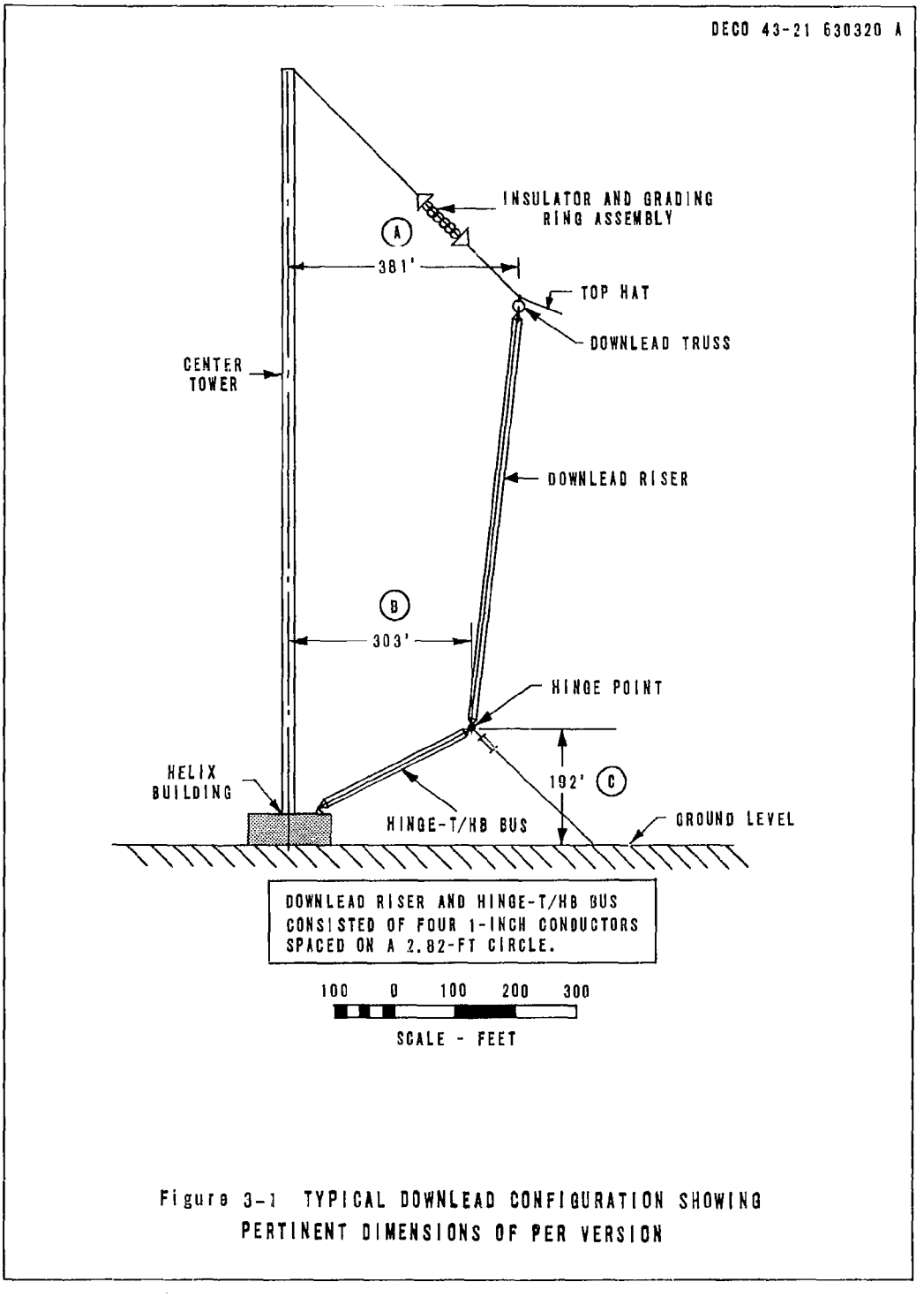

Figure 3-1 TYPICAL DOWNLEAD CONFIGURATION SHOWING PERTINENT DIMENSIONS OF PER VERSION

For each downlead configuration, the effective height and static capacitance as well as the base impedance were measured. Particular attention was devoted to impedance measurements near resonance.

Figures 3-2, 3-3, and 3-4 show the various downleads tested. For all types of downleads and all positions of the downlead truss, the elevation of the downlead truss was maintained approximately constant.

Tests 1 through 6 employed a 4-wire cage for the hinge-point-to-helix house bus; Tests 7 through 12 used a copper tube of approximately equivalent inductance per unit length. Beginning with Test 9, a completely new top hat replaced the earlier version which had been damaged by wind. These changes introduced very minor variations in performance which were not related to the particular downlead configuration involved.

3.3 Test Results

Table 3-1 shows the significant dimensions of the various downleads along with the effective height, static capacitance, and resonant frequency. Also included is the unloaded or lossless antenna bandwidth (bw_o) at the design frequency (15.5 kc) derived for comparison. All data given is referred to full scale operation.

Initially, it was proposed that three downlead pulloff points (i.e., A = 381, 481, and 581 feet in Figure 3-1) would be tested along with various hinge-point locations. However, in implementing the tests, it was decided that the intermediate (A = 481 feet) pulloff point would be tested only after the extreme position (A = 581 feet) proved effective.

The original goal for the resonant frequency was about 33.3 kc. This was established by assuming a 10-percent reduction due to residual

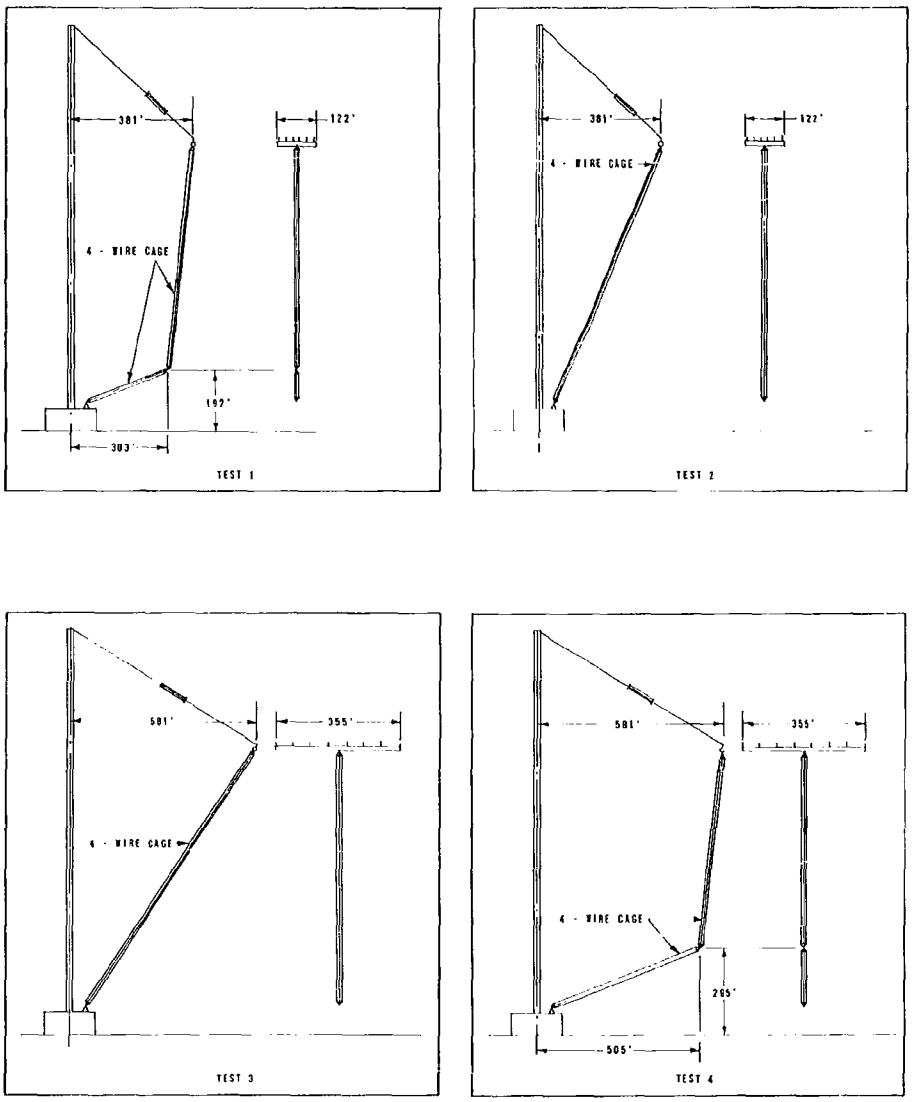

Figure 3-2 DOWNLEAD CONFIGURATIONS - TEST 1 THROUGH 4

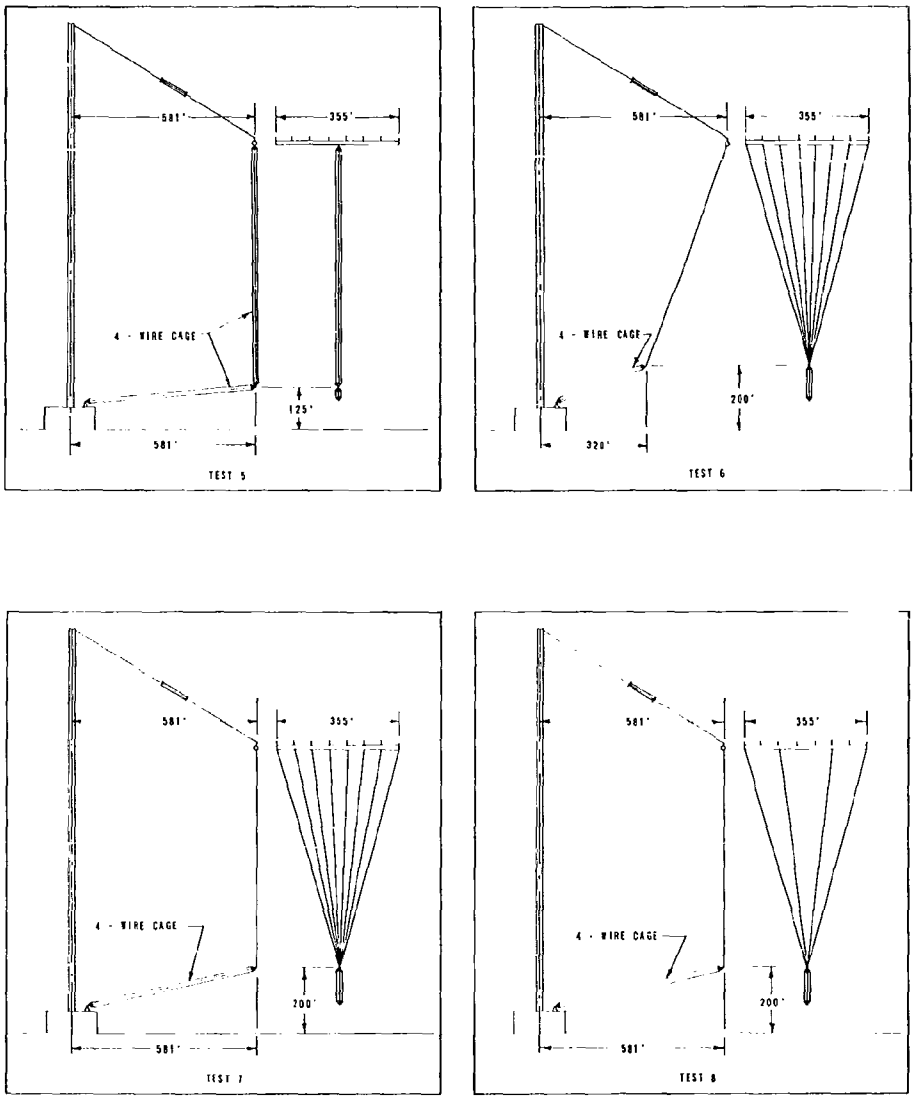

Figure 3-3 DOWNLEAD CONFIGURATIONS - TEST 5 THROUGH 8

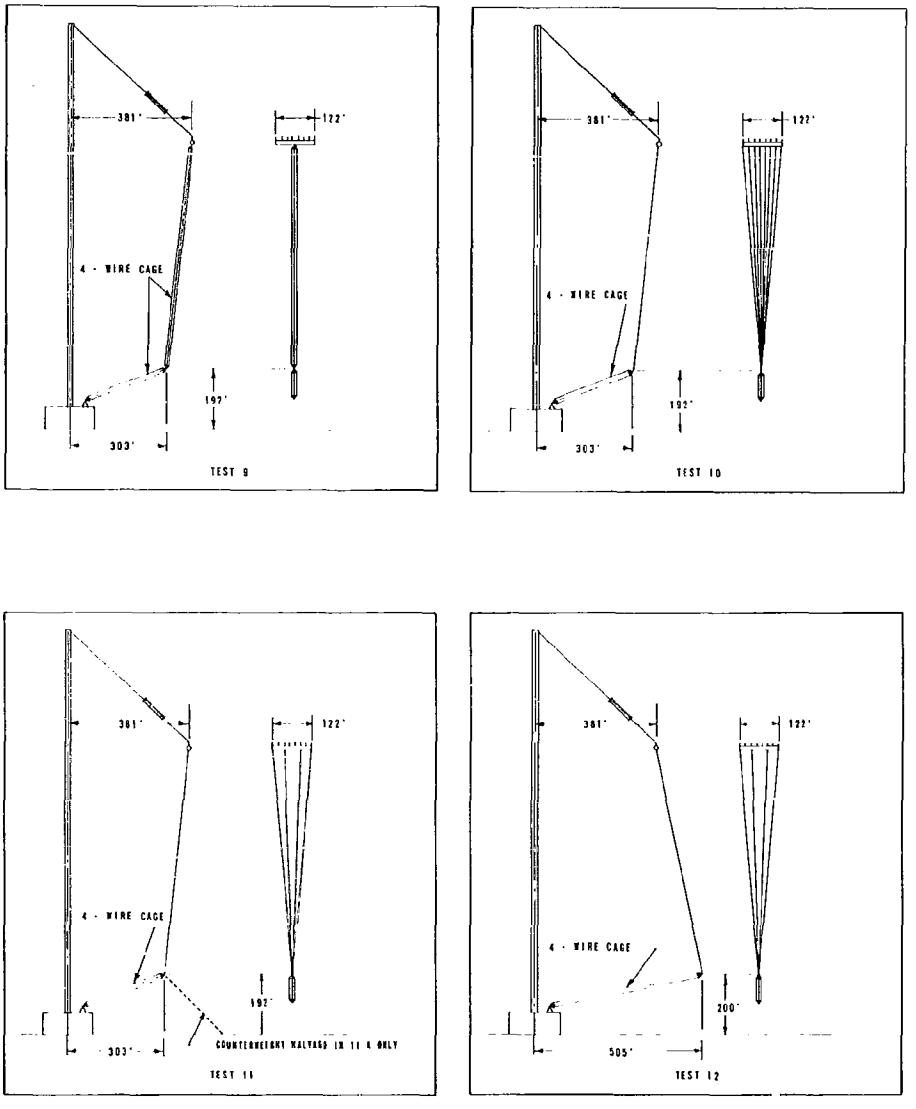

Figure 3-4 DOWNLEAD CONFIGURATIONS - TEST 9 THROUGH 12

TABLE 3-1

Resonant Frequency Test Results

Test No.	Downlead Vertical	Downlead Horizontal	A Truss Radius (feet)	B Hinge Radius (feet)	C Hinge Elevation (feet)	Effective Height (feet)	Static Capacitance (μf)	Resonant Frequency (kc)	Antenna Bandwidth at 15.5 kc (cps)
1	4-Wire Cage	4-Wire Cage	381	303	192	638	.1498	31.50	36.4
2	4-Wire Cage	4-Wire Cage	381	(No Hinge)		640	.1487	30.75	36.3
3	4-Wire Cage	4-Wire Cage	581	(No Hinge)		638	.1499	32.05	36.3
4	4-Wire Cage	4-Wire Cage	581	505	295	627	.1519	32.30	35.6
5	4-Wire Cage	4-Wire Cage	581	581	125	600	.1561	32.18	33.5
6	8-Wire Fan	4-Wire Cage	581	320	200	643	.1530	35.10	37.7
7	8-Wire Fan	Tubing	581	581	200	628	.1543	34.98	36.3
8	4-Wire Fan	Tubing	581	581	200	635	.1531	34.47	36.8
9	Tubing	Tubing	381	303	192	642	.1497	31.68	36.8
10	8-Wire Fan	Tubing	381	303	192	635	.1514	33.27	36.3
11	4-Wire Fan	Tubing	381	303	192	634	.1506	32.87	36.1
11A	Same as 11 with hinge pulloff halyard		381	303	192	639	.1505	32.87	36.7
11B	Same as 11 with 0.005 μf shunt in Helix Building		381	303	192	635	.1554	32.87	37.3
12	4-Wire Fan	Tubing	381	505	200	631	.1521	33.05	36.1

tuning and matching inductance and a minimum upper operating frequency of 30 kc. The exact effect of the residual inductance depends on tuning component design, which was not refined at that time. Therefore, the 10 percent margin was tentatively established for this purpose.

The first five tests explored the various positions of the 4-wire cage downlead (the full-scale version consisted of four 1-inch conductors positioned at the corners of a 2-foot square). No combination of dimensions in the range considered feasible was found which would yield the desired resonant frequency. At this point, the cage downlead was discarded in favor of a spread or fan arrangement to further reduce the downlead inductance. Test 6 employed an 8-wire fan downlead which was positioned at the extreme pulloff point (A = 581 feet) and resulted in a resonant frequency of 35.10 kc, well above the 33.3-kc goal. Test 7 introduced an increase in the hinge-tower separation (B) from 320 to 581 feet; this produced a small reduction in resonant frequency to 34.98 kc. At this time, the structural problems associated with this larger separation requiring a very large downlead truss and the windloading on the 8-wire fan dictated that further effort be made to reach a compromise version which would be economically acceptable.

Test 8 explored the possibility of reducing the number of conductors in the fan from 8 to 4. For the same A and B dimensions as the 8-wire fan in Test 7, the 4-wire version yielded a resonant frequency of 34.47 kc, a 0.51 kc reduction.

At this point, the model was damaged by ice and wind to the point that further work required a complete replacement of the top hat. After the new top hat was erected a control test (Test 9) was made to show any changes that had been introduced in the top hat replacement. Comparison of Tests 1 and 9 showed essentially no change except for a resonant

frequency increase of some 0.18 kc over the Test 1 results. However, Test 9 rather than Test 1 was used as a reference for Tests 10 through 12.

Tests 10 and 11 show the result of replacing the PER downlead (Test 9) with fans of 8 and 4 wires, respectively, with the same A, B, and C dimensions. This resulted in an increase in the resonant frequency to 33.27 kc for the 8-wire fan, and to 32.87 kc for the 4-wire fan. This result is marginal for the assumed 10 percent reduction due to residual inductance, but does indicate the feasibility of the fan-type downlead as a means of increasing resonant frequency.

Tests 11A and 11B involved two minor changes which were found to have no measurable influence on resonant frequency. In Test 11A, the hinge-point counterweight halyards and insulators were added. Test 11B introduced a small shunt capacitance (.005 μf full scale) inside the Helix Building across the antenna terminals. Both changes should not be expected to change the resonant frequency appreciably since a voltage node at the antenna base at resonance renders shunt elements ineffective at that point.

Test 12 shows the effect of increasing the B dimension to 505 feet (making the downlead slope away from the tower base) in a manner suggested by the structural designers. This produced a slight increase in resonant frequency to 33.05 kc, 0.18 kc above the value for Test 11. Since Tests 11 and 12 both employed 4-wire downleads, some further increase could be predicted for the 8-wire fan in the Test 12 configuration. Comparing Tests 7 and 8 and Tests 10 and 11 shows an average increase in resonant frequency of 0.45 kc for the 8 over the 4-wire fan. Extrapolating Test 12 results on this basis yields a predicted resonant frequency of 33.50 kc for the 8-wire fan in the Test 12 configuration. This value safely satisfies the 33.3 kc goal.

4. ANTENNA SELECTION

The initial configuration of the vlf antenna to be modeled in the final design phase was developed* through the consideration of the various design constraints of cost, performance, reliability, etc., in relation to analytical data developed in preliminary studies of structural and electrical properties of various alternatives. Specifically, model studies** provided information on the variation of electronic performance with structural variations of the following types:

(a) Size and aspect ratio of the antenna in comparison with the 1.28 Cutler design.

(b) Downlead configuration.

(c) Halyard slope, tower cantilever, and "B" tower-height compensation.

During the development of the final design, the various cost and performance constraints were continually reviewed to take advantage of every opportunity to improve performance or to reduce cost as a result of design trends established in the preliminary phases of planning.

---

* Further details on the selection procedures are contained in HNCD letter of 7 February 1962 to OIC, "VLF Pacific Antenna Selection" and an HNCD report "Basis of Selection of VLF Antenna Configuration," April 1963.

** Basic antenna studies relating to the 1.28 Cutler design were performed under Contract NBy-37598 and presented in the PER. Specific studies of the effects of halyard slope, cantilever length and B tower compensation, together with size and aspect ratio studies, were accomplished under Change Order F of that contract. The effect of downlead configuration on resonant frequency was explored under the early phases of Contract NBy-37636; the results are presented under Section 3 of this report.

Particularly, it was recognized that the achievement of optimum bandwidth was not compatible with the originally specified upper operating frequency of 30 kc without employing additional capacitive tuning circuitry. Consequently, by direction of cognizant Navy offices, a revised minimum upper operating frequency of 28.5 kc was established.

4.1 Cost-Performance Study

Based on the final phases of the PER and early studies in the final design program, the modified Cutler design was selected with the following provisions:

(a) The size of one Cutler-type element was increased by a factor of 1.28 to provide adequate bandwidth and power radiating capability.

(b) Vertical halyards were employed and cantilever lengths were reduced to 10 feet, requiring an increase of 45 feet in the intermediate tower heights to compensate for the cantilever reductions.

These values depart from corresponding PER conditions of sloping halyards, 57-foot cantilever, and 57-foot compensation, but provide roughly equivalent electrical performance.

Considering both structural and electrical aspects, the antenna recommended for final design was considered to have the greatest potential of meeting the requirements summarized below:

(a) Antenna bandwidth (100 percent efficiency) not less than 37.5 cycles at the design frequency of 15.5 kc.

(b) Upper operating frequency not less than 28.5 kc.

(c) No tuning capacitors required to meet (b) above.

(d) Estimated cost not to exceed that of the Single Modified (1:28) Cutler Antenna.

Figure 4-1 summarizes the data developed for the cost-performance study relating the antenna bandwidth and resonant frequency to the size, aspect ratio, and cost. The data of Figure 4-1 is typical of the inter-relations considered in arriving at a final configuration. Since bandwidth occupies a dominant role in the antenna selection, this factor is emphasized. Considering the bandwidth and cost constraints, the acceptable combinations of $\underline{a}$ and $\underline{s}$ in Figure 4-1 are seen to lie in the region above the 37.5 cps line and below the PER cost line. The maximum antenna resonant frequency in this region was about 30.6 kc for the PER design (4-wire cage downleads), which yields an upper operating frequency of only about 27.5 kc with the 10 percent tuning and coupling margin.

Having recognized the resonant frequency problem prior to the start of the final design, the resonant frequency study (Section 3) was undertaken to develop means of increasing resonant frequency without degrading other performance aspects. For the modified 1.28 Cutler configuration ($\underline{a} = \underline{s} = 1$), the 8-wire fan downlead resulted in an increase in resonant frequency of approximately 5 percent over the value obtained with the 4-wire cage downlead in a similar configuration. Estimates were made of the effects of the deviation from unity aspect ratio and scale factor which, together with a 10 percent margin for the tuning-coupling effect and 1 percent tolerance limit, located the maximum operating frequency (28.5 kc) line on Figure 4-1.

Considering the three constraint lines (cost, bandwidth, maximum operating frequency) in Figure 4-1, the point for $\underline{a} = 0.925$ and $\underline{s} = 1.05$ determined the antenna configuration recommended by HNCD. This choice provides for adequate bandwidth (with no safety margin) and maximum operating frequency at an estimated cost not greater than

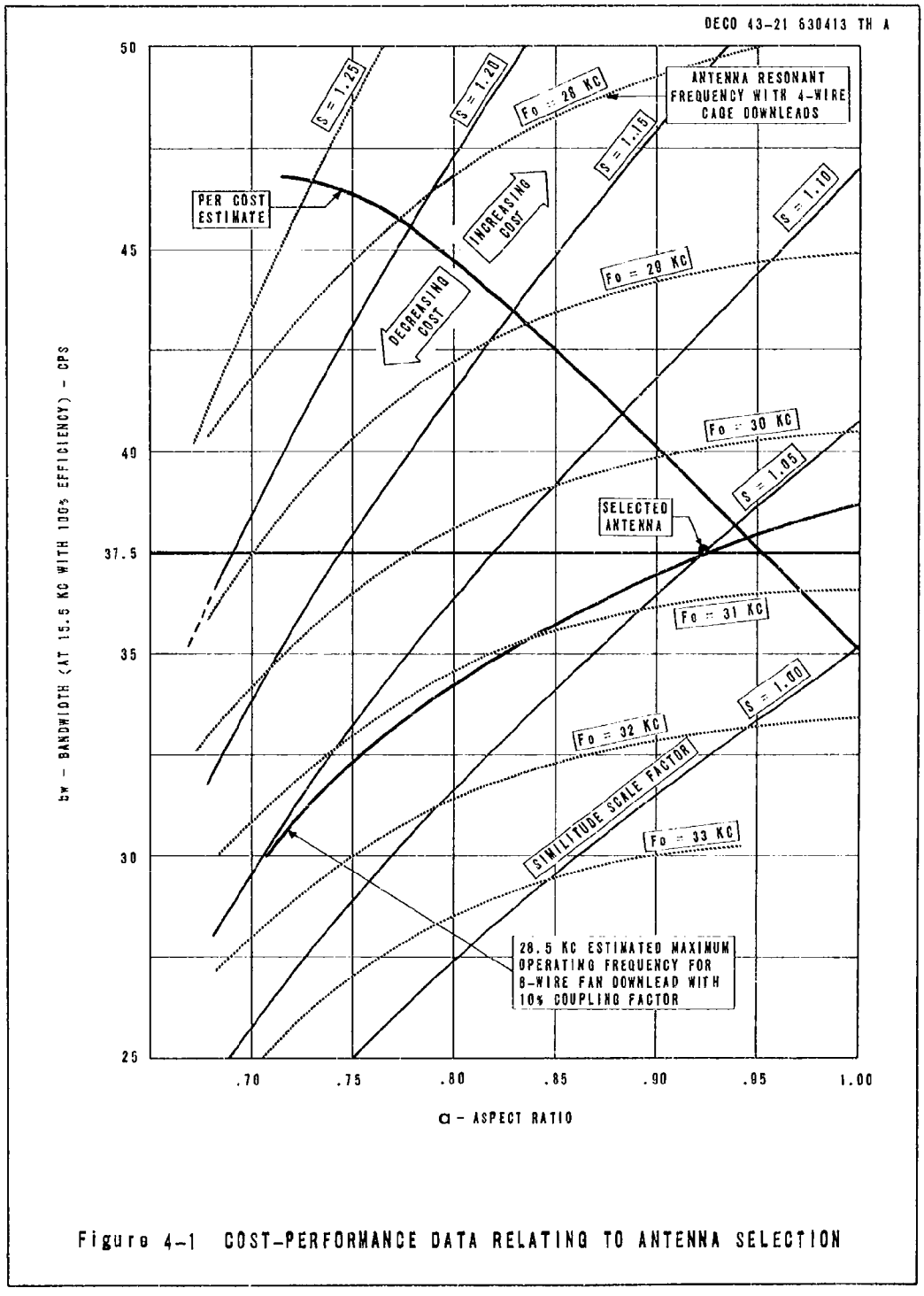

Figure 4-1 COST-PERFORMANCE DATA RELATING TO ANTENNA SELECTION

that of the PER design. The decision to delete a safety margin to account for prediction tolerance in the bandwidth parameters was made with the concurrence of cognizant Navy offices. The recommendation was predicated on the inclusion of a bandwidth control element in the transmitter which could compensate for a minor degradation of antenna bandwidth with some attendent reduction in efficiency. The recommended configuration was accepted by the Navy and modeling proceeded on the basis of this selection.

5. ANTENNA MODEL STUDY

5.1 Initial Configuration

As a result of the antenna selection study (Section 4), the antenna configuration initially constructed for further model study in the final design stage differed from the previously modeled PER design (1.28 Cutler) in the following aspects:

(a) The aspect ratio $\underline{a}$ and similitude scale factor $\underline{s}$ were changed from unity in the PER version to $\underline{a} = 0.925$ and $\underline{s} = 1.05$ for the initial configuration. These changes resulted in towers approximately 25 percent higher and spans approximately 35 percent greater than Cutler.

(b) The tower heights were further increased to maintain the average height with the non-counterweighted top hat and the corresponding increase in sag.

(c) An 8-wire fan downlead replaced the 4-wire cage previously used.

(d) The downlead hinge point was positioned at a 500-foot radius from the center tower and elevated 186 feet above ground.

(e) A combined Transmitter/Helix Building replaced the PER helix building at the base of the center tower. Also, the tower was nested in a well in the building rather than directly on the roof.

(f) The busses combining the downleads at the Transmitter/Helix Building were external rather than internal as in the PER design. These initially entered the building through a single bushing rather than the previous three.

(g) Initially, the internal circuitry was not installed in the tuning and coupling area of the T/HB. A short vertical lead simulating a 10-inch

bus provided a convenient measuring point at an opening in the model T/HB floor.

Figure 5-1 shows a plan view of a typical panel of the top hat. As initially proposed, the panel consisted of four outer conductors (Nos. 1, 2, 7, and 8) of aluminum clad (approximately 7 mils of aluminum) nominally 1-inch outside diameter cable, whereas the four inner conductors were of 1-inch ACSR (i.e., with a solid aluminum outer lay). Also, the outer two conductors of each side were enlarged to 1-1/2 inch diameter in the region near the intermediate towers. The ACSR conductors were proposed where structurally feasible in an attempt to reduce losses. Figure 5-2 shows an elevation view of a longitudinal panel cross section with an exaggerated vertical scale to emphasize the sag. For the model version, each catenary was approximated by establishing two sag points as shown in Figure 5-3. This top hat (designated Top Hat I) has a centroid elevation of 900 feet.

5.1.2 Transmitter/Helix Building

In the proposed design, the transmitter and the tuning/coupling circuitry were housed in the same structure (T/HB). This eliminated an extensive transmission line as well as provided other structural economies. Figure 5-4 shows the external features of the T/HB as initially proposed. The center tower was placed in a well approximately 25 x 40 feet in the building. The model version of the building was made of sheet brass and included the tower well and the internal switch rooms which form a corridor beneath the bushing entrance area.

5.1.3 Bushing

The T/HB shown in Figure 5-4 used only one entrance bushing instead of three as in the PER version. At the beginning of the study,

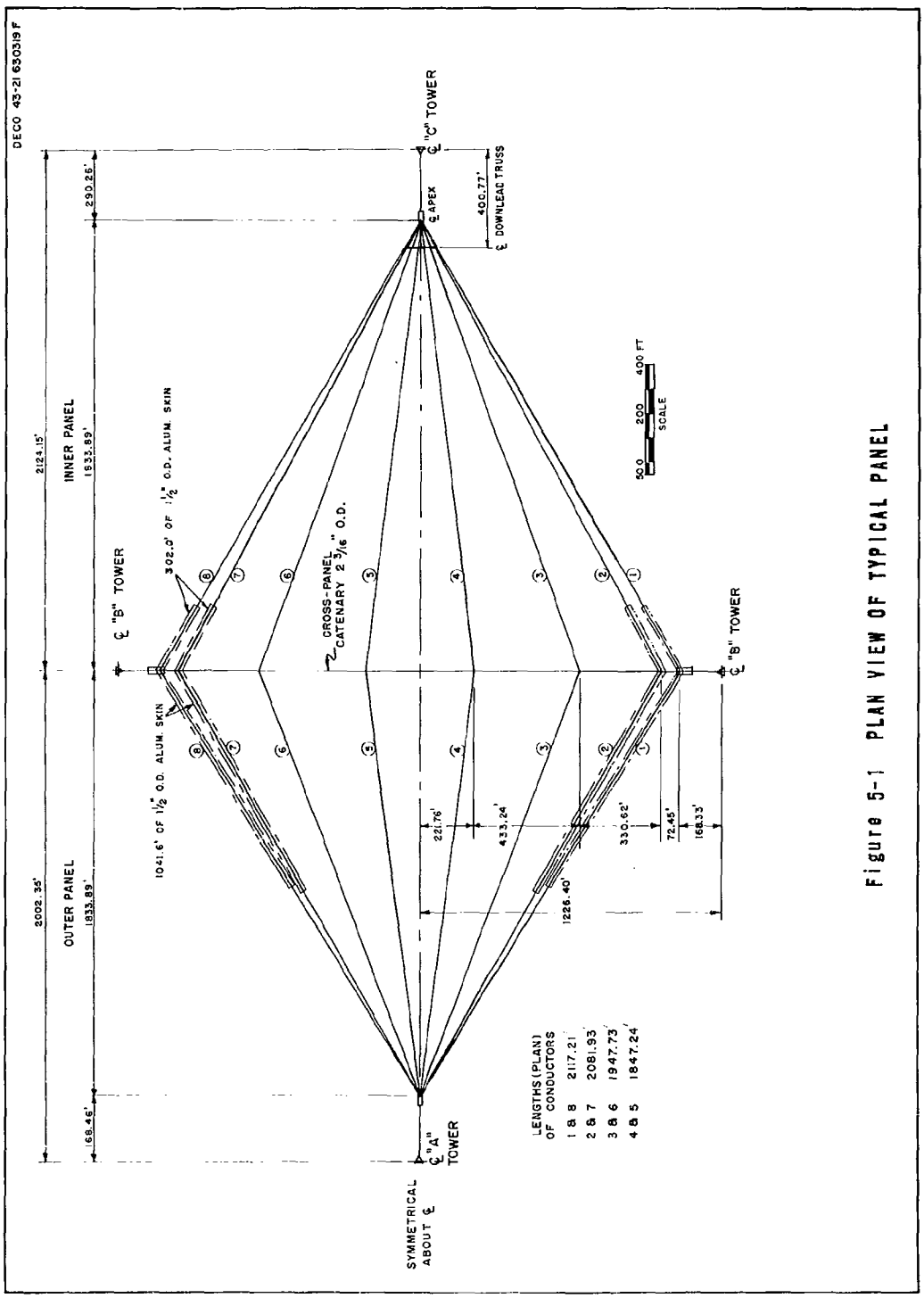

Figure 5-1 PLAN VIEW OF TYPICAL PANEL

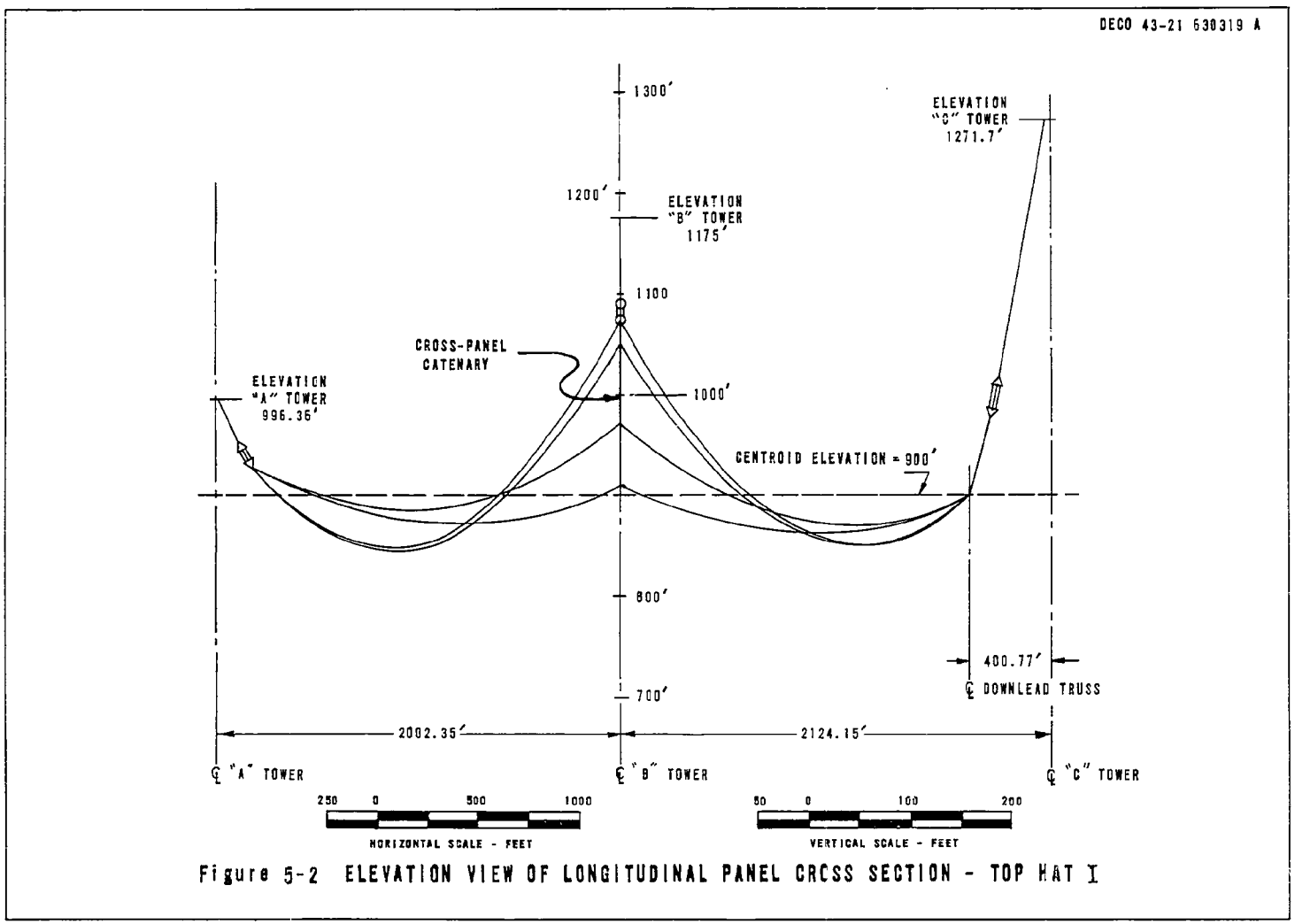

Figure 5-2 ELEVATION VIEW OF LONGITUDINAL PANEL CROSS SECTION - TOP HAT I

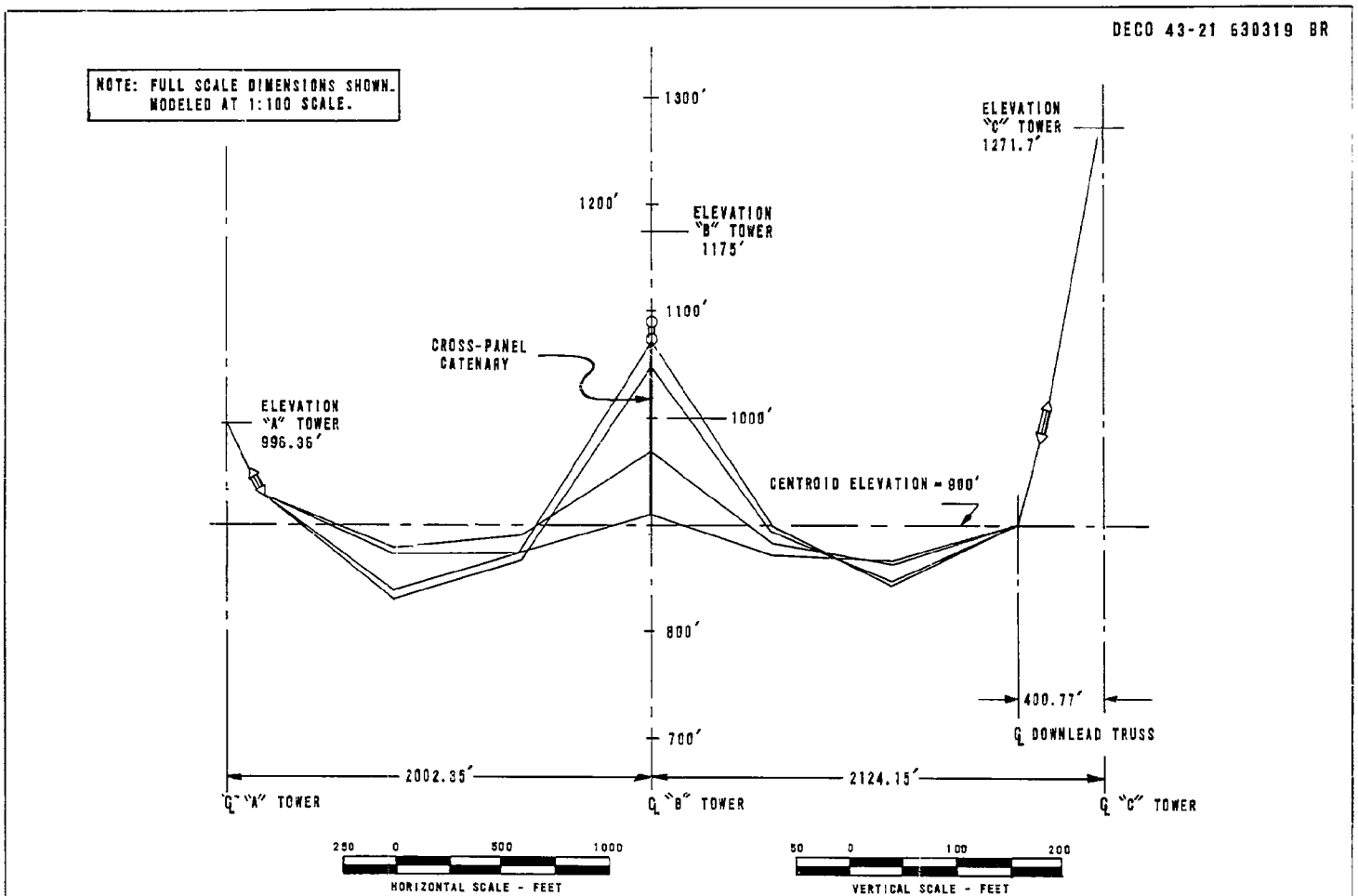

Figure 5-3 ELEVATION VIEW OF LONGITUDINAL PANEL CROSS SECTION AS MODELED - TOP HAT I

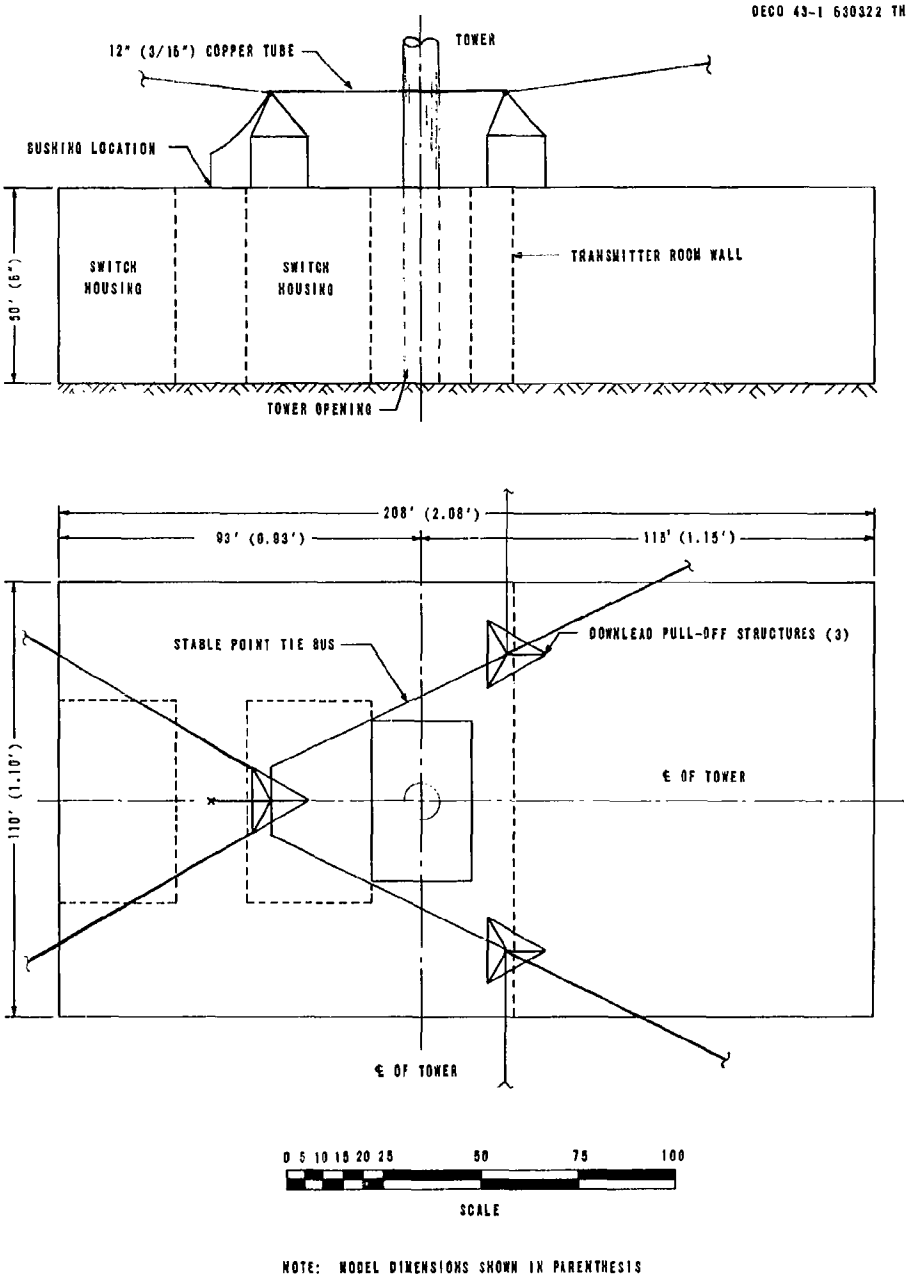

Figure 5-4 INITIAL TRANSMITTER/HELIX BUILDING

it was not known whether a single bushing could be obtained which could carry the entire base current, but the advantages of the single-bushing approach warranted its inclusion in the initial model. This approach uses external bus work to combine the six downleads rather than the internal bus work used in the PER design. Although this required three insulated downlead pulloff structures on the roof, it resulted in a reduced inductance with a correspondingly higher resonant frequency.

5.1.4 Downleads

An 8-wire fan downlead was selected to provide a sufficiently high resonant frequency from the results obtained under the resonant frequency study (Section 3). Figure 5-5 shows the details of the downlead arrangement. The spacing of the top hat conductors, designed to equalize the charge distribution, was preserved at the top of the fan with a tapering to uniform spacing at the hinge point. At the hinge, the 4-wire cage bus continues to the T/HB roof area.

5.2 Evaluation of Initial Configuration

Upon conclusion of the antenna selection study, the initial configuration was evaluated on the model range. This configuration was subjected to a series of measurements to determine its performance characteristics. The measurement program consisted of determining the basic antenna parameters from which performance under emergency and normal operating conditions were derived. Detailed data is presented in Appendix A.

5.2.1 Five-Panel (Emergency) Performance

Prior to the erection of the sixth panel, tests were made to establish the performance characteristics of the antenna in a simulated emergency situation with only five panels in operation. It was expected that

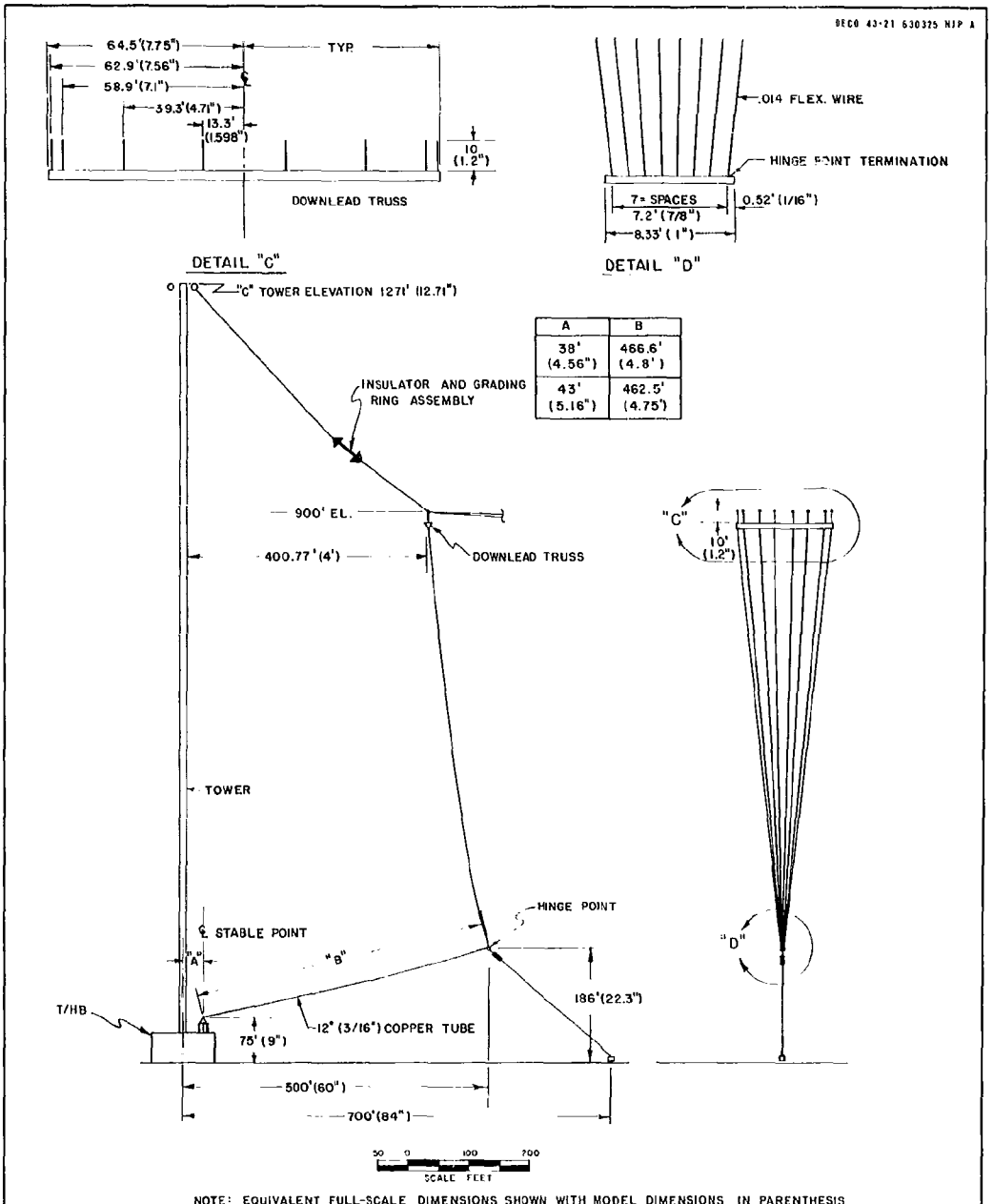

NOTE: EQUIVALENT FULL-SCALE DIMENSIONS SHOWN WITH MODEL DIMENSIONS IN PARENTHESIS

Figure 5-5 DOWNLEAD DETAILS

this would reduce the capacitance and, hence, the power radiating capability.

The basic full-scale parameters determined together with the derived characteristics for performance at 15.5 kc with 1 megawatt radiated power are presented in Table 5-1. Base impedance data over the entire frequency range, taken at a point at the floor of the T/HB, is presented in Figure 5-6.

TABLE 5-1

Parameters and Performance of Initial Configuration

	5-Panel Emergency	6-Panel Normal
Parameters		
Effective Height (h_0)	625 feet	625 feet
Static Capacitance (C_s)	0.1412 μf	0.1633 μf
Resonant Frequency (f_0)	33.05 kc	32.18 kc
Performance Characteristics		
Unloaded Bandwidth (bw_0)	32.7 cps	37.7 cps
Base Reactance (X_b)	-56.7 ohms	-48.3 ohms
Base Voltage (V_b)	144 kv	124 kv
Top Hat Voltage (V_t)	185 kv	161 kv
Base Current (I_0)	2559 amperes	2559 amperes
Radiation Resistance (R_0)	0.153 ohms	0.153 ohms

The reduction in capacitance from the 6-panel case may be seen from the data for the 6-panel operation which is also presented in Table 5-1. For 6-panel operation, the static capacitance is 0.1633 μf. The 5-panel situation would be expected to have more than 5/6 or 83.3

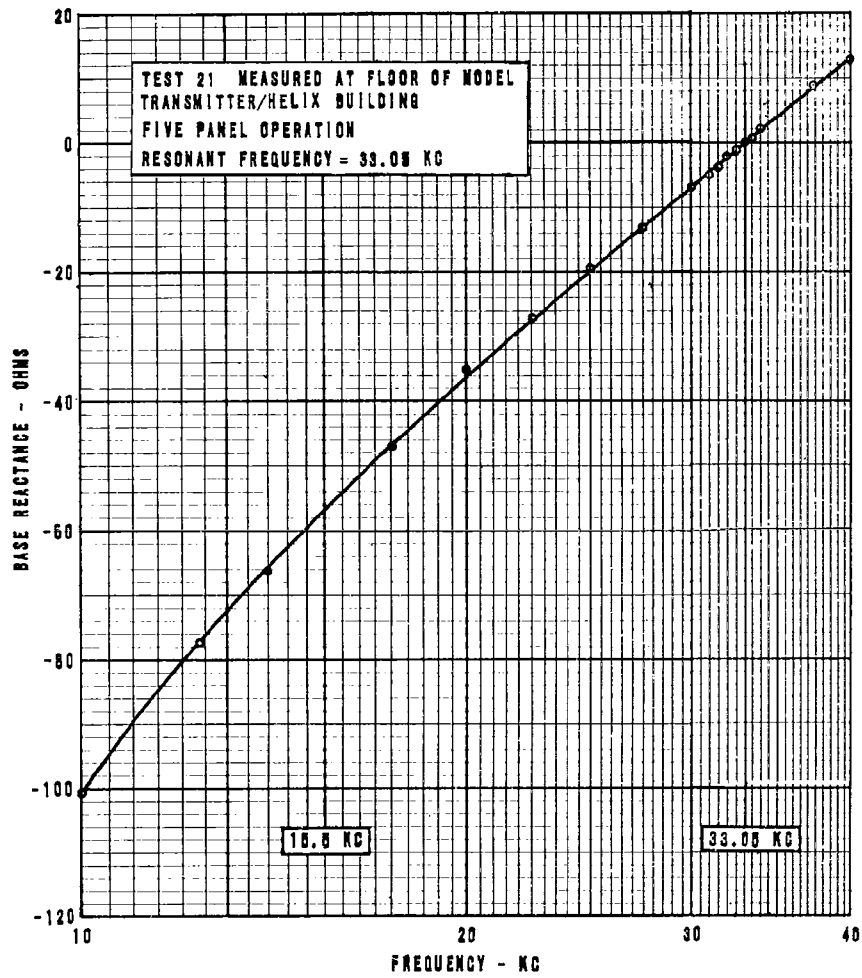

Figure 5-6 MEASURED BASE REACTANCE - 5-PANEL OPERATION

percent of the normal capacitance, since some fringing occurs into the area occupied by the missing panel. The actual 5-panel value is 86.5 percent of the normal capacitance. Reducing the antenna capacitance increases the top hat voltage (for equal radiated power) above the 161 kv design value. Also, the reduction in unloaded bandwidth is apparent. As shown by Table 5-1, the effective height is not affected by the removal of a panel.

5.2.2 Six-Panel (Normal) Performance

Following the 5-panel tests, the final panel was installed and all measurements repeated to establish the performance under a normal operating situation.

Basic full-scale parameters and derived operating characteristics for the 6-panel situation are shown in Table 5-1. Base-impedance data over the operating frequency range is shown in Figure 5.7, referred to the floor of the T/HB as before.

The resonant frequency shown in Table 5-1 does not include the expected reduction due to residual tuning/coupling inductance. For the estimated 10 percent reduction factor for this effect, the maximum expected operating frequency is approximately 28.96 kc, slightly above the 28.5 kc upper operating frequency established during the antenna selection study.

The 6-panel model data confirmed all design predictions for full-power performance and established the capabilities of the proposed radiator as a satisfactory approach. Although a wider margin in resonant frequency and bandwidth might have been desirable, these two factors are inversely related necessitating a rather critical compromise in this area.

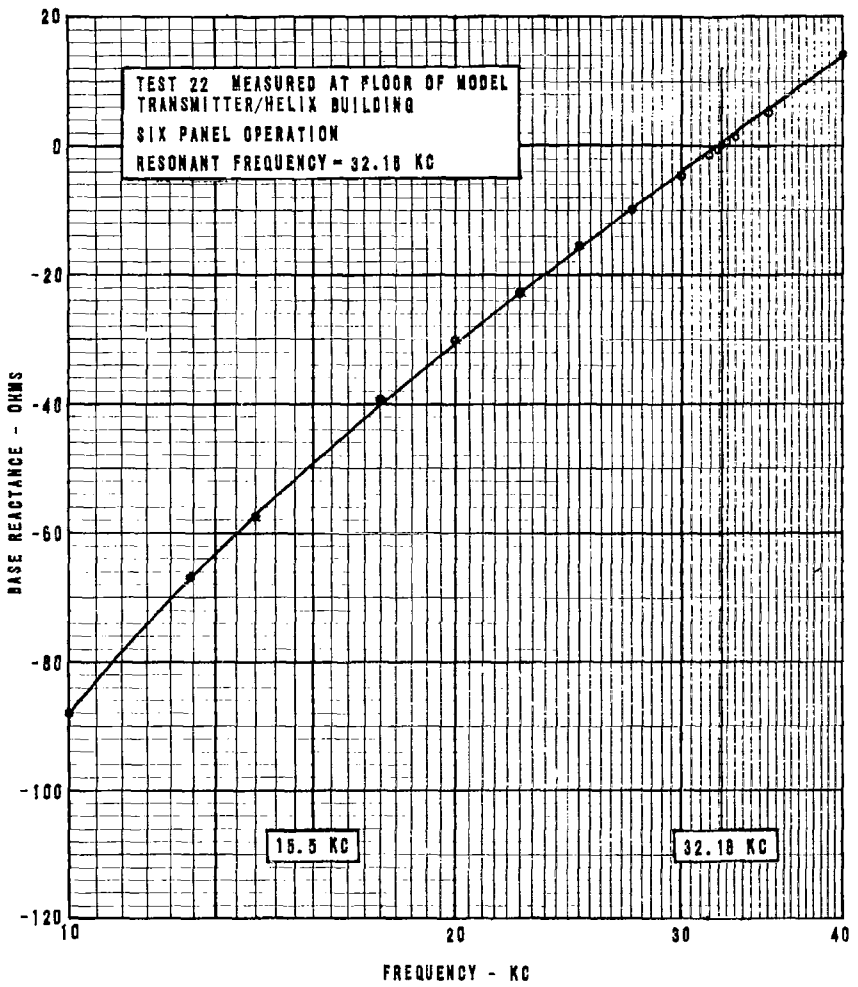

Figure 5-7 MEASURED BASE REACTANCE - 6-PANEL OPERATION

5.2.3 Gradient Distribution

The distribution of gradient on the antenna conductors was determined from current distribution studies performed on the model. Figure 5-8 shows the current distribution on the typical static panel under normal full-power operation (i.e., 1 megawatt radiated) at 15.5 kc as derived from model data. Details of this technique appear in Section 2.2.4, and the theoretical analysis in Appendix B. A photographic study of corona on the model under 60-cycle excitation appears in Appendix E.

Areas of maximum gradient can be determined from the data presented in Figure 5-8 for points along the conductors where the slope of the current as a function of distance along the wire is greatest. The maximum gradient occurs on the two innermost (Nos. 4 and 5) conductors just beyond (outer half) the cross-panel catenary, reaching a maximum value of 0.74 kv/mm, somewhat below the 0.8 kv/mm design limit. It should be noted that the outer two conductors on each panel half (Nos. 1 and 2, 7 and 8) are enlarged to 1-1/2 inch diameter in the region of the intermediate towers. This enlargement, from the 1-inch diameter figure for the bulk of the top hat, results in tolerable gradient levels which would otherwise be excessive. For example, the 1-1/2 inch outer conductor exhibits a maximum gradient of 0.62 kv/mm just beyond the cross-panel catenary, while a 1-inch diameter conductor in this area would operate at a gradient of 0.94 kv/mm for 1 megawatt radiated at 15.5 kc. This value exceeds the 0.8 kv/mm maximum acceptable value, thereby supporting the requirement for the larger diameter conductor in this area.

The discontinuity in the current distribution along each top hat conductor at the cross-panel catenary (as shown in Figure 5-8) results from the diversion of the current from the conductors out along the catenary. Since the catenary is of considerably larger diameter (2-3/16 inch)

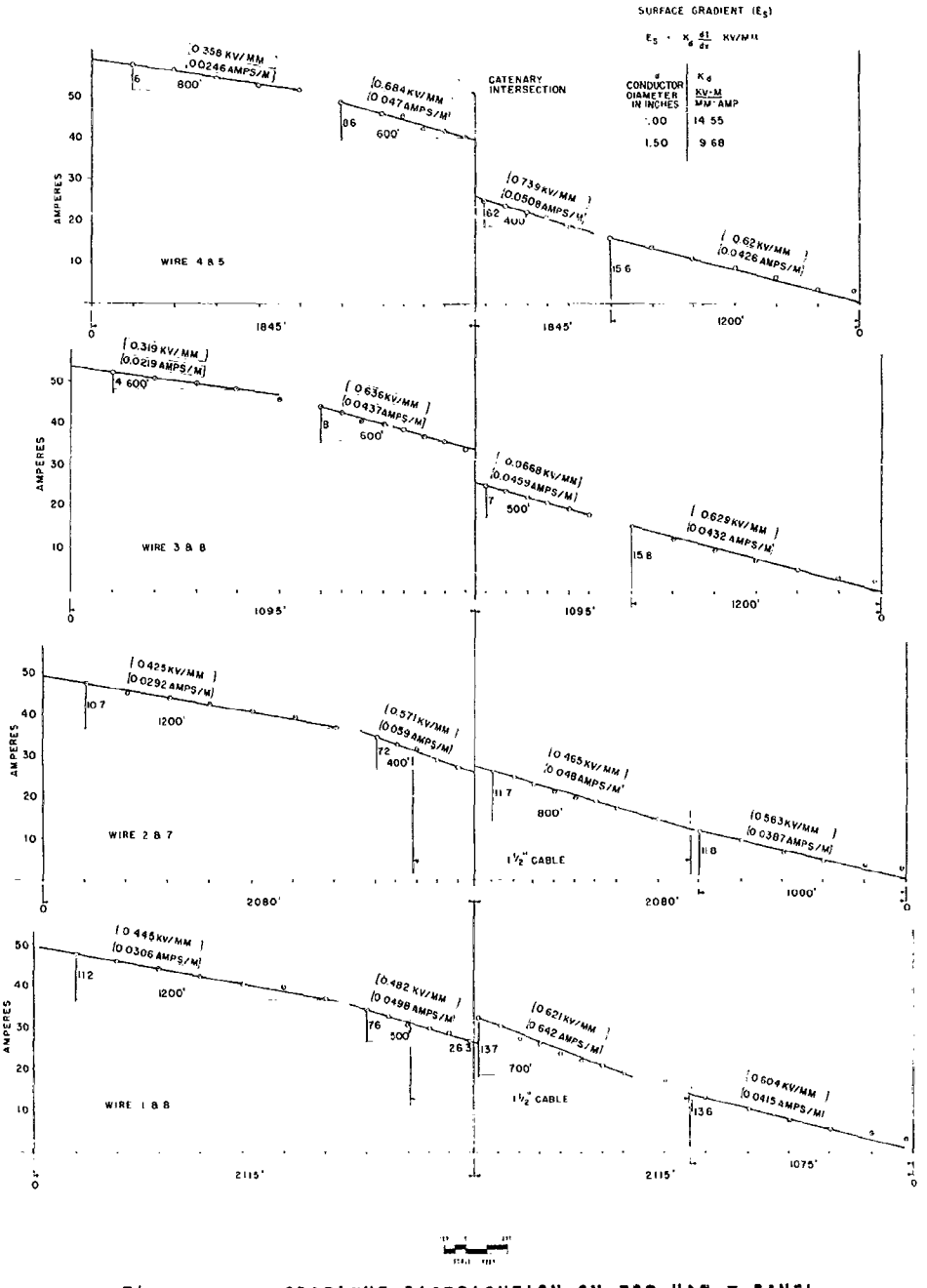

Figure 5-8 GRADIENT DISTRIBUTION ON TOP HAT I PANEL

than the other conductors, it provides a greater area from which displacement current flows to ground. Because of its large diameter, gradients along its surface are even lower than on the rest of the top hat. For this reason, a detailed gradient study of this cable was not considered necessary.

Gradient data obtained for the 8-wire fan downleads is shown in Figure 5-9. This data was obtained in the same manner as that obtained on the top hat. Except at the lower elevations, the gradient on the downlead conductors is lower than on the top hat. While measurement accuracy in the lower portion of the fan is rather poor, some relatively high gradient areas are indicated near the hinge point. However, these are not expected to lead to corona problems since additional shielding will be provided at the hinge (in the form of corona rings) which tends to reduce conductor gradients on the fan.

5.3 Development of Final Configuration

5.3.1 Revised Transmitter/Helix Building

Several changes made in the T/HB warranted model verification. Requirements for increased equipment space resulted in a general enlargement of the building. The internal features of the tuning/coupling portion of the building (as shown in Figure 5-10) were developed and modeled for operation at 28.5 kc. Provisions were made in the model for measuring antenna characteristics through the appropriate circuitry, as well as through a short vertical lead as in the previous tests. A further provision was made to allow measurements to be made directly at the common feed point below the entrance bushings.

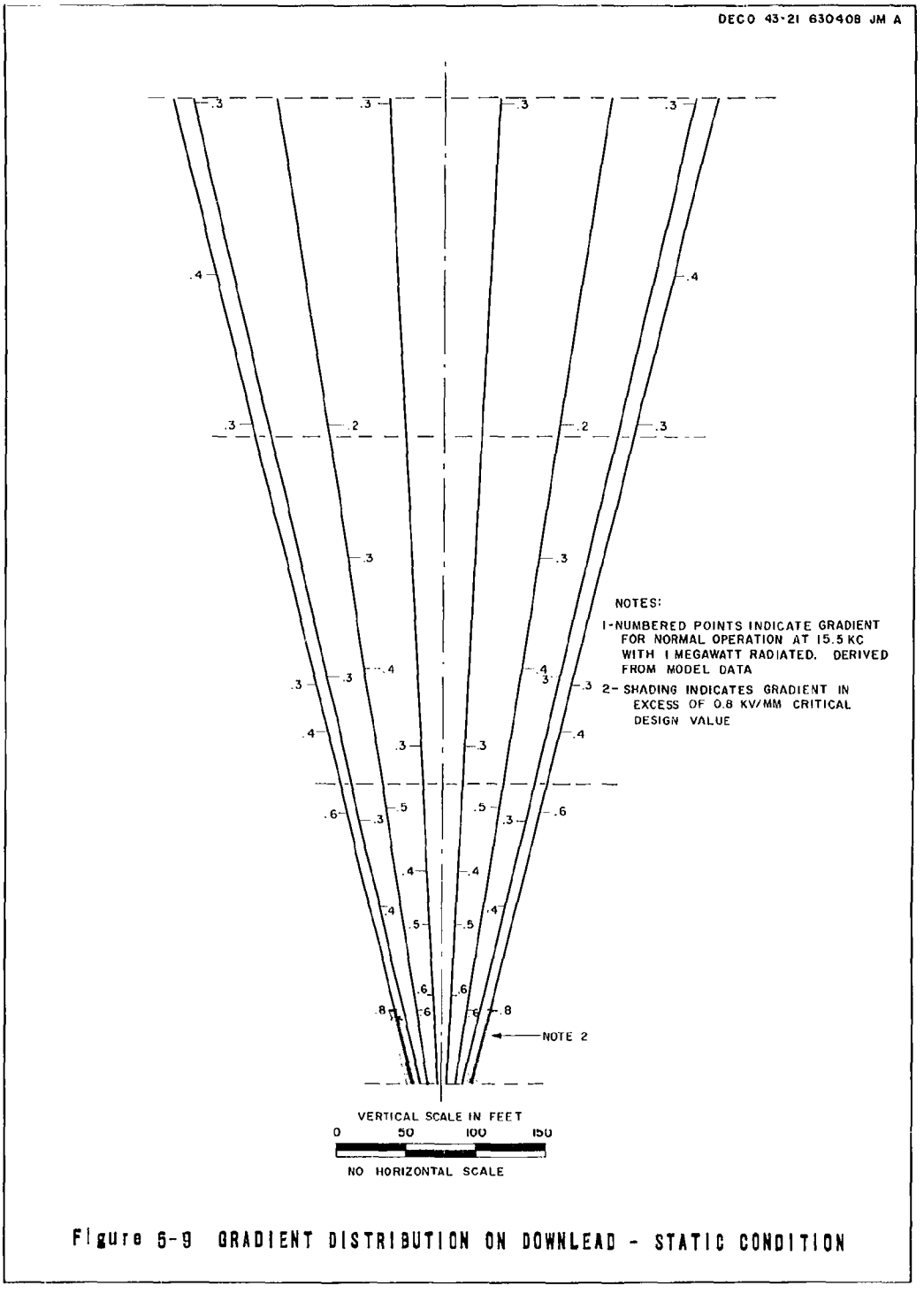

Figure 5-9 GRADIENT DISTRIBUTION ON DOWNLEAD - STATIC CONDITION

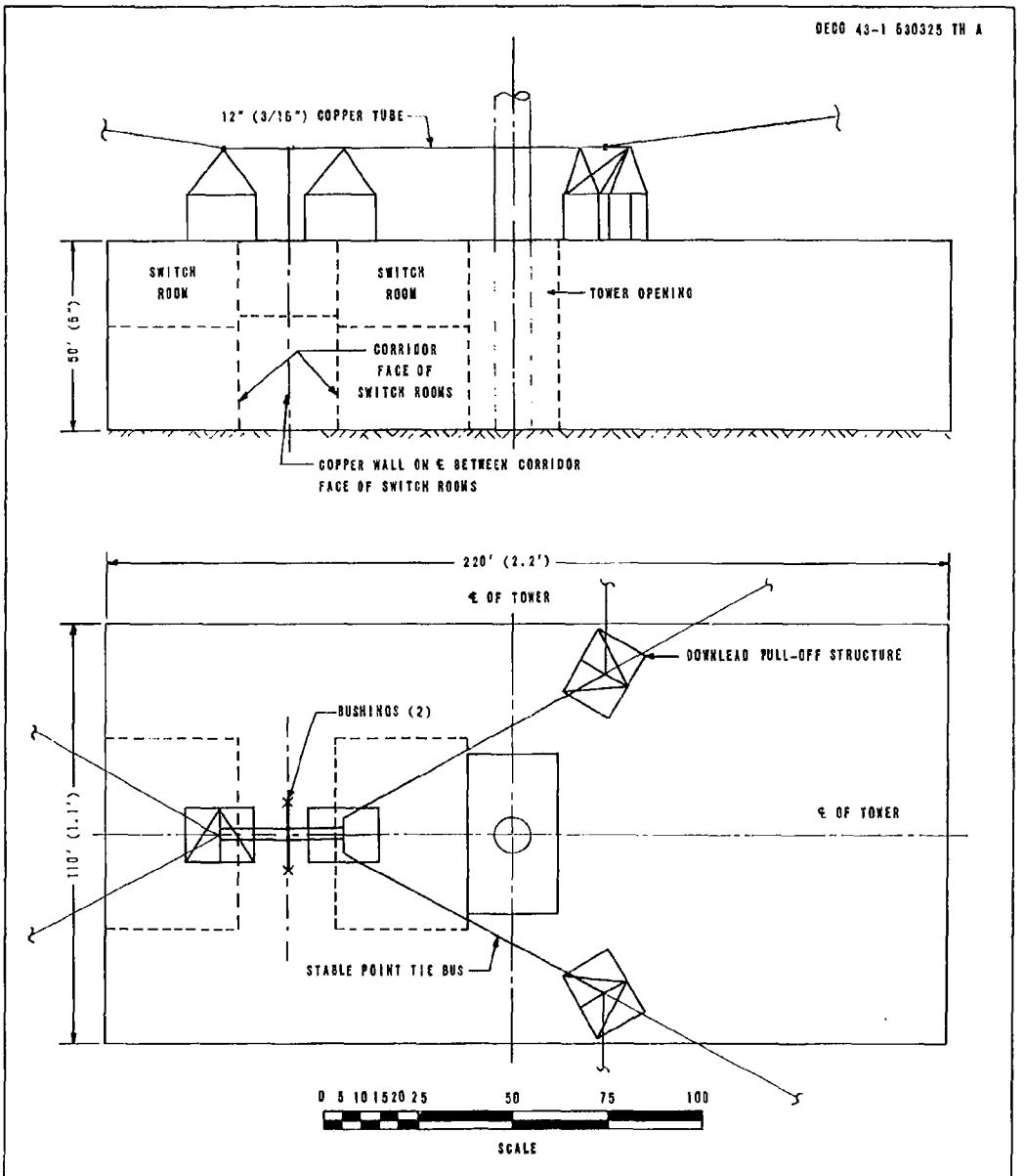

Figure 5-10 REVISED TRANSMITTER/HELIX BUILDING

Dual Entrance Bushings

As part of the revision of the T/HB dual entrance bushings replaced the single bushing originally modeled. This change reflected the need for higher current-carrying capability and for higher reliability than could be obtained with a single bushing. Along with this change, a rearrangement in the downlead buswork on the T/HB roof was required. Figure 5-10 also shows the revised bus configuration over the roof area. Some minor reduction of series inductance was expected as a result of the change.

Six-Panel Performance (Top Hat I)

For the enlarged T/HB with dual bushings, the basic antenna parameters determined at the floor of the building through a simulated 10-inch vertical bus to the common feed point were: effective height, 623 feet; static capacitance, 0.1634 μf; and resonant frequency, 32.25 kc. Aside from a very minor reduction in effective height and a similar increase in resonant frequency, practically no change resulted in basic antenna characteristics.

Base reactance data measured at both the floor terminal of the model and the common point below the bushings is shown in Figure 5-11. The floor terminal measurements reflect the insertion of a small inductance attributed to the connecting lead. The normal measuring point throughout the model study was at the T/HB floor terminal. This point was selected for convenience and also for repeatability because of a somewhat better connector configuration. The measurements at the common point near the bushings required a short flexible lead whose position was only approximately repeatable. However, from measurements at both inputs the approximate effect of a short section of "bus"

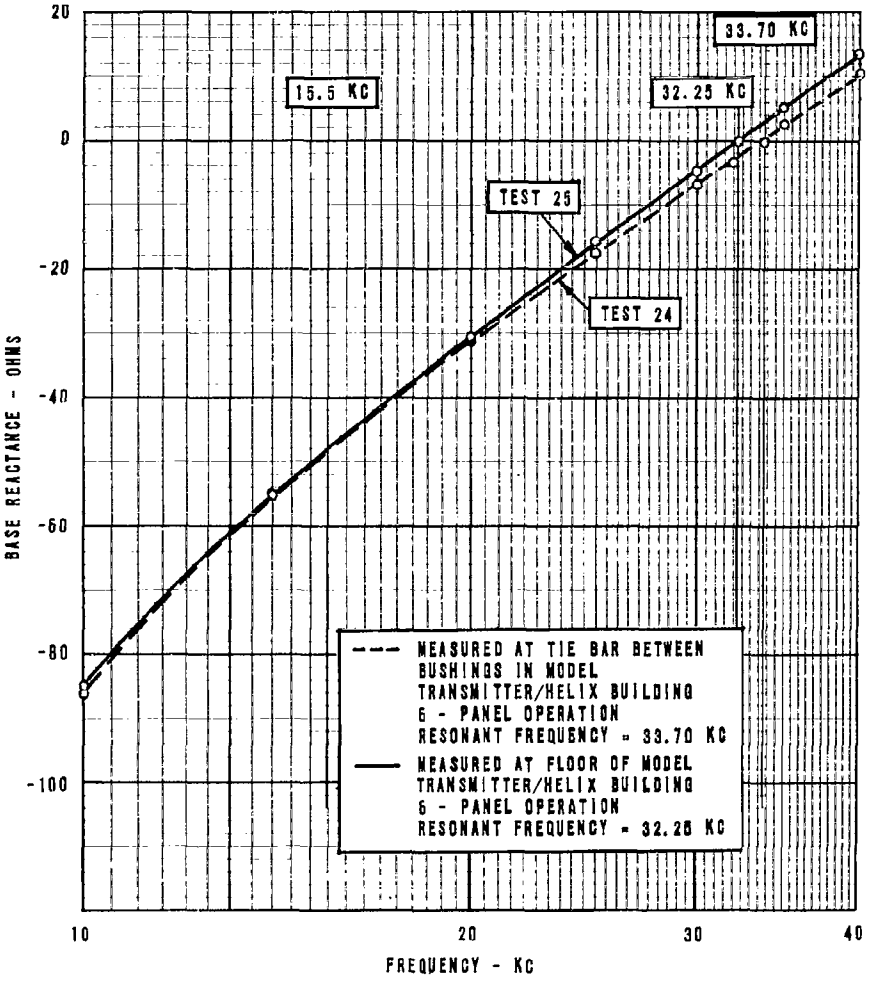

Figure 5-11 MEASURED BASE REACTANCE AT TWO REFERENCE POINTS

was determined. Since the residual inductance in the tuning/coupling circuitry at the high end of the frequency range is a determining factor in the critical area of maximum operating frequency, it is necessary to consider all reactance data referred to the appropriate terminals.

Effect of Tuning/Coupling Circuitry on Resonance

The approximate configuration of the tuning/coupling component arrangement and appropriate values for the upper end of the frequency range were modeled as shown in Figures 5-12 and 5-13. Figure 5-14 shows the measured input reactance through the tuning/coupling circuitry in the frequency range near resonance. The maximum operating or self-resonant frequency is seen to be 29.6 kc. This value is about 4 percent above the minimum acceptable value (28.5 kc) previously established.

5.3.2 Revised Top Hat Shape

A structural analysis of stresses in the top hat conductors under conditions of maximum wind loading showed that the proposed Top Hat I design did not have acceptable safety-factor margins. The ultimate yield of the ACSR cables was degraded by the aluminum outer layer to such a point that their use was precluded. Therefore, a new top hat design (Top Hat II) utilizing only aluminum-clad conductors was developed to maintain acceptable structural safety-factor margins during periods of maximum wind loading.

Increased Top Hat Sag

Top Hat II, composed entirely of aluminum-clad steel conductors has greater sag and, for the same tower heights, a lower average physical height than Top Hat I. Specifically, Top Hat II (as shown in Figure 5-15) has an average height of 891 feet as compared to 900 feet for Top

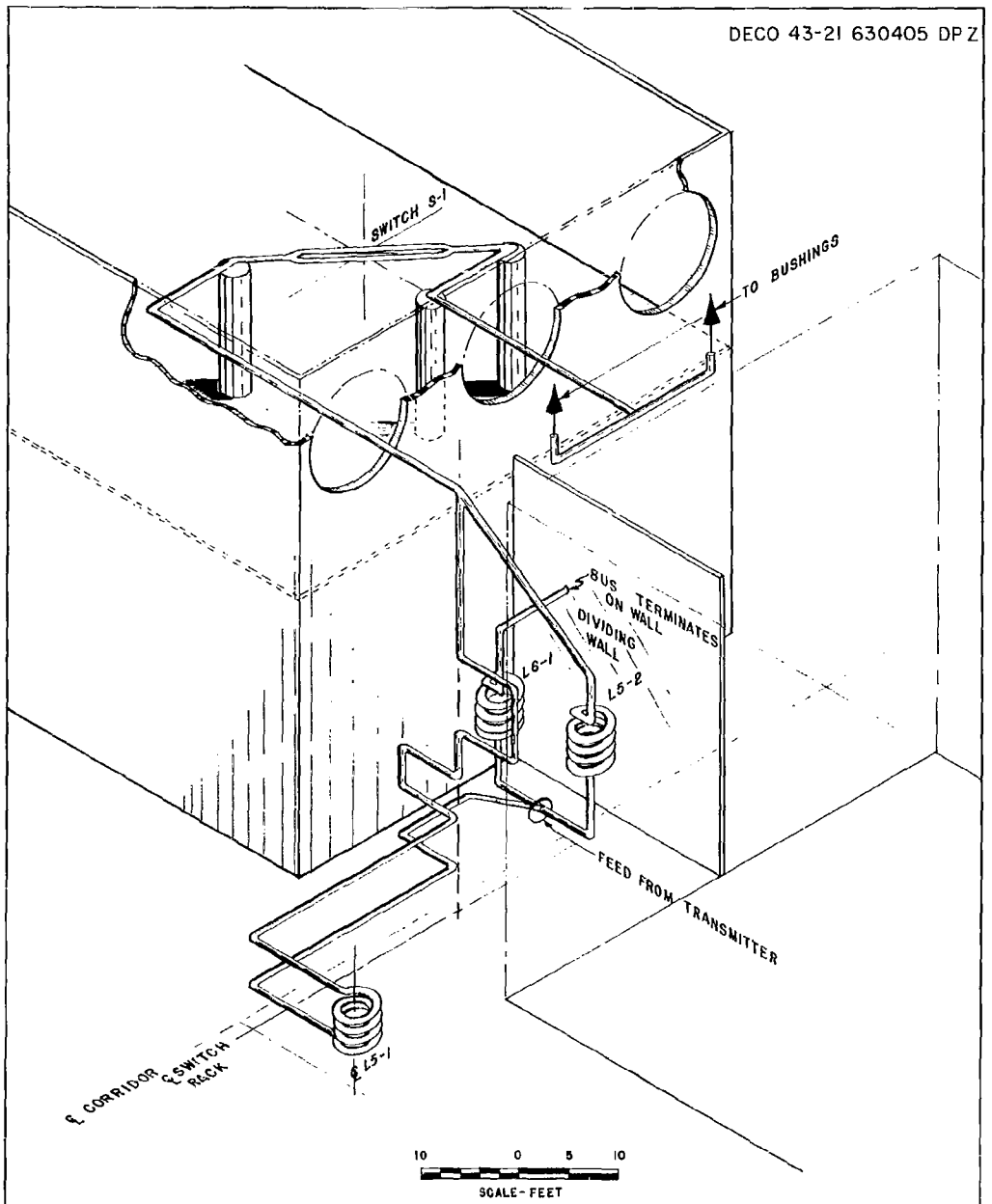

Figure 5-12 PICTORIAL SCHEMATIC OF MODELED TUNING/COUPLING CIRCUITRY AT 28.5 KC

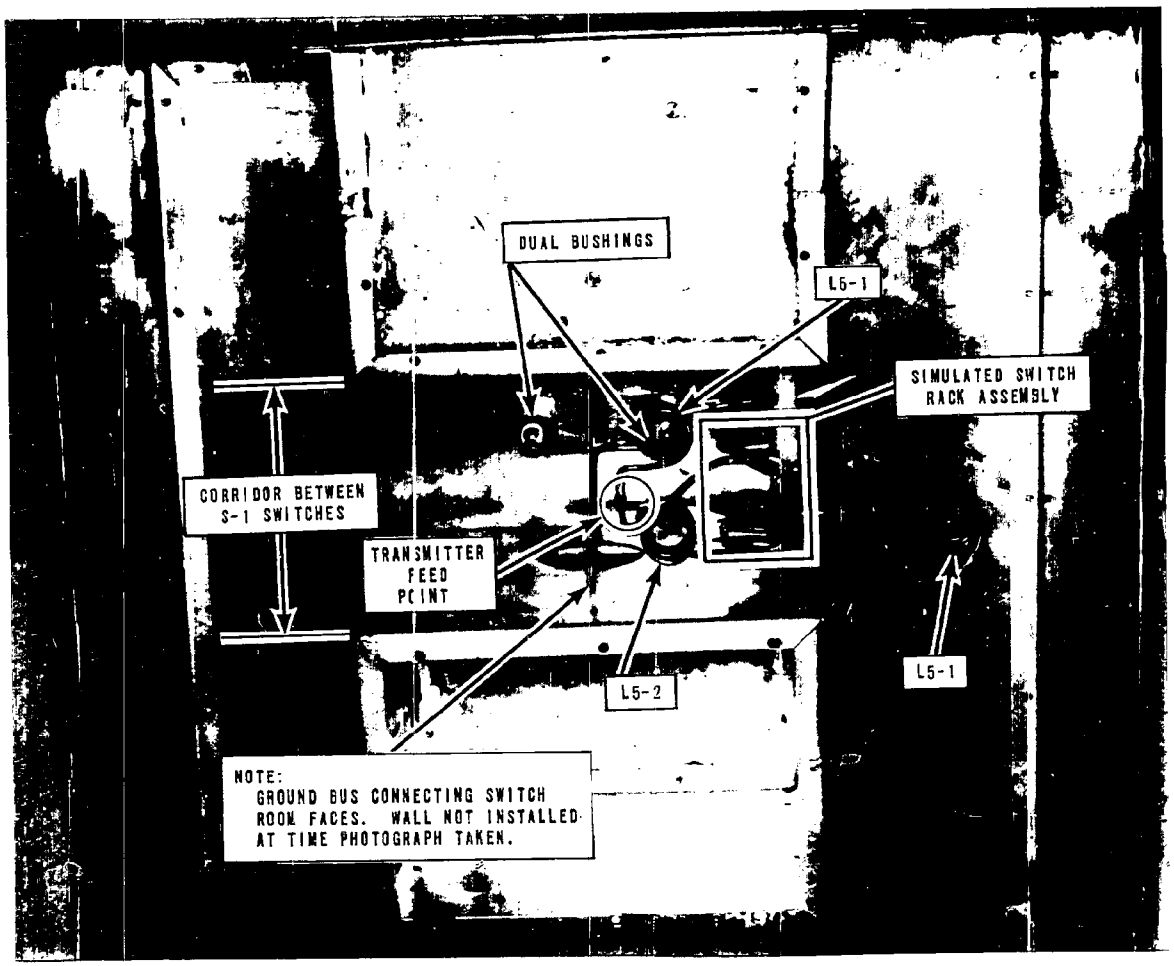

Figure 5-13 PHOTOGRAPH OF MODELED TUNING/COUPLING CIRCUITRY VIEWED FROM BENEATH T/HB

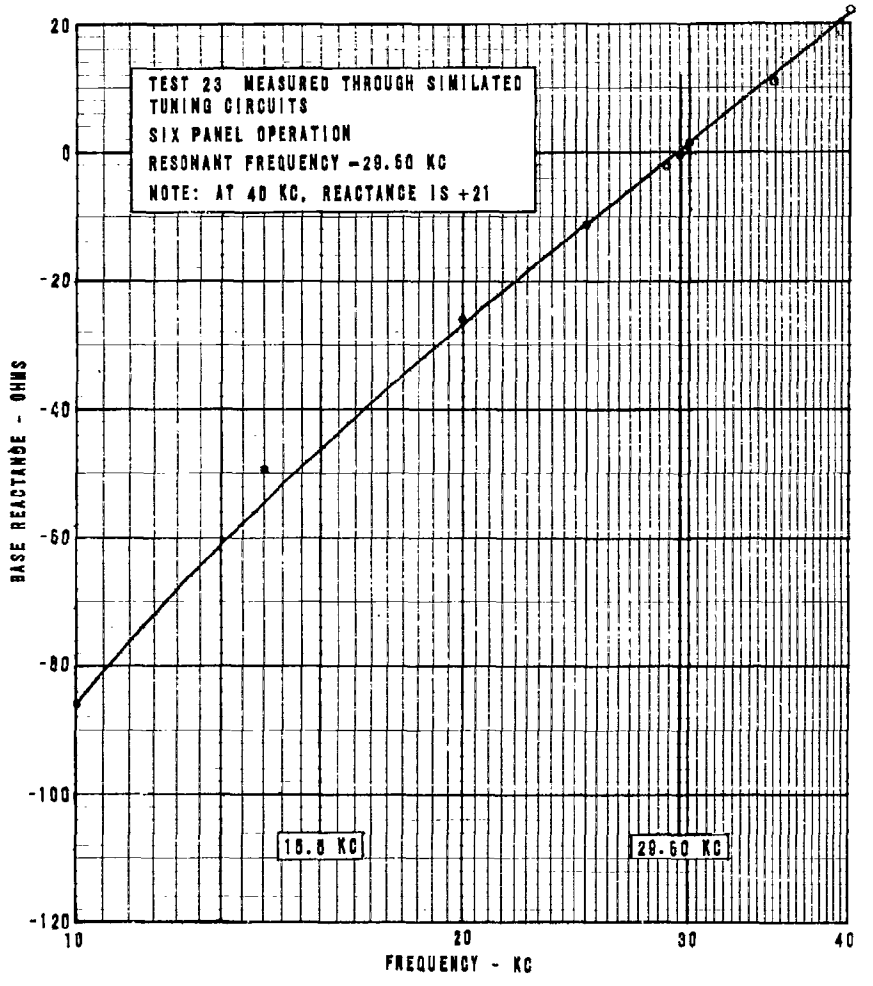

Figure 5-14 MEASURED BASE REACTANCE INCLUDING TUNING/COUPLING CIRCUITRY

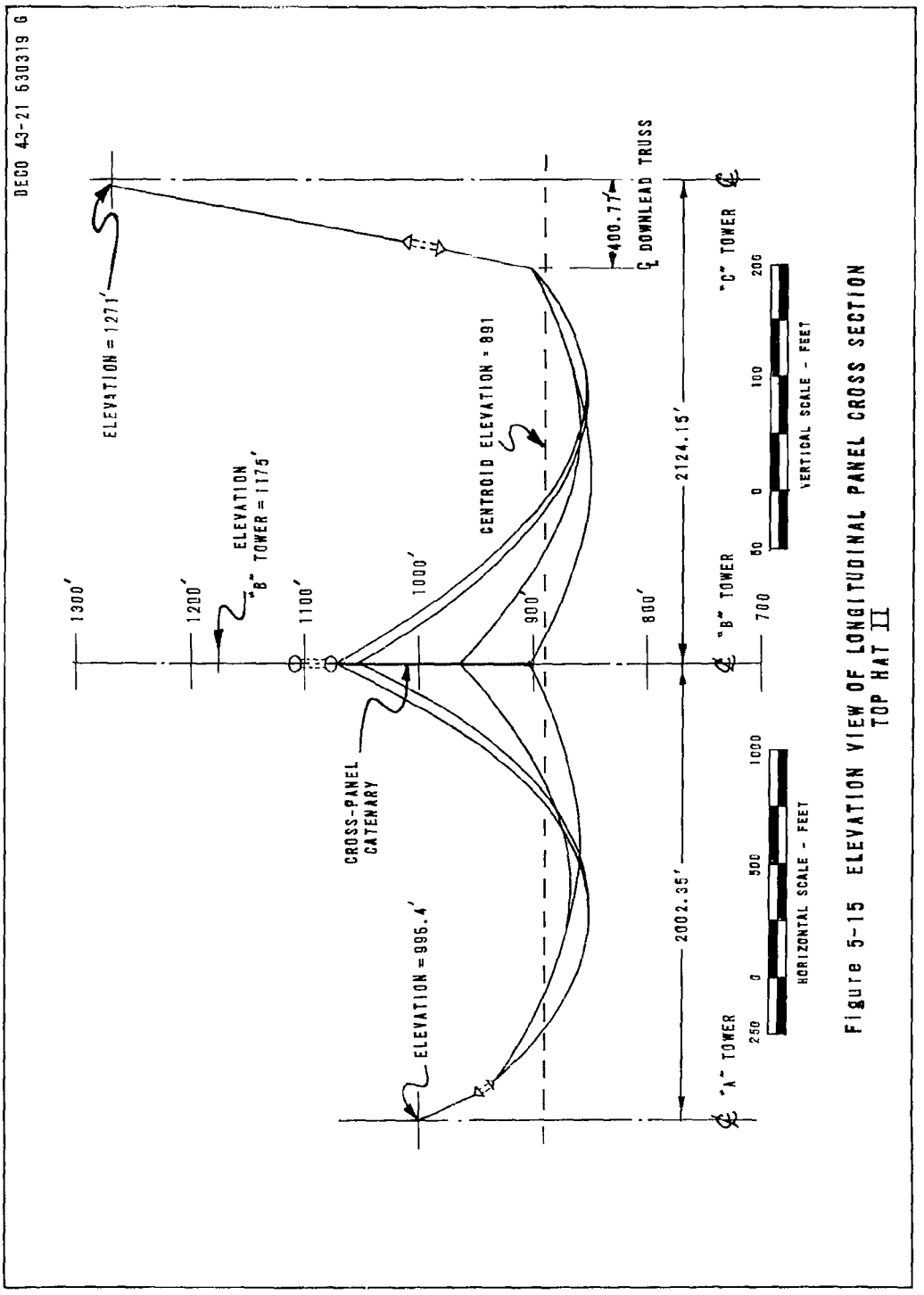

Figure 5-15 ELEVATION VIEW OF LONGITUDINAL PANEL CROSS SECTION TOP HAT II

Hat I. To determine the extent of degradation resulting from this loss in average height, the Top Hat II configuration was modeled with the two-point sag approximation shown in Figure 5-16. This required an entirely new set of model top hat panels since the revised design employs longer conductors and increased sags.

Six Panel Performance (Top Hat II)

The reduction in average physical height of the top loading was expected to produce a corresponding reduction in effective height. Basic full-scale antenna parameters measured at the normal T/HB floor were determined from the model (Test 26, Appendix A). These parameters were: effective height, 610 feet; static capacitance, 0.1642 μf; and resonant frequency, 32.45 kc.

Comparing the effective height of Top Hat II (Test 26) to that of Top Hat I (Test 25) shows a reduction of 13 feet, i.e., somewhat greater than but comparable to, the 9 foot reduction in average physical height. The indication from this comparison is that with the increased sag, the average height should be elevated at least to the previous 900 feet to achieve the same value of effective height. Since the descrepancy of 4 feet between the variation of effective height and average physical height is well within the ±2 percent predicted test accuracy, no further compensation is justified. For small changes in the "B" tower elevations, it can be shown that the average height changes by one-half the increment of change. On this basis, a recommendation was made to elevate the "B" towers 20 feet to compensate for increase sag.

Three tests were run with the Top Hat II in position. Test 26 relates to the basic antenna viewed through the normal T/HB terminals. Test 27 relates to data derived from measurements made at the common

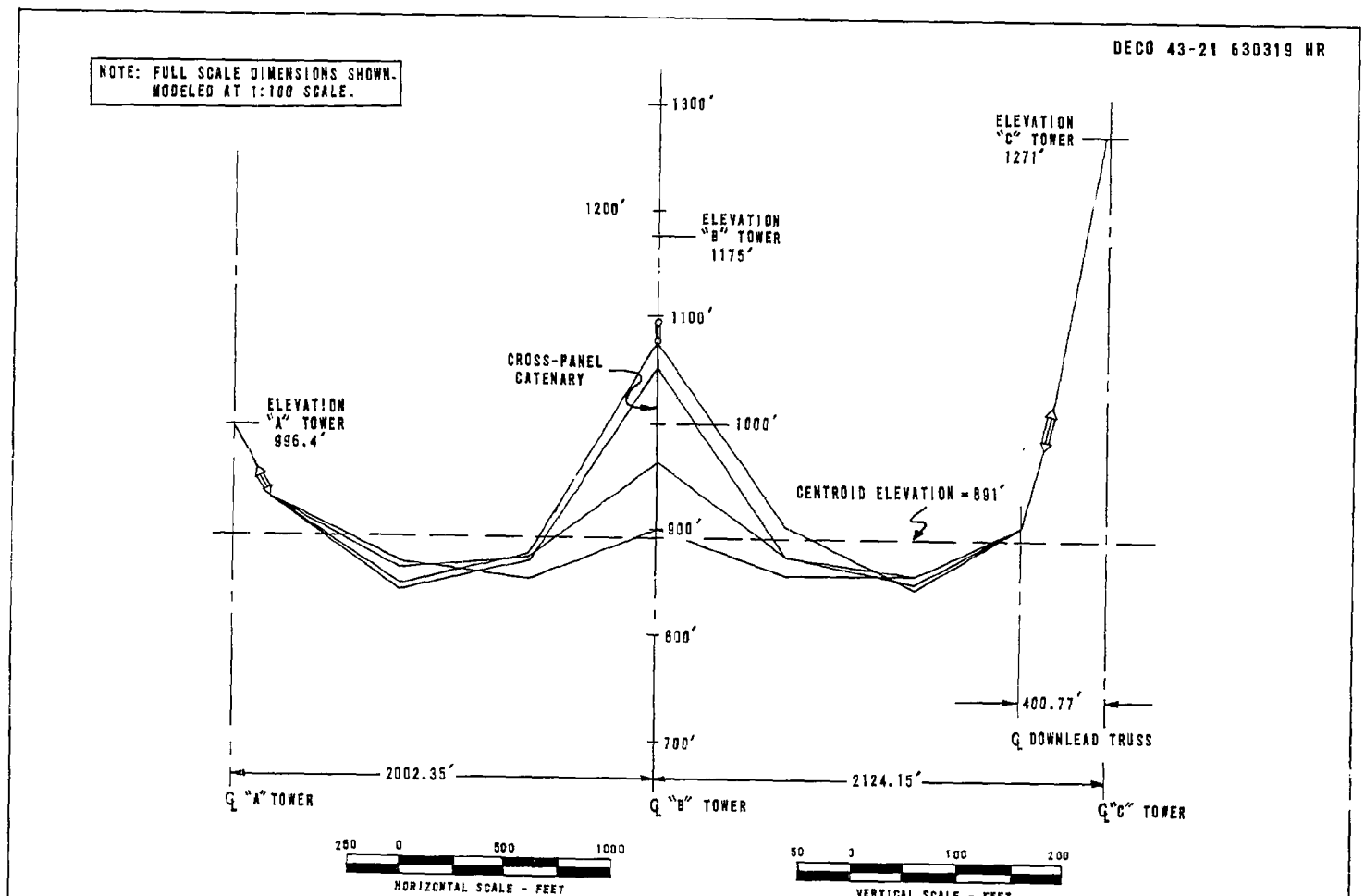

Figure 5-15 ELEVATION VIEW OF LONGITUDINAL PANEL CROSS SECTION AS MODELED - TOP HAT II

lead point near the entrance bushings (i.e., excluding the roof-to-floor bus inductance). Test 28 defines the maximum operating frequency to be 29.43 kc including the effect of the tuning/coupling circuitry (see Appendix A).

5.3.3 Revised Tower Heights

"B" Tower Compensation

To restore antenna performance (particularly effective height) to values achieved prior to the increased sag of Top Hat II, the elevation of the intermediate "B" towers was increased by 20 feet to 1195 feet. This brought the average top hat elevation to approximately 901 feet, or 1 foot above the Top Hat I value. Although the top hat sags and conductor lengths remained virtually unchanged for this small variation in the "B" tower elevations, the revised configuration is referred to as Top Hat III for reference. Figure 5-17 shows a longitudinal panel cross section of Top Hat III in elevation. The modeled version of this design is shown in Figure 5-18. For modeling purposes, the top hat panels used were identical to those of Top Hat II.

For the revised top hat with the recommended 20-foot "B" tower compensation, the basic antenna parameters measured at the T/HB floor were: effective height, 629 feet; static capacitance, 0.1633 μf; and resonant frequency, 32.45 kc.

Comparing these values with those obtained with Top Hat I (which involved only one bushing), it is apparent that the compensation for increased sag was sufficient to restore, or slightly increase, the effective height while the static capacitance remained the same. Some minor reduction of series inductance through two bushings instead of one apparently accounts for a slight increase in the resonant frequency from 32.18 kc to the 32.45 kc value shown above.

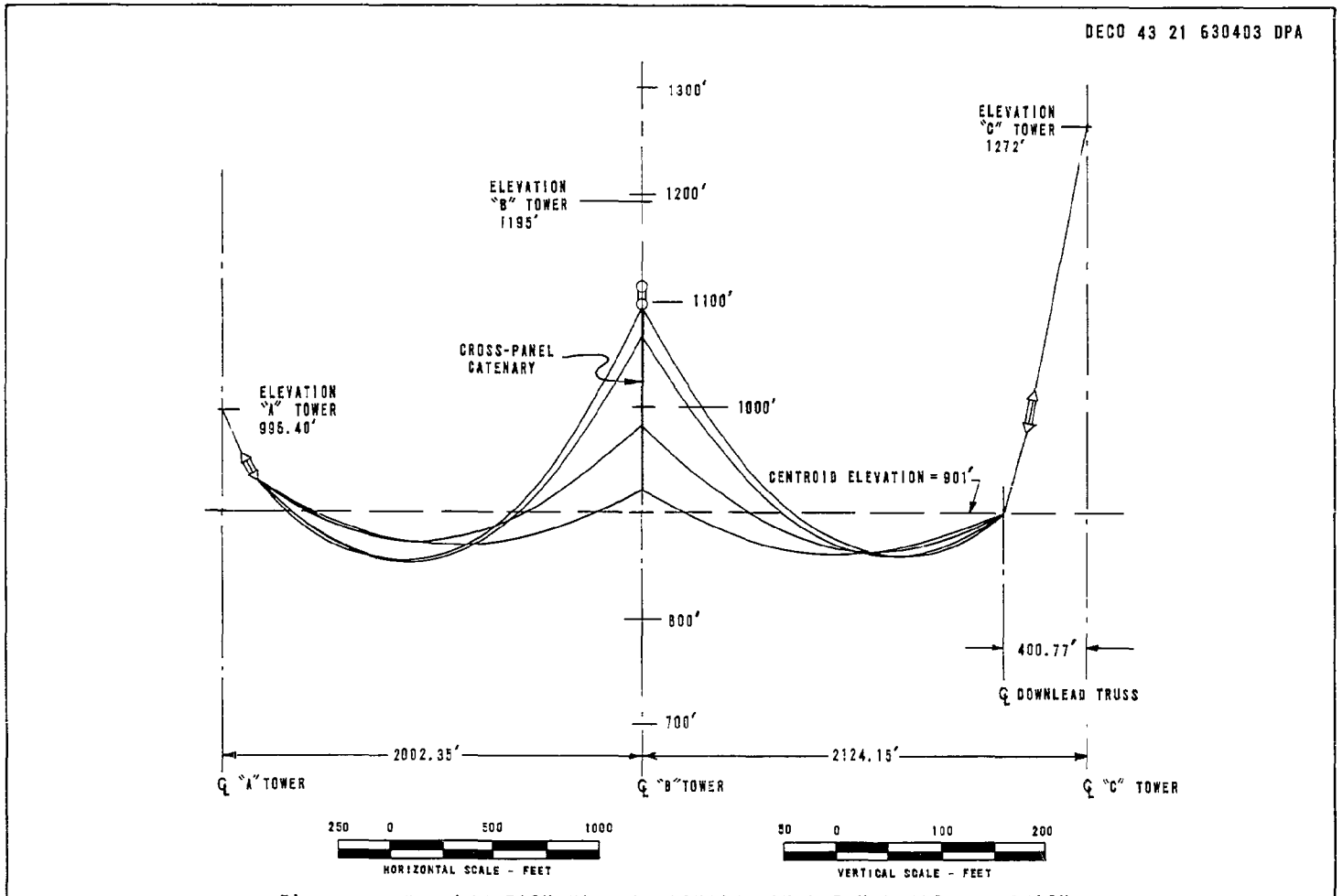

Figure 5-17 ELEVATION VIEW OF LONGITUDINAL PANEL CROSS SECTION TOP HAT III

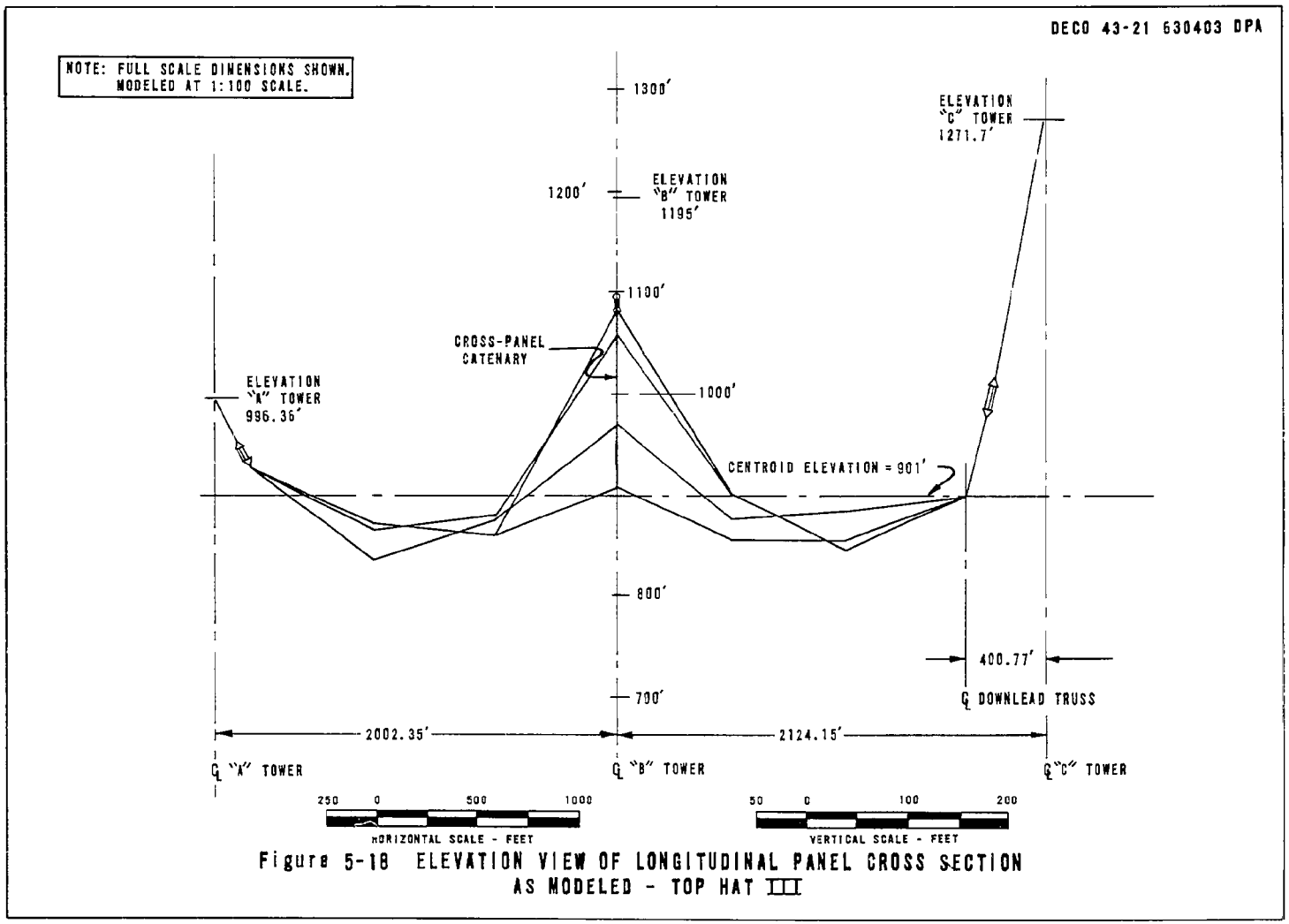

Figure 5-18 ELEVATION VIEW OF LONGITUDINAL PANEL CROSS SECTION AS MODELED - TOP HAT III

Figure 5-19 shows the input reactance measured at both the T/HB terminal (Test 31) and at the common point below the dual bushings (Test 30). Comparing the two sets of data shows that the difference can be described by a series inductance of approximately 14.3 μh (full scale value). Using this value, it is possible to refer all reactance data from the floor terminal to the common point.

The maximum operating frequency was determined for the Top Hat III configuration in Test 29. With the modeled tuning/coupling circuitry at the upper portion of the frequency range, the system resonant frequency was reduced to 29.45 kc, only 0.5 percent below the value achieved with the initial configuration (Top Hat I).

5.3.4 Wind Distortion Study

To establish the performance reliability of the antenna to perform under extreme wind distortion, a model study was made for the distorted configuration. For design purposes a maximum wind of 130 mph velocity (at 30-foot elevation) was established. Computations were carried out for various wind directions with respect to a typical panel, and conductor positions were established. The particular wind orientation chosen for the model study was one in which two panels were subjected to a direct cross wind as shown in Figure 5-20. Although the choice of this case was aribtrary, it was felt that it represented an extreme distortion and, as such, was likely to indicate the extreme degradation of electrical characteristics.

From the computed positions of the top hat conductors (Top Hat III), large-scale plan and elevation drawings were made of each conductor span. On these drawings a two-point approximation was constructed to simulate the distorted condition. Each half panel was intersected by two "distortion planes", the intersection of each individual

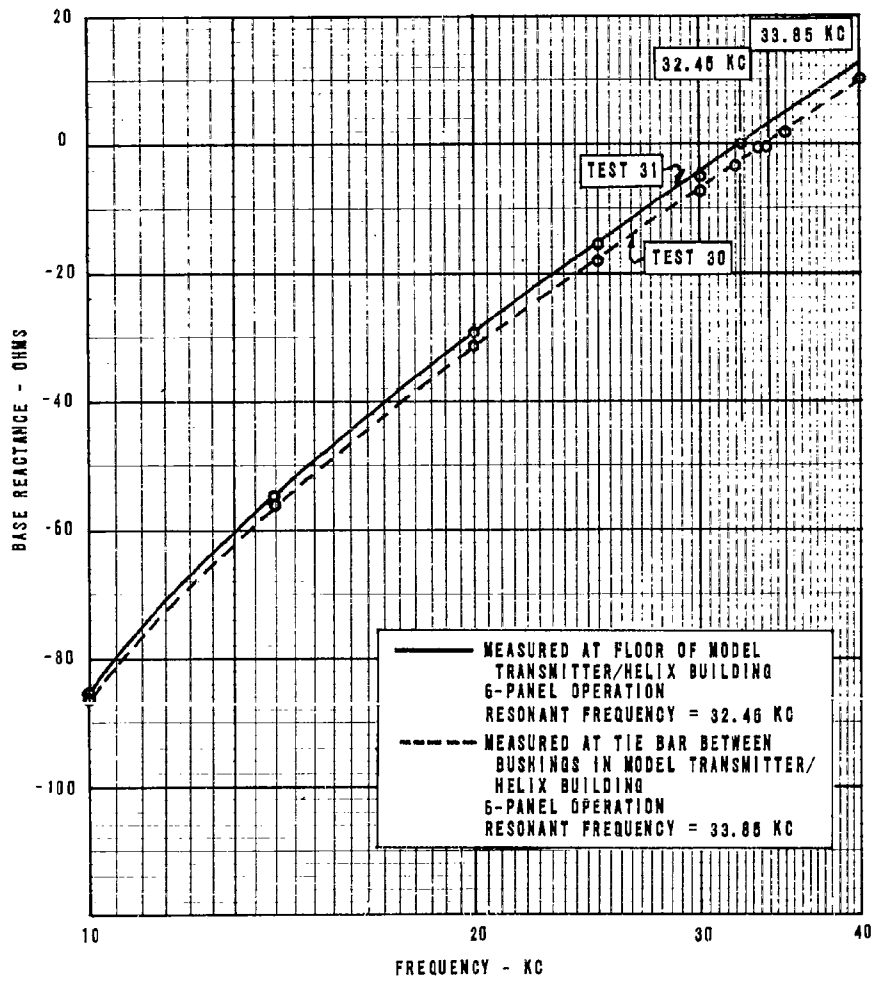

Figure 5-19 MEASURED BASE REACTANCE AT TWO REFERENCE POINTS

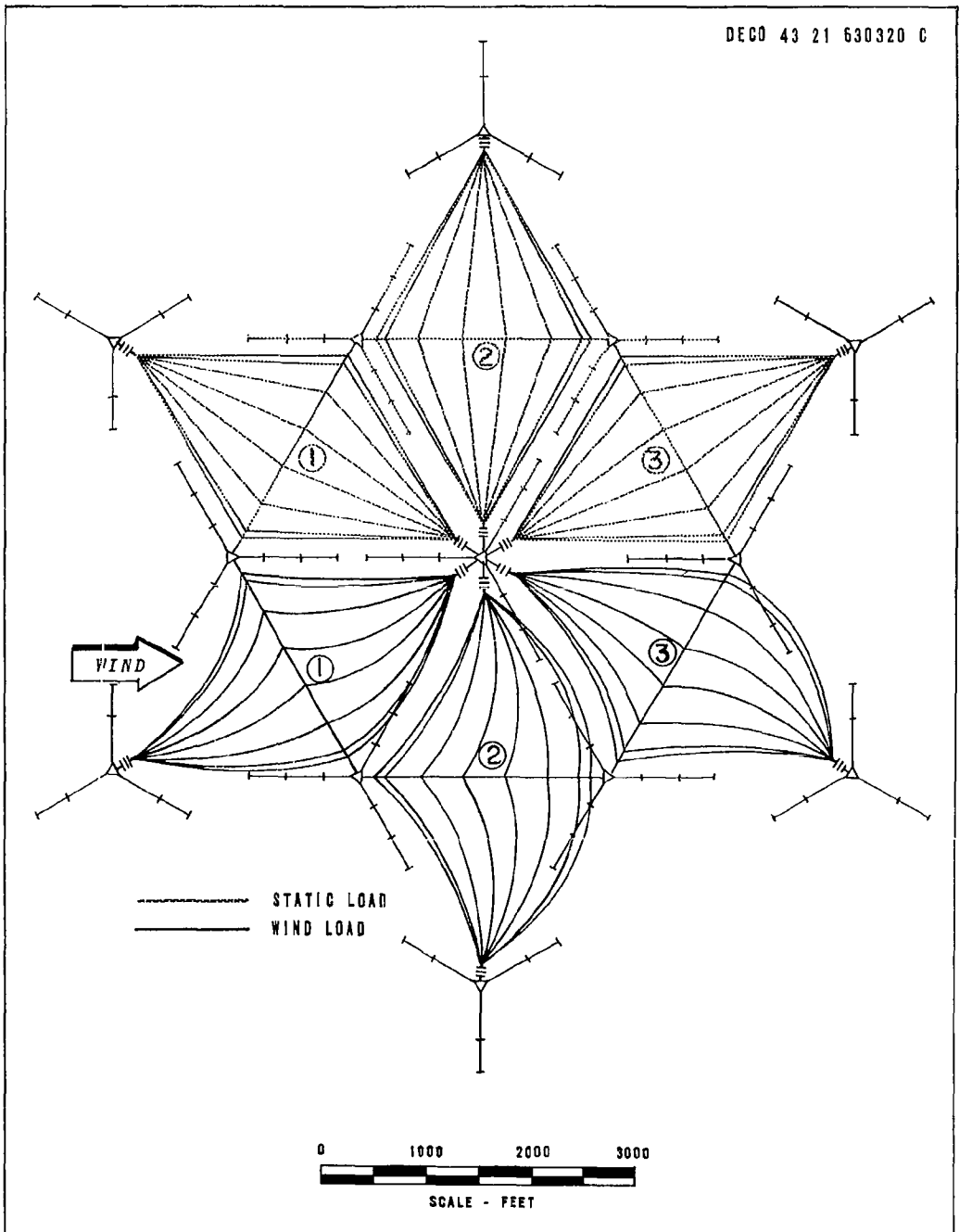

Figure 5-20 PLAN VIEW OF ANTENNA UNDER MAXIMUM WIND DISTORTION

conductor with the distortion planes being derived from the drawings. Poles were then rigged on both sides of each panel in the distortion planes to support nylon lines constraining the model conductors in their proper positions.

Figures 5-21, 5-22, and 5-23 show the three wind attack angles. The plan position and elevation of each control point determines the top hat shape.

As the top hat is lifted and displaced, the associated downleads are similarly distorted. Figures 5-24, 5-25, and 5-26 show the various downlead positions used on the model to simulate maximum wind (130 mph). It was observed that of the three representative downleads, only the No. 2 fan approaches the center tower guys. Consequently, it was expected and confirmed by measurement that the critical area of corona formation occurred at the point where the No. 2 fan is displaced into close proximity with the top two guy levels (See Figure E-3 , Appendix E). Detailed structural analysis revealed a similar deflection of the offending guys in the direction of the wind which tended to alleviate the problem. However, it was found necessary to study the effect of providing additional fan-guy separation appropriate to lower wind velocities.

Six-Panel Performance

After all positioning poles were erected for the distortion rigging, but before the model was actually distorted, the basic antenna properties were measured to establish the effect, if any, of the 36 holes and numerous nylon lines. Although considerable care was taken in preparing the wooden poles by drying and shellacing, it was expected that some minor effect would probably result. In general, the effect can be explained by

MODEL ELEVATIONS IN FEET			
POINT	ELEVATION	POINT	ELEVATION
1	9.69	23	10.29
2	9.45	24	11.11
3	9.51	25	11.30
4	9.39	26	10.56
5	9.19	27	10.27
6	9.32	28	9.90
7	9.61	29	9.14
8	9.87	30	8.93
9	9.90	31	9.19
10	10.44	32	9.83
11	10.33	33	10.03
12	9.81	34	9.71
13	9.22	35	9.62
14	8.98	36	9.27
15	9.37	37	9.17
16	9.76	38	9.27
17	9.77	39	9.83
18	10.82	40	9.95
19	9.57	41	10.17
20	9.61	42	—
21	9.14	43	10.06
22	9.47		

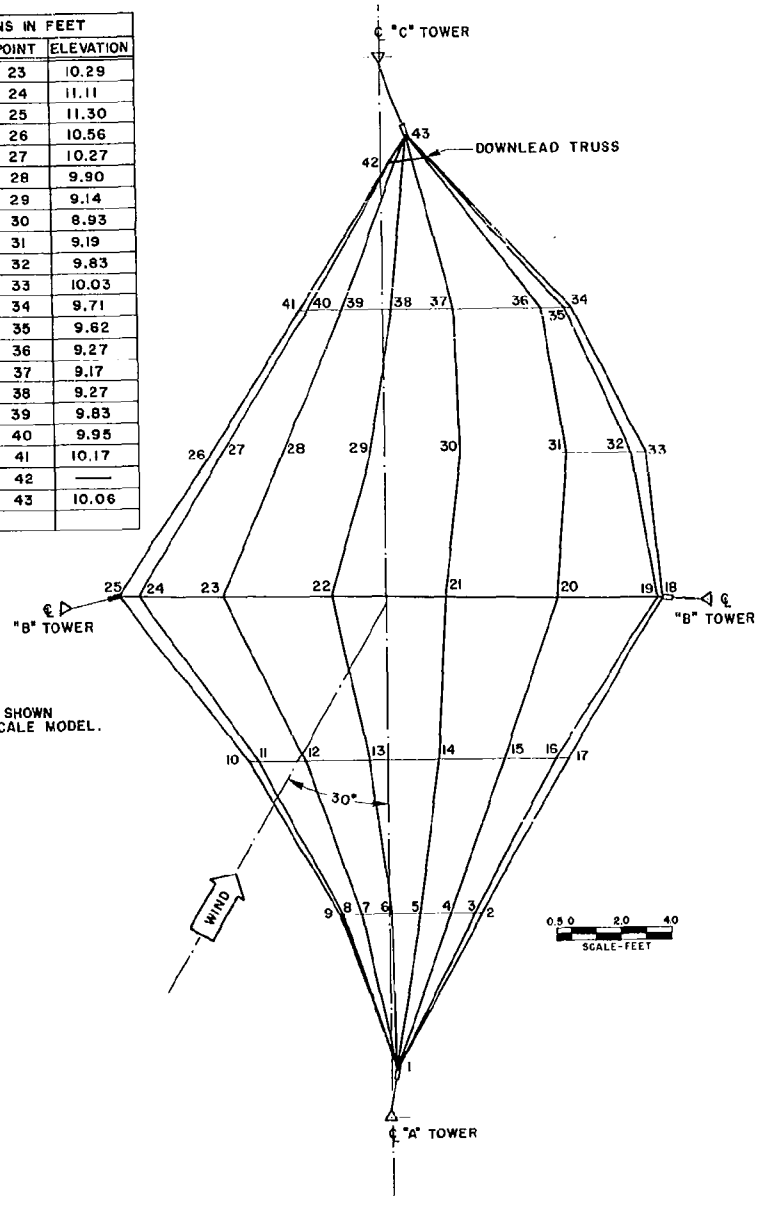

NOTE: DIMENSIONS SHOWN APPLY TO SCALE MODEL.

Figure 5-21 PLAN VIEW OF PANEL 1 UNDER MAXIMUM WIND DISTORTION

MODEL ELEVATIONS IN FEET			
POINT	ELEVATION	POINT	ELEVATION
1	9.72	23	10.73
2	9.52	24	11.34
3	9.45	25	11.47
4	9.34	26	10.98
5	9.39	27	10.91
6	9.60	28	10.55
7	9.85	29	10.04
8	9.97	30	9.75
9	9.99	31	9.74
10	10.56	32	9.99
11	10.50	33	10.08
12	10.18	34	10.18
13	9.71	35	10.15
14	9.35	36	10.11
15	9.35	37	10.15
16	9.68	38	10.34
17	9.82	39	10.59
18	10.60	40	10.77
19	10.35	41	10.80
20	9.74	42	—
21	9.59	43	10.90
22	10.03		

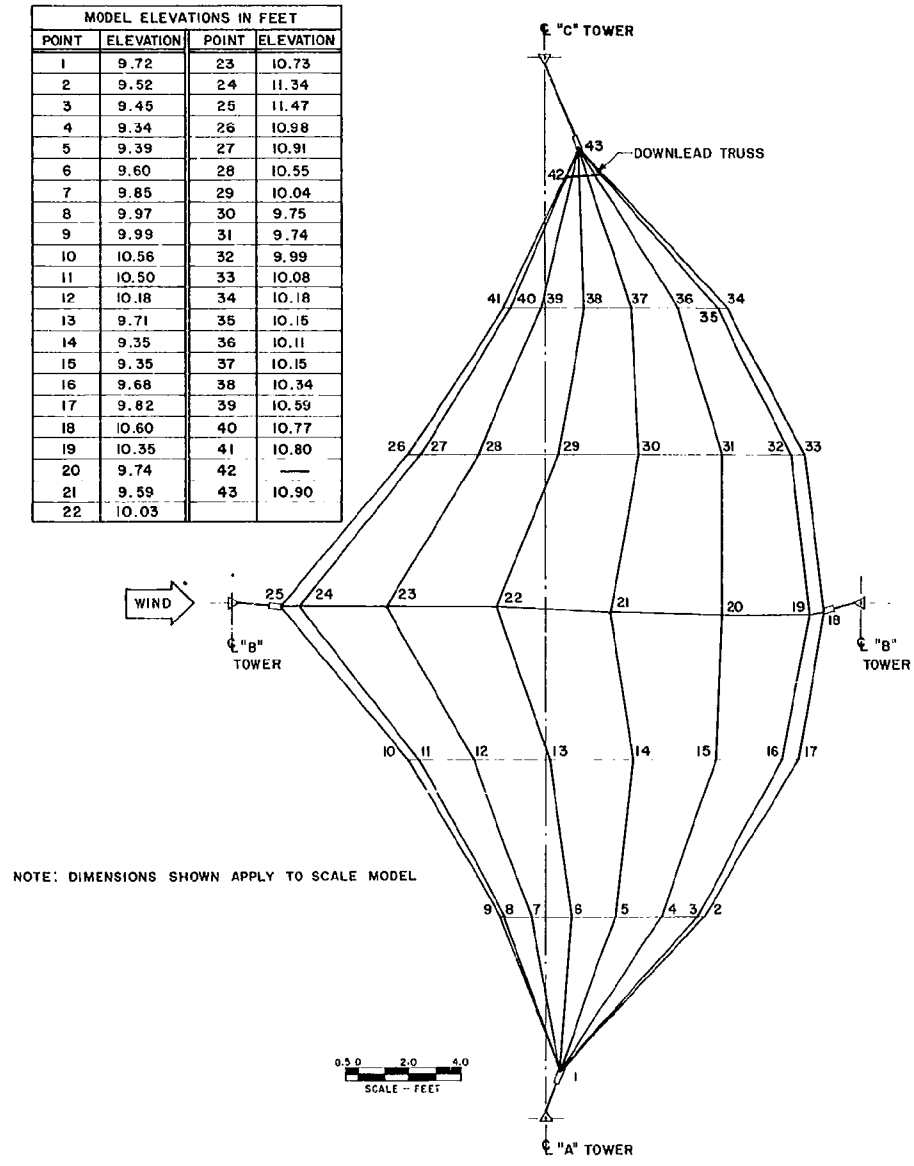

NOTE: DIMENSIONS SHOWN APPLY TO SCALE MODEL

Figure 5-22 PLAN VIEW OF PANEL 2 UNDER MAXIMUM WIND DISTORTION

MODEL ELEVATIONS IN FEET			
POINT	ELEVATION	POINT	ELEVATION
1	9.32	23	11.41
2	9.23	24	11.10
3	9.15	25	11.28
4	8.70	26	10.64
5	8.51	27	10.56
6	8.48	28	10.08
7	8.89	29	9.64
8	9.25	30	9.50
9	9.34	31	9.76
10	9.99	32	9.54
11	9.86	33	9.18
12	9.27	34	9.14
13	8.53	35	9.53
14	8.62	36	10.00
15	9.02	37	9.83
16	9.62	38	9.90
17	9.81	39	10.17
18	10.87	40	10.39
19	10.69	41	10.46
20	9.97	42	—
21	9.61	43	10.66
22	9.79		

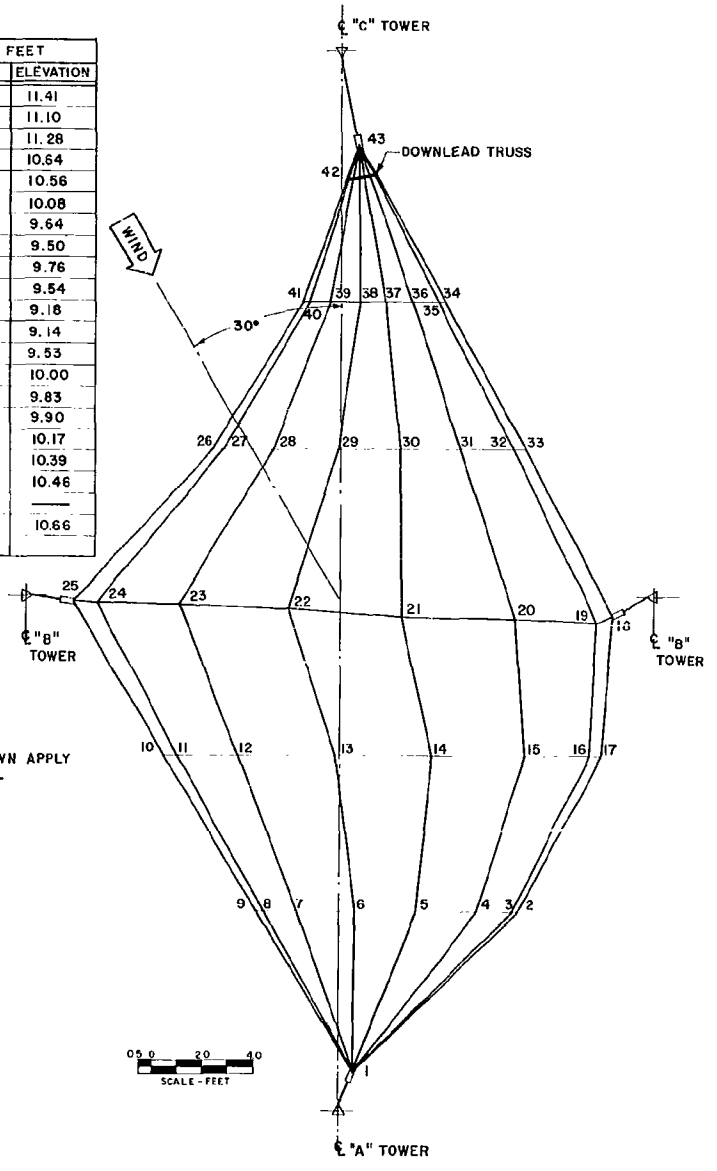

NOTE: DIMENSIONS SHOWN APPLY TO SCALE MODEL

Figure 5-23 PLAN VIEW OF PANEL 3 UNDER MAXIMUM WIND DISTORTION

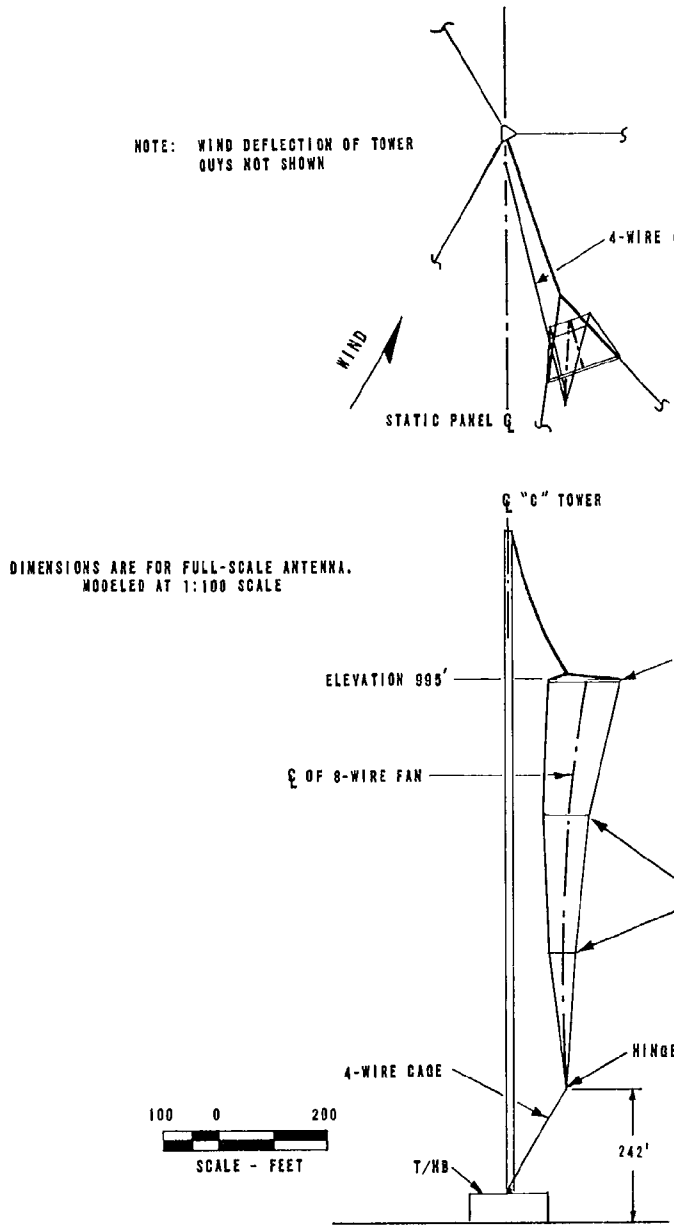

Figure 5-24 PANEL 1 FAN DOWNLEAD UNDER MAXIMUM WIND DISTORTION

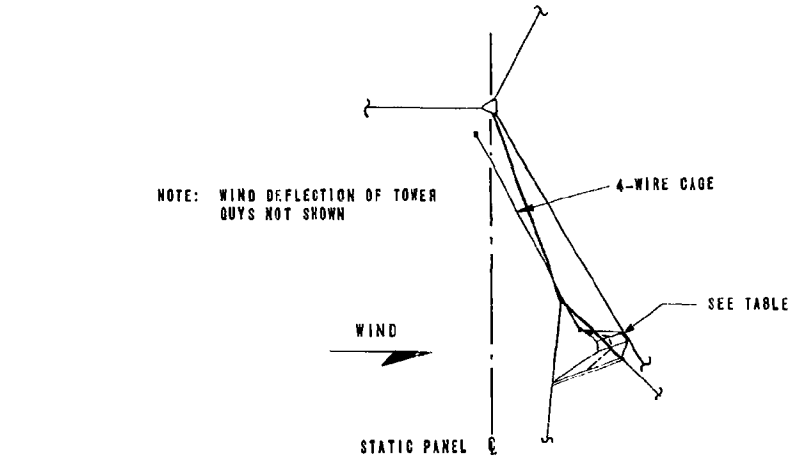

DIMENSIONS ARE FOR FULL-SCALE ANTENNA.
MODELED AT 1:100 SCALE.

WIND VELOCITY	CRITICAL GUY-FAN SEPARATION
MAX. 130 MPH	20 FT
110 MPH	45 FT
90 MPH	70 FT

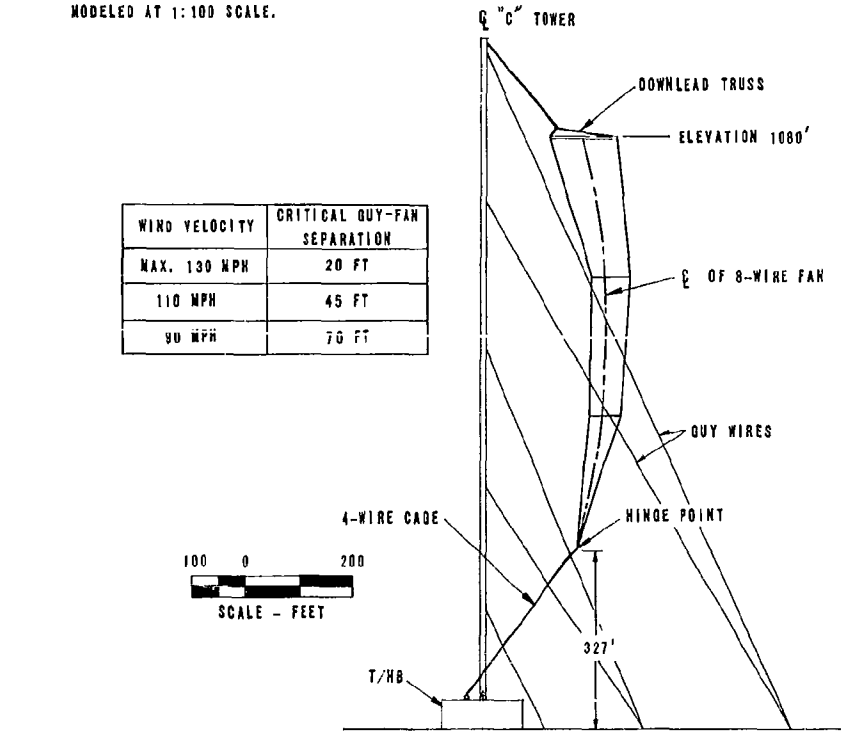

Figure 5-25 PANEL 2 FAN DOWNLEAD UNDER WIND DISTORTION

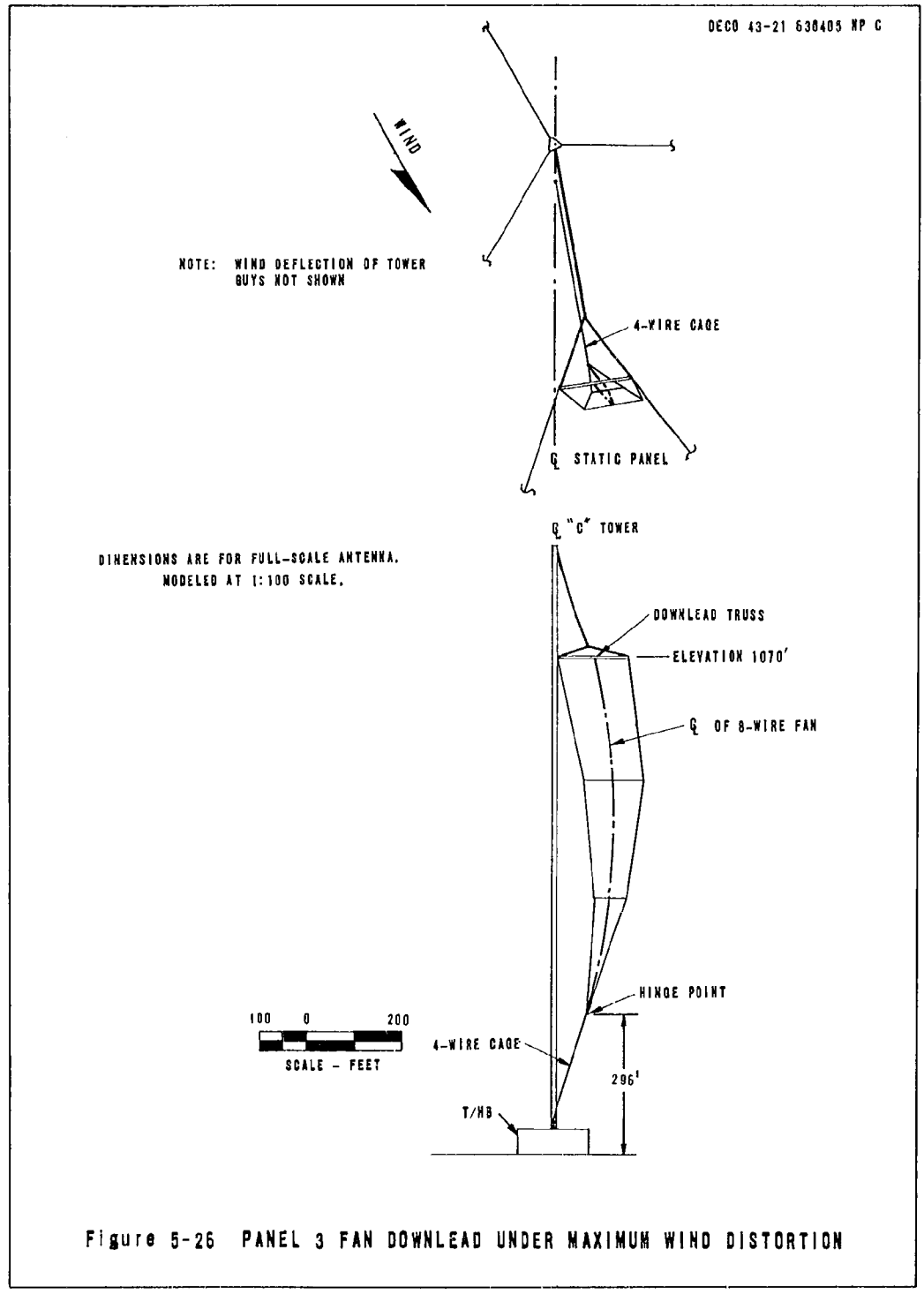

Figure 5-26 PANEL 3 FAN DOWNLEAD UNDER MAXIMUM WIND DISTORTION

considering the poles and rigging as a path for excess polarization current[2], that is, vertical displacement current in excess of the current which would flow in the absence of the dielectric rigging. If the rigging effect increases the relative dielectric constant K for the region of the antenna, the capacity C_s can be expected to increase and the effective height to decrease according to the following relations:

Dielectric	Air	Air + Rigging
• Effective Height	h_o	h_o/K
• Static Capacitance	C_s	KC_s
• Dielectric Constant	1	K

Comparing Tests 35 (Air) and 36 (Air + Rigging) for the undistorted top hat (III) yields the following full scale values:

	Air	Air + Rigging	Percent Change
• Effective Height	628 ft.	619 ft.	-1.8
• Static Capacitance	0.1637 μf	0.1640 μf	+0.18
• Resonant Frequency	32.28 kc	32.38 kc	0

Although the trend of effective height and capacitance change are as expected, the relation of these parameters to an effective dielectric constant K is not exact. Apparently the distribution of poles and rigging near the top hat is not sufficiently uniform to permit the simple relations described above to be applied. Since, however, the total change in

---

[2] S. A. Shelkunoff and H. T. Friis, Antennas, Theory and Practice. John Wiley and Sons (1952). (See Section 10.14, Magnetically and Dielectrically Loaded Antennas.)

effective height is less than 2 percent (the predicted tolerance on this parameter) and the capacitance change even less, it appears that the effect of the distortion rigging was practically negligible.

For the top hat (6 panels) under maximum wind distortion, the following data was obtained at the normal T/HB floor terminal (Test 36): effective height, 684 feet; static capacitance, 0.1575 μf; and resonant frequency, 30.68 kc.

Base reactance data for the wind-distorted configuration is plotted in Figure 5-27. Physically, the horizontal wind loading has the effect of rotating the plane of each sagging top hat span toward the horizontal, the degree of rotation depending on the angle between the wind and the span. This has the effect of raising the average top hat elevation, thus increasing the effective height, and reducing the capacitance. If the antenna could be represented by a single (top loading) capacitance and a single thin, conducting downlead, free of the perturbing influence of grounded towers and long, relatively low, horizontal runs of cage conductors, then the increase in effective height due to an increase in the average top hat height would be approximately the same as the decrease in capacitance. However, for an antenna with a considerable near-base capacitance and many parasitic conducting structures, the two effects are not comparable. In particular, elevating the horizontal downlead bus-work (connecting the hinge points and the pulloff points on the T/HB) greatly reduces the near-base capacitance. This has the effect of raising the apparent effective height (i.e., reducing the loading effect of the near-base capacitance) and adding to the increase in the average top-loading which yields an exaggerated (positive) change in effective height compared to the (negative) change in static capacitance. (See Appendix D.)

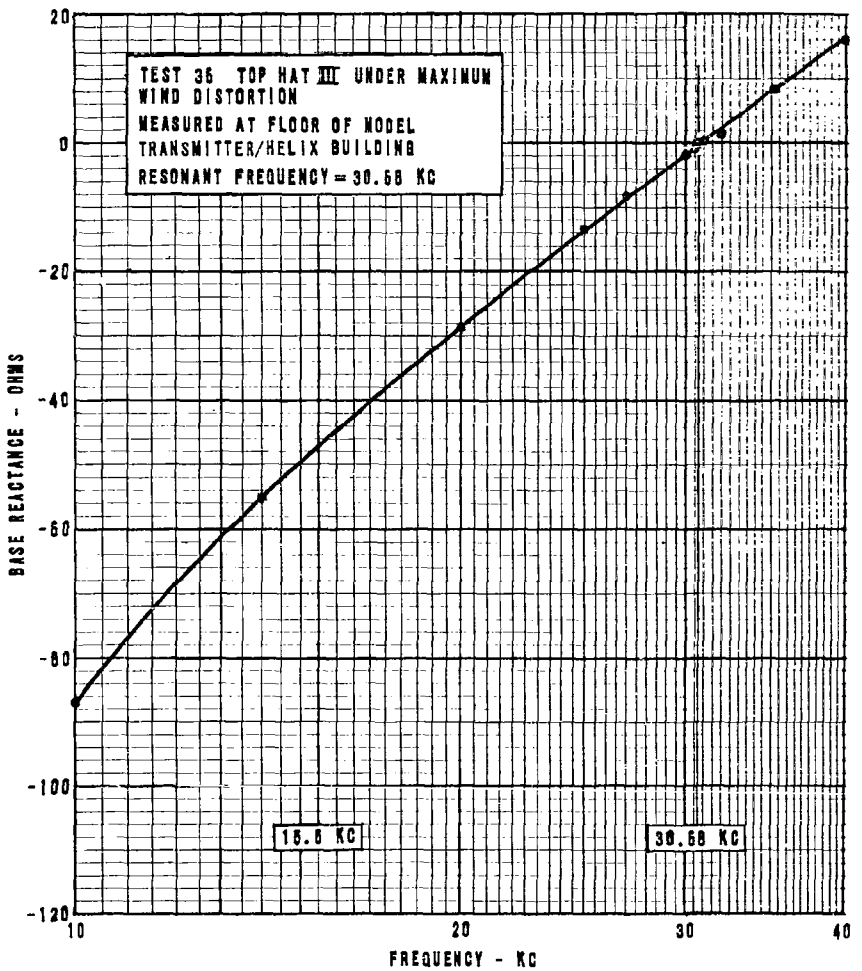

Figure 5-27 MEASURED BASE REACTANCE FOR TOP HAT III UNDER MAXIMUM WIND DISTORTION

Comparing the measured antenna characteristics under static and maximum wind conditions yields the following full-scale data:

	Test 35 Static Loading	Test 36 Max. Wind Loading	Percent Change
• Effective Height	619 feet	684 feet	+10.5
• Static Capacitance	0.1640 μf	0.1575 μf	-3.96
• Resonant Frequency	32.28 kc	30.68 kc	-4.94

Since all the downlead trusses are lifted by the wind, the downlead bundle acquires a somewhat longer and thinner shape. This, together with the increase in average top hat elevation, accounts for the associated increase in inductance and reduction in resonant frequency.

Under the condition of maximum wind distortion, the simulated tuning/coupling circuitry appropriate to operation at the upper end of the frequency range was inserted (Test 39), and input reactance was measured to determine resonance. For this arrangement resonance occurs at a scaled frequency of 28.25 kc, some 0.25 kc below the 28.50 kc figure specified. However, since the predicted frequency of occurrence of 130 mph winds is approximately once in 50 years, the situation was considered tolerable.

Gradient Distribution

Current distribution measurements were performed at a scale frequency corresponding to 15.6 kc (i.e., 1560 kc) using the shielded oscillator probe in a manner similar to that outlined in Section 2.2.4 for the case of Top Hat I under static loading. From the current distribution, the electric field gradient is determined from the change in current per unit area of top hat conductor (See Appendix B).

Under conditions of maximum wind loading, the antenna conductors are displaced from their static or dead-load position, changing the various spacings between conductors and between conductors and ground. This distortion changes the current distribution, increasing the gradient in some areas. Critical areas of increased gradient were expected at points where top hat and downleads were blown towards grounded towers and guys.

Figures 5-28 through 5-33 show the distribution of gradient on the three wind-distorted top-hat panels appropriate to the maximum wind orientation chosen for study.

Although the expected increase in maximum gradient on the top hat was observed, the critical area of interest was on the No. 2 panel downlead fan. This particular downlead is displaced toward a guy plane for the chosen wind. Some advantage is gained by virtue of a similar deflection of the guys, but not sufficiently to preclude the possibility of a limited area of corona formation. The other downleads (Nos. 1 and 3) are not deflected to positions near towers or guys, so that only the No. 2 fans are critical.

To provide detailed information on the No. 2 fans, three wind velocities were studied which would indicate several situations expected during periods of storm activity. Figures 5-34, 5-35, and 5-36 show the critical downlead under 130, 110, and 90 mph winds, respectively. Under these conditions the following relations were obtained:

Gust Velocity at 30 feet	No. 2 Downlead--Guy Separation	Maximum Gradient (1 Mw Radiated)	Power Radiated (0.8 Kv/mm Gradient)	Frequency of Occurrence
130 mph	20 feet	1.3 kv/mm	380 kw	1 in 50 yrs.
110 mph	45 feet	0.9 kv/mm	480 kw	1 in 15 yrs.
90 mph	70 feet	0.8 kv/mm	1000 kw	1 in 6 yrs.

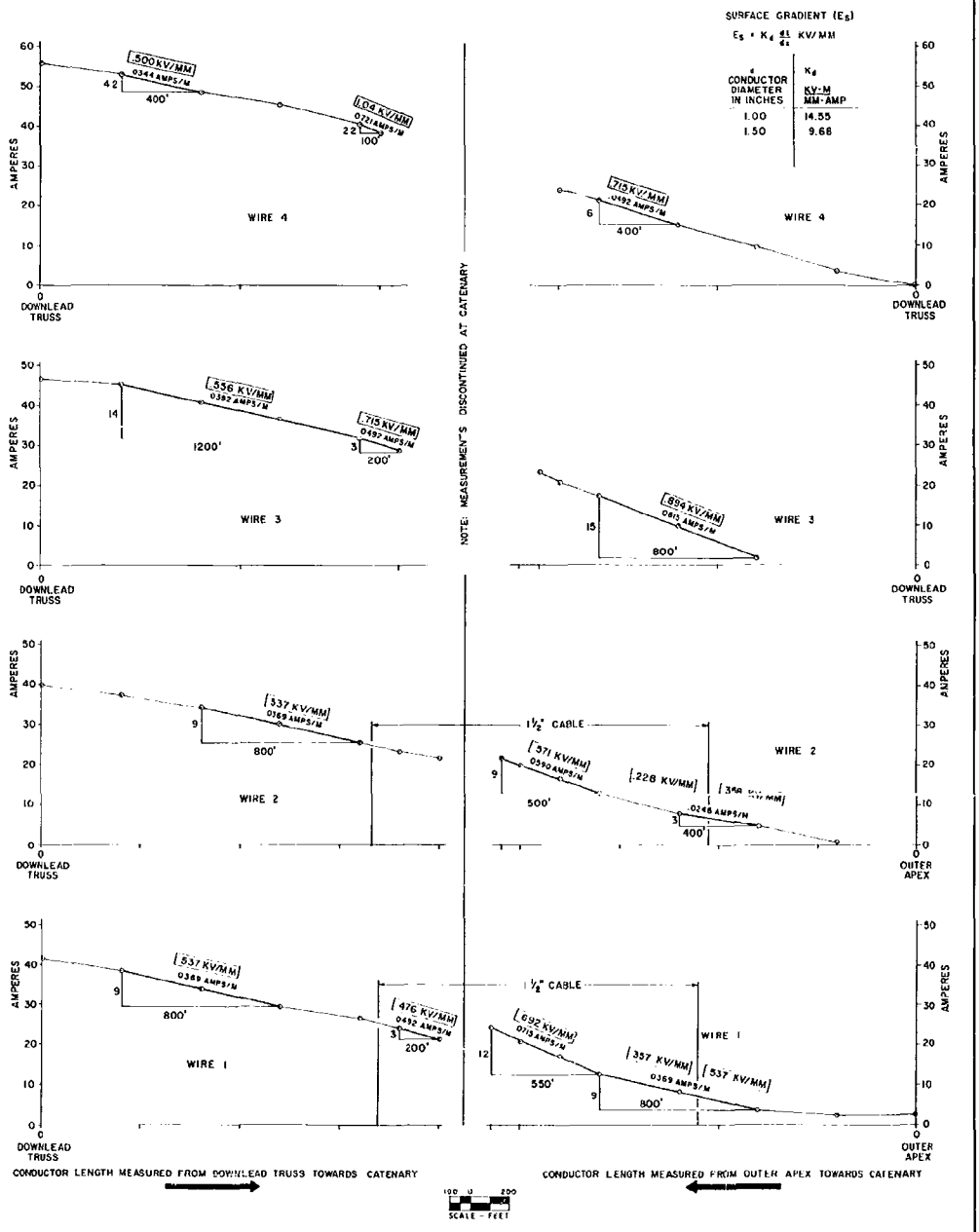

Figure 5-28 GRADIENT DISTRIBUTION UNDER MAXIMUM WIND ON PANEL 1 (WIRES 1-4)

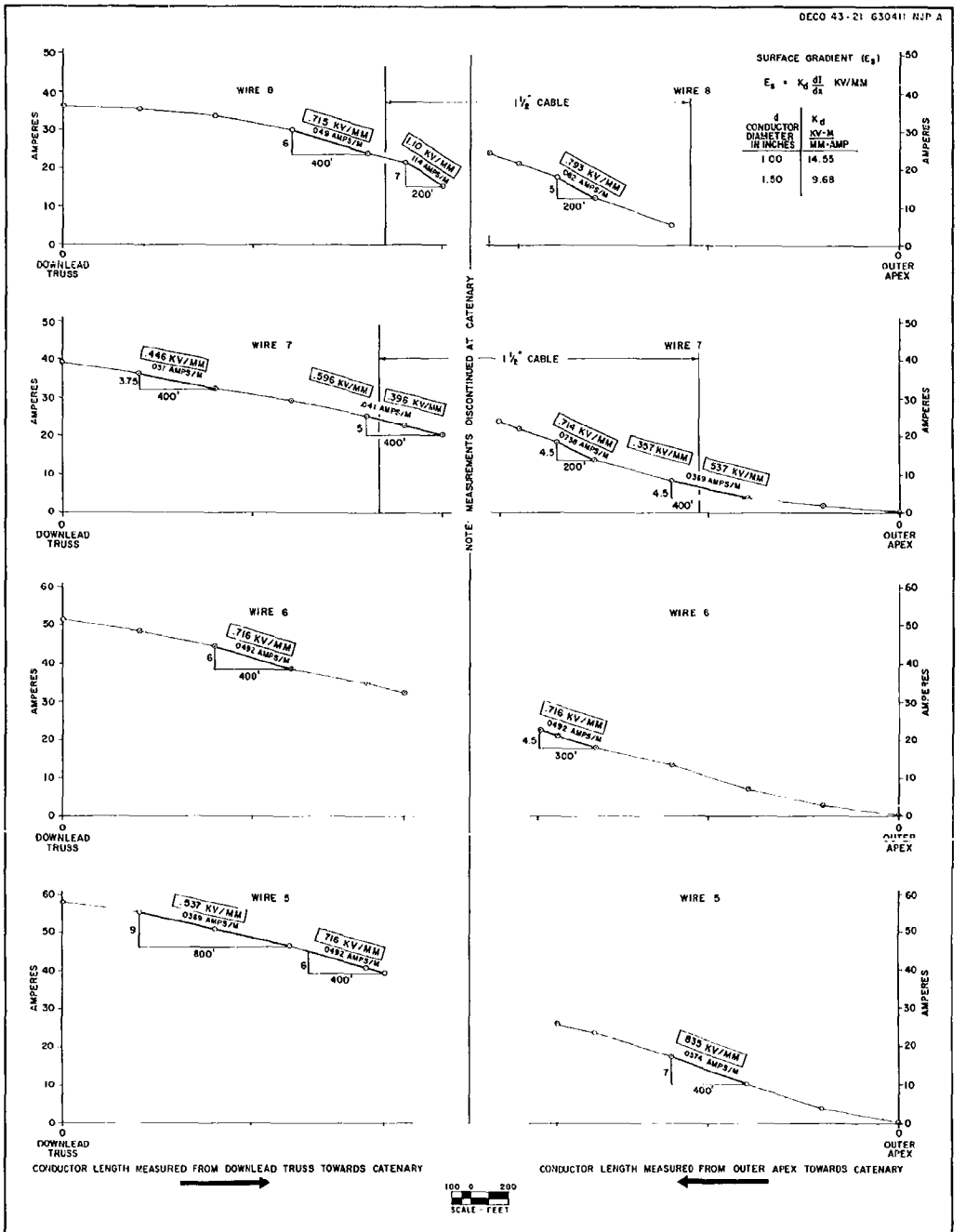

Figure 5-29 GRADIENT DISTRIBUTION UNDER MAXIMUM WIND ON PANEL 1 (WIRES 5-8)

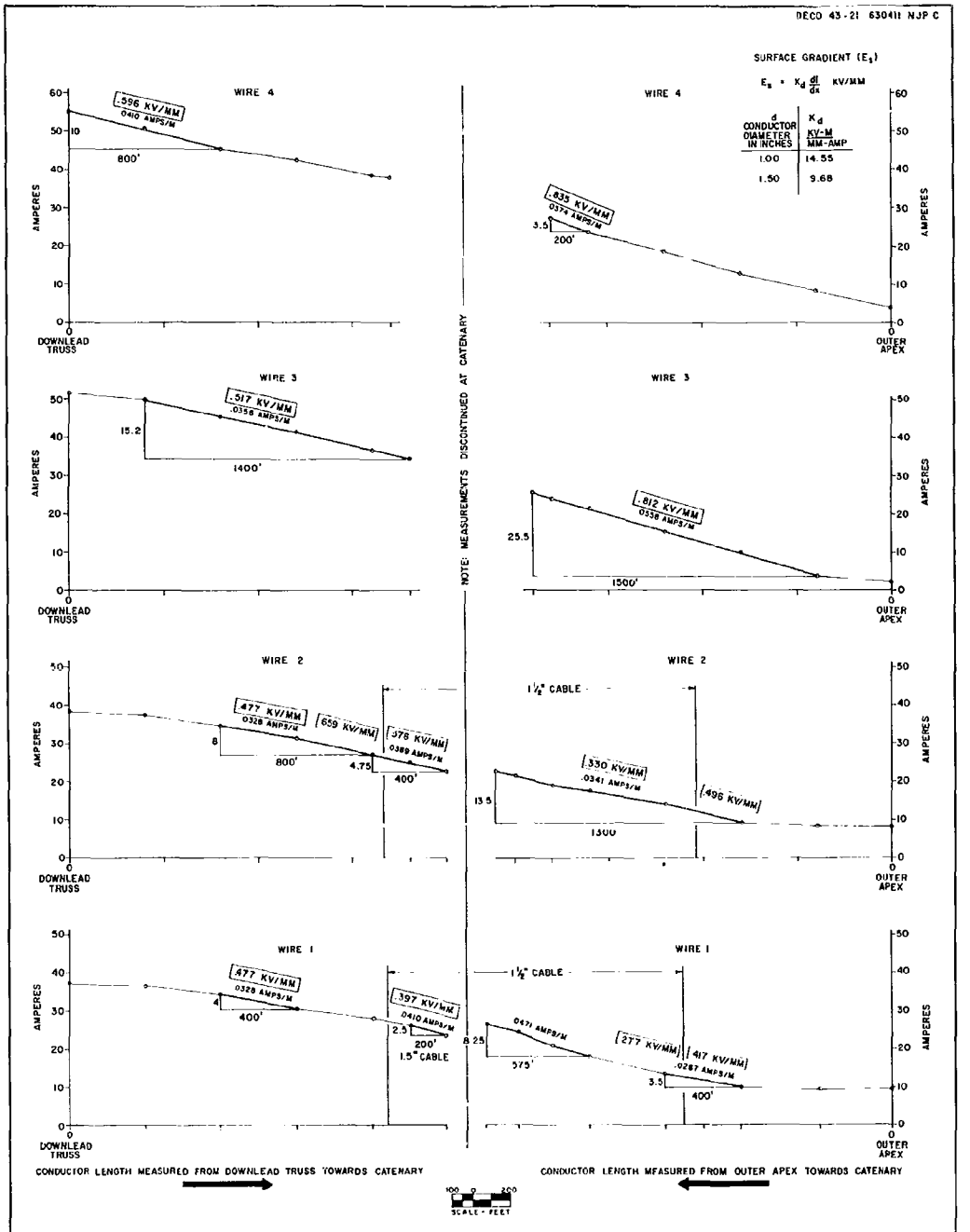

Figure 5-30 GRADIENT DISTRIBUTION UNDER MAXIMUM WIND ON PANEL 2 (WIRES 1-4)

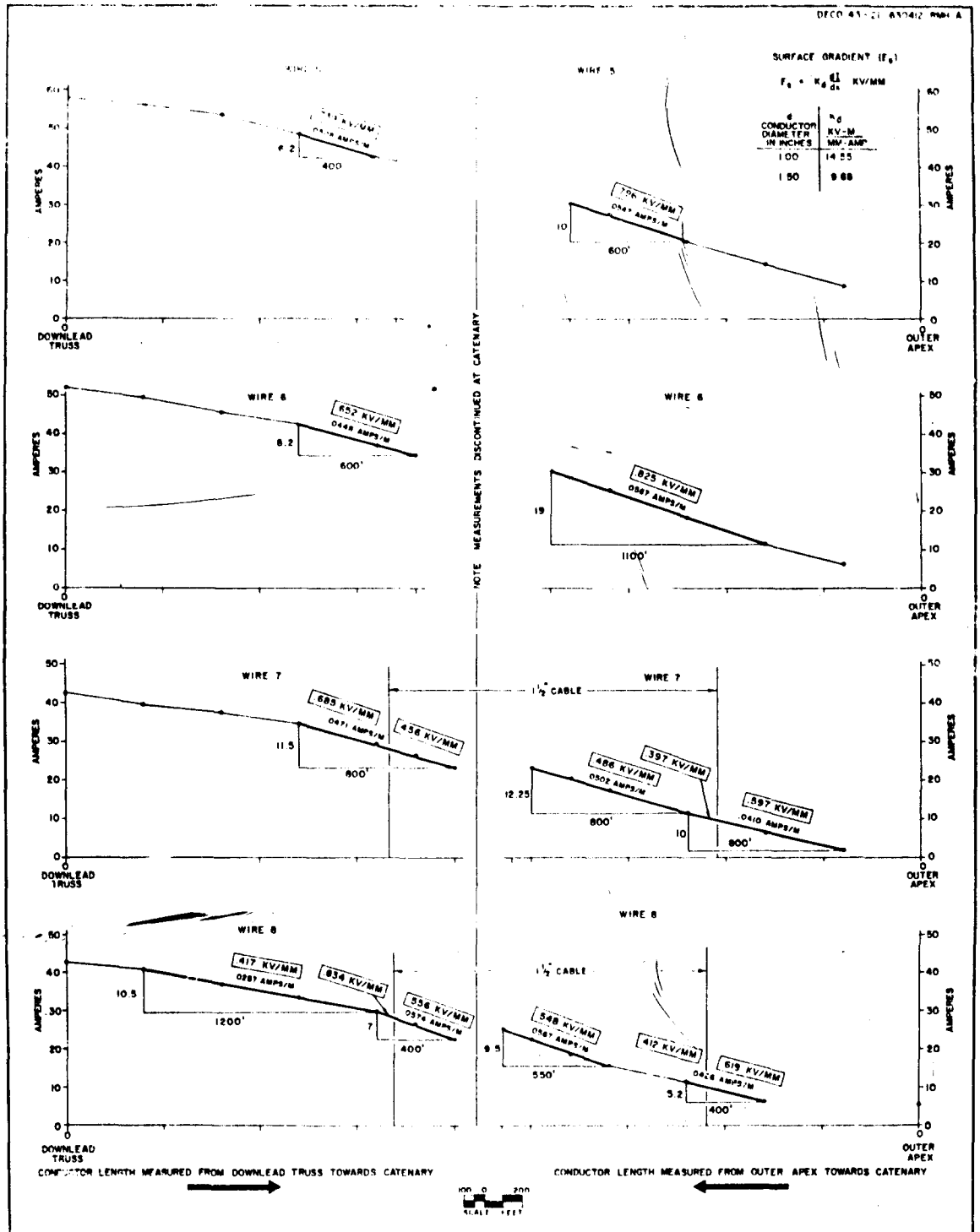

Figure 5-31 GRADIENT DISTRIBUTION UNDER MAXIMUM WIND ON PANEL 2 (WIRES 5-8)

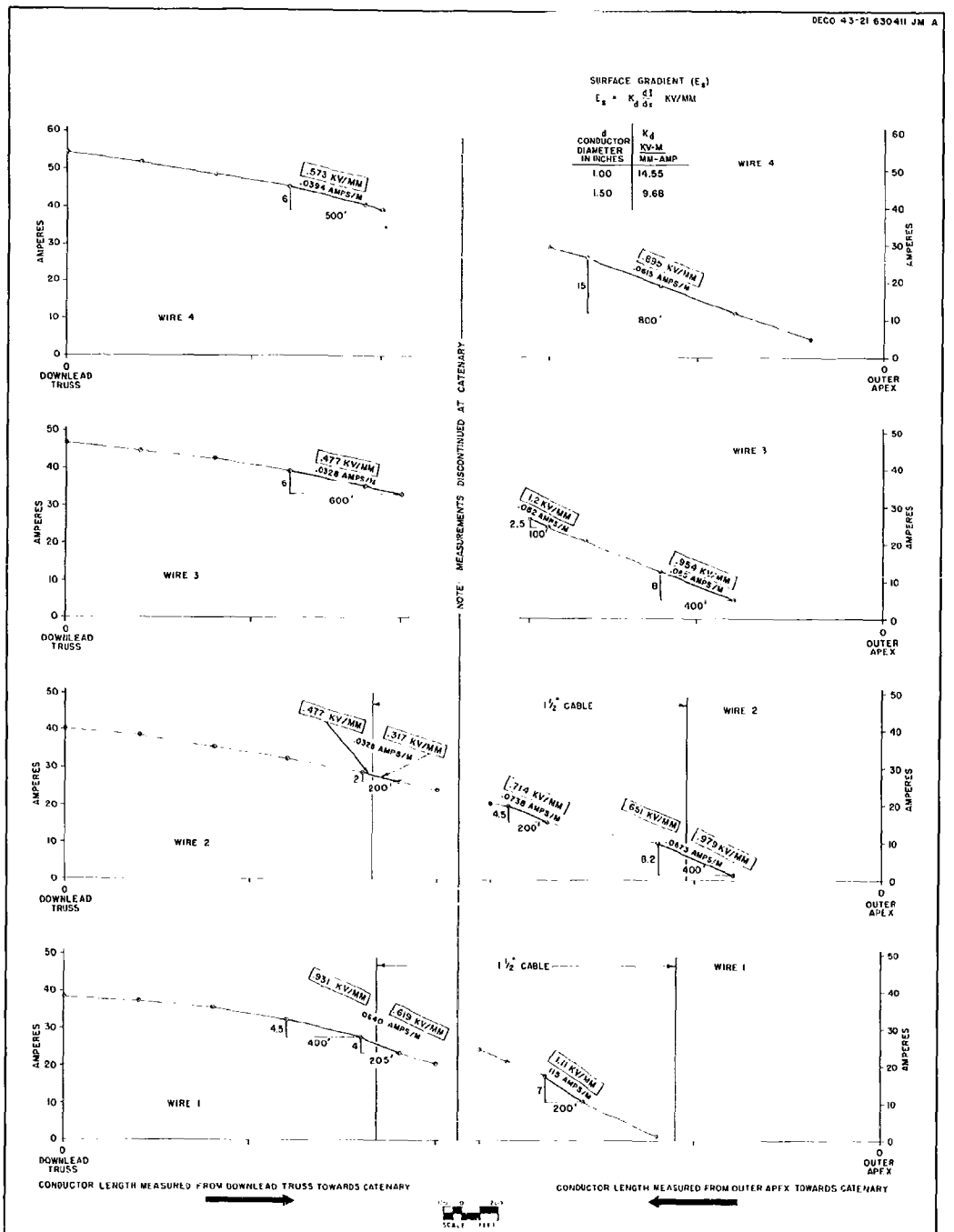

Figure 5-32 GRADIENT DISTRIBUTION UNDER MAXIMUM WIND ON PANEL 3 (WIRES 1-4)

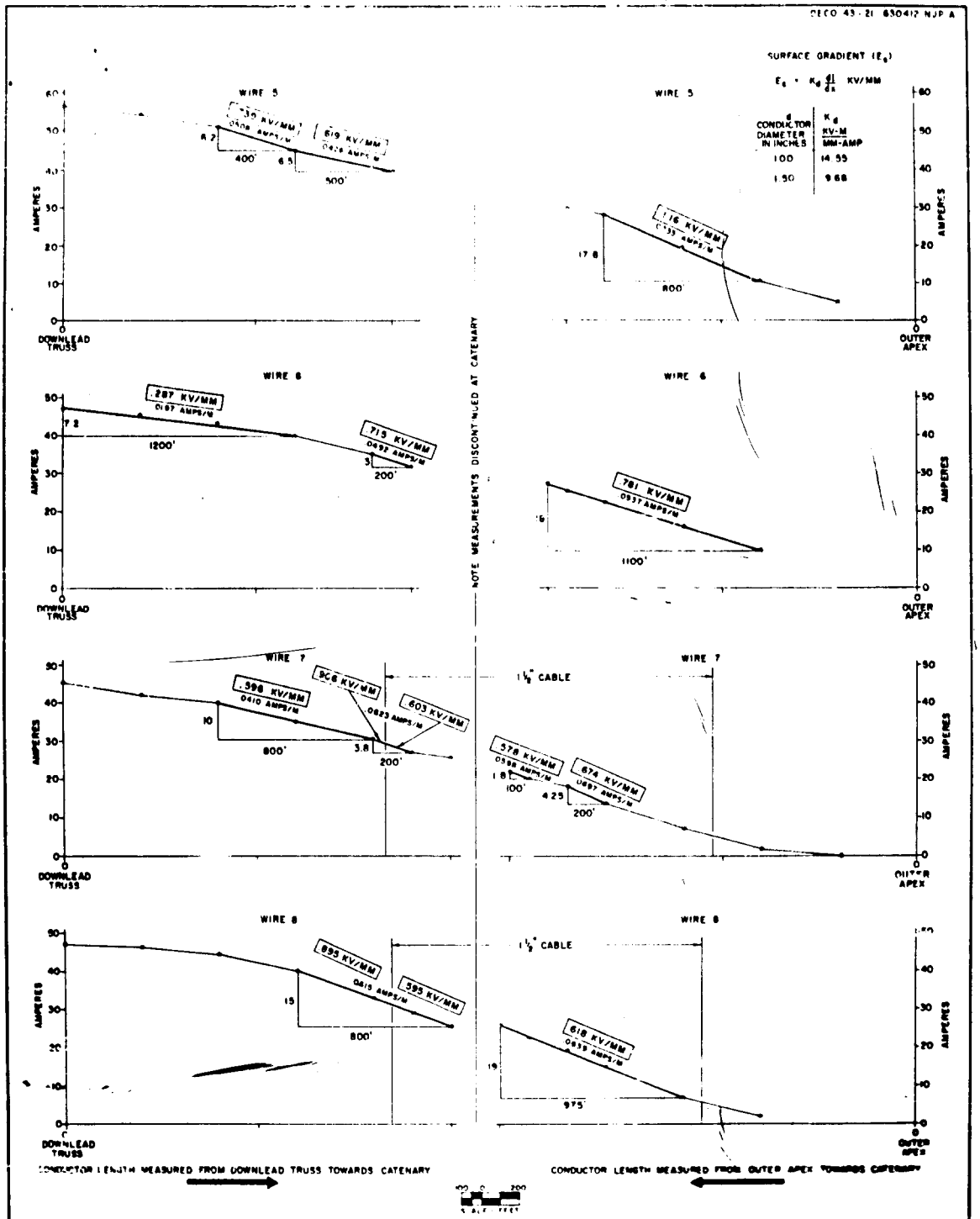

Figure 5-33 GRADIENT DISTRIBUTION UNDER MAXIMUM WIND ON PANEL 3 (WIRES 5-8)

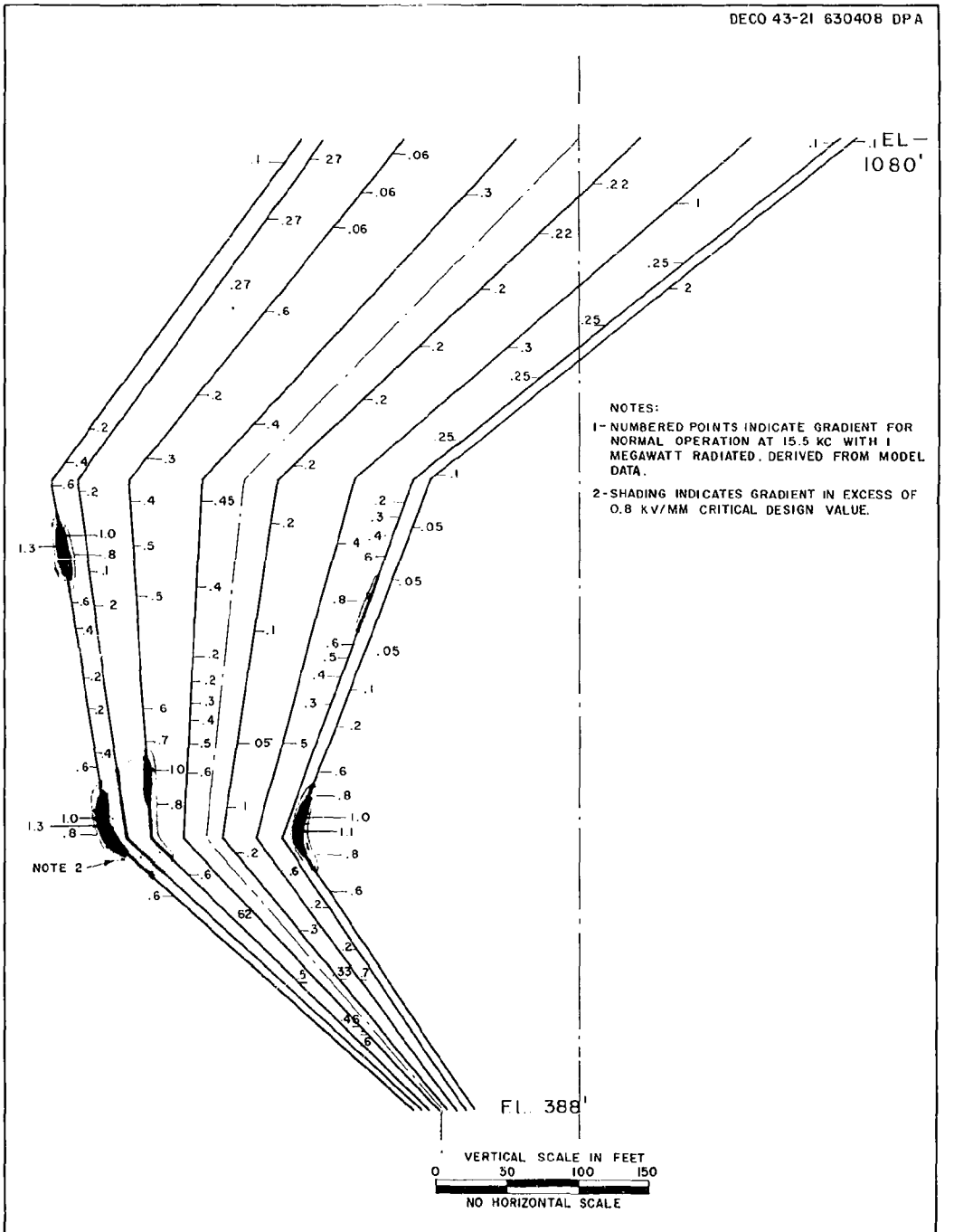

Figure 5-34 GRADIENT DISTRIBUTION ON CRITICAL (No. 2 FAN) DOWNLEAD UNDER 130 MPH WIND

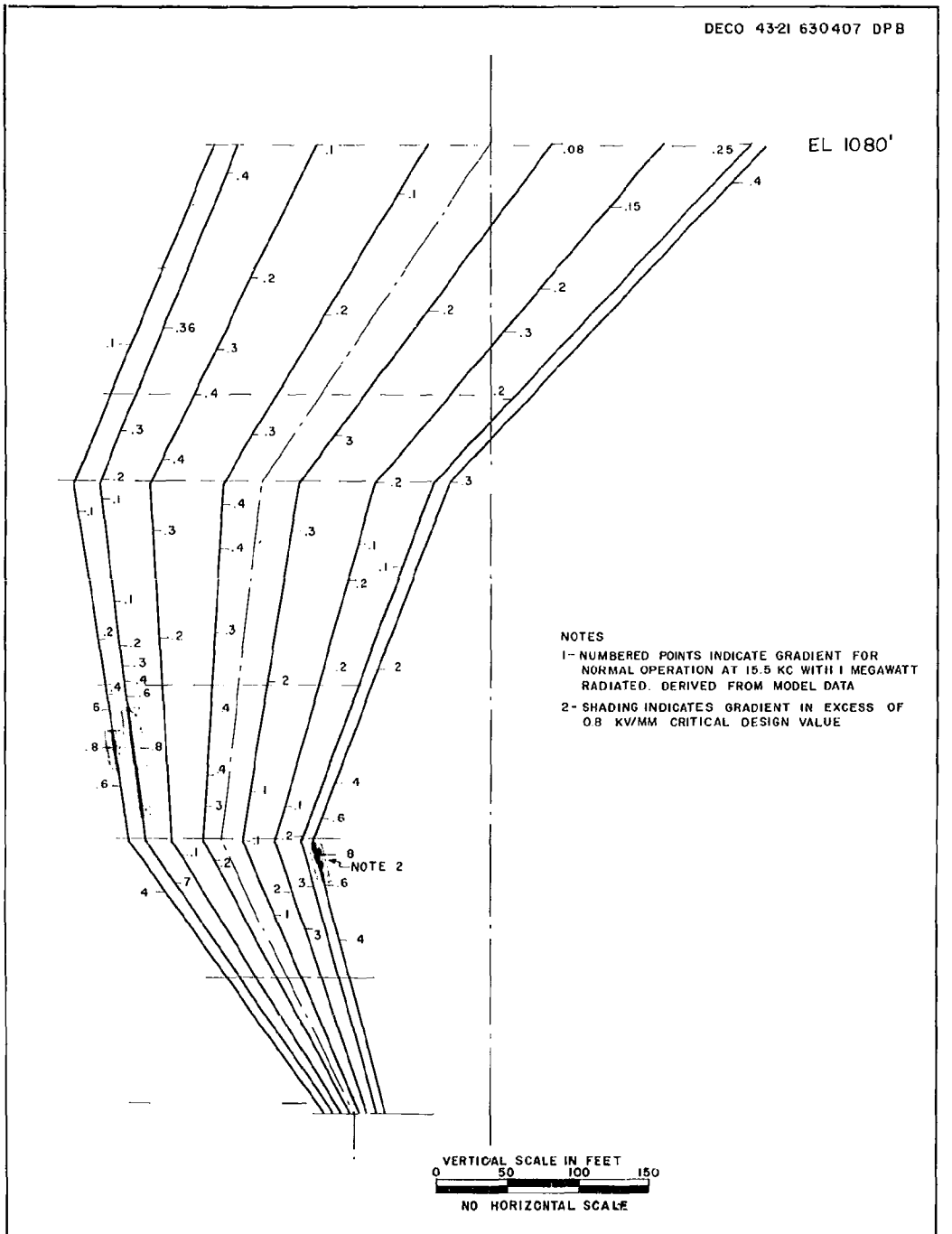

Figure 5-35 GRADIENT DISTRIBUTION ON CRITICAL (No. 2 FAN) DOWNLEAD UNDER 110 MPH WIND

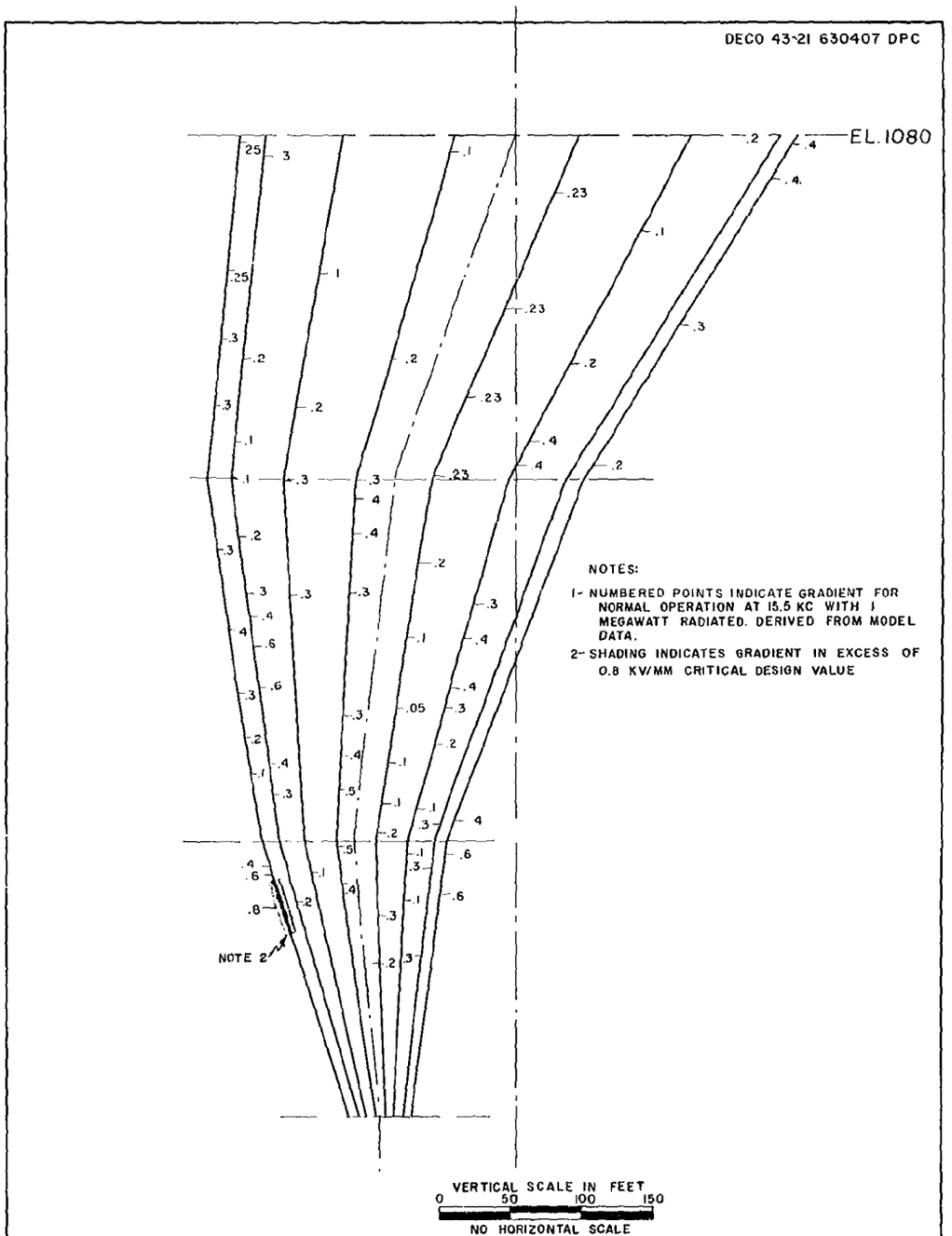

Figure 5-36 GRADIENT DISTRIBUTION ON CRITICAL (No. 2 FAN) DOWNLEAD UNDER 90 MPH WIND

6. SUMMARY OF PREDICTED PERFORMANCE

This report presents the results of the antenna model study which was carried out for the development of the design of the VLF PAC antenna. Beginning with an evaluation of the initial configuration (Section 5.1) this study includes the results of a continuous model program involving detailed structural revisions which occurred as part of the refined design. These revisions included changes in top hat shape, intermediate tower elevations, entrance bushings and Transmitter/Helix Building. In general, the effects of such revisions were reflected by relatively minor changes in electrical performance as derived from model measurements. Consequently, the measurement of some aspects of performance which were not considered of primary importance or were not expected to change appreciably were not repeated for the final revisions.

For comparison, Table 6-1 summarizes both the predicted full-scale basic antenna parameters and the derived operating characteristics relating to full-power (1 megawatt radiated) operation at the design frequency (15.5 kc). This data is given for (a) normal (6 panel, no wind) operation, (b) emergency (5 panel, no wind) operation, and (c) for the condition of 6 panels and maximum wind (130 mph) distortion. The normal and wind-distorted data were obtained from the final model with all pertinent revisions included. However, the emergency condition was evaluated only on the initial configuration. Since no major changes were determined in the performance for the normal condition (compare, for example, the results of Tests 22 and 34) it was considered unnecessary to repeat the emergency condition measurements.

The base reactance values shown in Table 6-1 include all corrections and are referred to the bushing entrance on the antenna. Figure 6-1 is a plot of the corrected input reactance over the entire

TABLE 6-1

Summary of Performance

Basic Parameters:	(1) Normal Operation 6 panels, no wind	(2) Emergency Operation 5 panels, no wind	(3) Maximum Wind 6 panels
Effective Height - ft.	628	625	684
Static Capacitance - μf	.1637	.1412	.1515
Resonant Frequency - kc	32.28	33.05	30.68
Performance Characteristics:			
(15.5 kc, 1000 kw radiated)			
3 db Bandwidth - cps	38.2	32.7	43.5
Base Reactance - ohms	-46.9	-56.7	-47.7
Base Voltage - kv	123.	144.	113.
Top Hat Voltage - kv	160	185	152
Input Current - amps	2545	2559	2336
Radiation Resistance - ohms	.154	.153	.183
Average Gradient - kv/mm	.43	.52	.43
Maximum Gradient	.74	>.84	1.30
With Coupling Circuitry:			
Maximum operating freq. - kc	29.45	--	28.25
Miscellaneous Data:			
Apparent Inductance - μh	149	164	171
Antenna Q (15.5 kc)	406	474	356

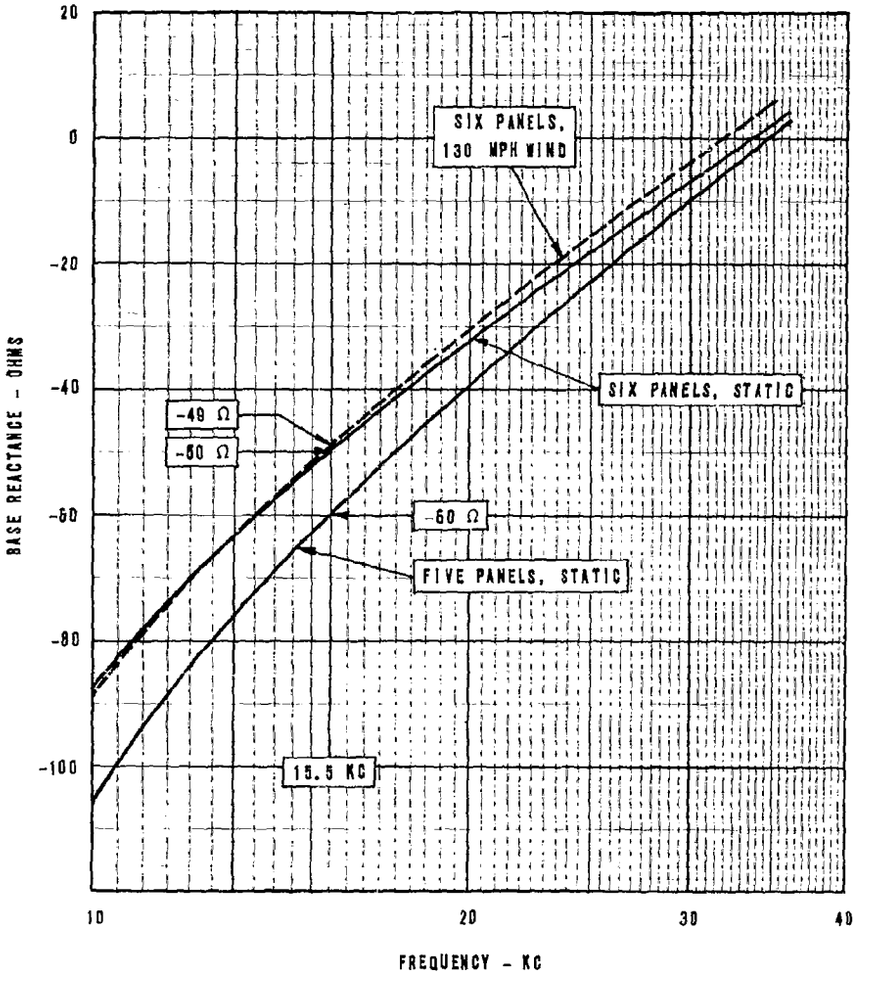

Figure 6-1 BASE REACTANCE AS A FUNCTION OF FREQUENCY

range of operating frequencies referred to the bushing entrance. Note that the resonant frequencies (zero reactance) indicated in Figure 6-1 differ slightly from the tabulated values taken directly from model data, reflecting the corrections and different reference point involved in the figure.

Considering the results of the model study, the configuration selected adequately meets the design goals. The bandwidth requirement (not to be less than 37.5 cps) is exceeded slightly under normal conditions and only degraded under emergency operation where such degradation was considered acceptable. Similarly, the maximum operating frequency (not to be less than 28.5 kc) was exceeded by almost 1 kc under normal operation and violated only under maximum wind distortion by 0.25 kc. In all cases considered, the average gradient on the antenna conductors fell below the design limit (average not to exceed 0.65 kv/mm), with the maximum value exceeding the tolerable limit (maximum not to exceed 0.80 kv/mm) only for full-power operation with 5-panels and for maximum wind distortion. Since the full-power requirement is relaxed for 5-panel operation, this represents no problem. Similarly (see Section 5.3.1) the excess gradient under wind distortion was not considered intolerable considering the relative infrequency with which such such high winds are incident to the site.

Appendix A: MODEL DATA

This appendix contains the data obtained on the VLF-PAC model during the measurement program. Table A-1 presents the effective heights, static capacitances, and resonant frequencies for Tests 21 through 39; tower heights, number of panels, and dates of tests, are also included. Table A-2 presents a tabulation of the base reactances measured on the model at various stages of development.

Detailed descriptions of the test procedures and theoretical background are given in other sections of this report; however, certain comments are repeated here for reference.

- Effective heights — An average was taken of several runs made on each test. This average was corrected for the effect of the input susceptance of the cathode follower driving the voltmeter.

- Static capacitances -- The average of several readings was divided by 1.027 to correct for the effect of the wires on the model being slightly larger than 1/100 of the full-scale size.

- Resonant frequencies — The resonant frequency was obtained by interpolating to the frequency at which the measured base reactance was zero.

- Measured base impedances — The resistive term is tabulated for completeness only, but should not be considered indicative of radiation resistance or full-scale losses because of the inability to accurately model ground plane and cable conductivities.

TABLE A-1

Model Data Summary

Test No.	Date	Test Conditions	Measuring Point (Note 1)	Effective Height h_e (feet)	Static Capacitance C_o (μf)	Resonant Frequency f_o (kc)
21	29 Mar. '62	"Emergency" operation single bushing, Modeled T/HB See Note 3	d	625.	0.1451	33.05
22	2 Apr. '62	"Normal" operation, single bushing	a	625.	0.1633	32.18
23	22 May '62	T/HB enlarged, two bushings	b	637.	0.1647	29.60
24	23 May '62	T/HB enlarged, two bushings	c	628.	0.1634	33.70
25	25 May '62	T/HB enlarged, two bushings	a	622.	0.1634	32.25
26	28 May '62	New top hat with increased sags	a	610.	0.1642	32.45
27	31 May '62	New top hat with increased sags	c	607.	0.1638	33.57
28	1 June '62	New top hat with increased sags	b	608.	0.1647	29.43
29	6 June '62	Raised "B" Tower 20'	b	623.	0.1644	29.45
30	6 June '62	Raised "B" Tower 20'	c	627.	0.1630	33.85
31	7 June '62	Raised "B" Tower 20'	a	629.	0.1633	32.45
32	7 June '62	Measured at floor T/HB through one bushing	d	627.	0.1630	31.95
33	8 June '62	"Block and Tackle" installed on Panel "A"	d	629.	0.1630	31.95
34	14 June '62	Revised downlead pull-off structures to 4-legged version	a	628.	0.1638	32.28
35	26 June '62	36 wood poles in place for wind distortion	a	619.	0.1640	32.28
36	9 July '62	130 mph wind distorted condition	a	685.	0.1575	30.68
37	27 July '62	Critical fan-to-guy spacing (Panel "D") increased to 45'			See Note 4.	
38	28 July '62	Critical fan-to-guy spacing (Panel "D") increased to 70'			See Note 4.	
39	12 July '62	Observe shift in resonant frequency due to simulated tuning network	b			28.25

Notes:

1. Measuring Points
   a. Normal, at Transmitter/Helix Building floor.
   b. Through simulated tuning/coupling circuitry.
   c. At tie bar between two entrance bushings.
   d. At Transmitter/Helix Building floor, with only one entrance bushing used (as for emergency operation).
2. The full-scale tower heights were as follows.

	A	B	C
Tests 21-28	996 feet	1175 feet	1271 feet
Tests 29-39	996 feet	1195 feet	1271 feet

3. All tests were for 6-panel operation, except test 21, which was run with 5 panels.
4. Tests 37 and 38 were for gradient studies only.
5. Corrected model antenna data scaled to full-sized antenna.
6. Tests 21 through 25 for Top Hat I; tests 26 through 28 for Top Hat II; tests 29 through 39 for Top Hat III.

TABLE A-2

Measured Base Impedance (Referred to Full-Scale Antenna)

TEST 21

Frequency KC	Impedance Ohms	Frequency KC	Impedance Ohms
10.00	0.21 - j102.0	31.50	0.86 - j3.82
12.45	0.20 - j77.9	32.00	0.89 - j2.19
14.00	NR - j66.1	32.50	0.91 - j1.54
17.50	0.36 - j47.2	33.00	0.92 - j0.15
20.00	0.41 - j35.0	33.50	0.97 + j0.75
22.50	0.50 - j26.9	34.00	0.99 + j1.80
25.05	0.55 - j19.8	35.00	1.03 + j4.00
27.50	0.65 - j13.1	37.50	1.20 + j8.55
30.00	0.79 - j6.87	40.00	1.40 + j13.0
31.00	0.85. - j4.84		

TEST 22

Frequency KC	Impedance Ohms	Frequency KC	Impedance Ohms
10.00	0.16 - j88.0	31.50	0.85 - j1.43
12.45	0.24 - j66.7	32.00	0.88 - j0.41
14.00	NR - j57.1	32.25	0.88 + j0.06
17.50	0.32 - j38.9	32.50	0.90 + j0.62
20.00	0.40 - j30.0	33.00	0.92 + j1.50
22.50	0.48 - j22.7	35.00	1.01 + j5.23
25.05	0.55 - j15.6	37.50	1.20 + j10.0
27.50	0.62 - j9.83	40.00	1.40 + j14.0
30.00	0.76 - j4.33		

TEST 23

Frequency KC	Impedance Ohms	Frequency KC	Impedance Ohms
10.00	NR - j86.0	29.50	0.80 - j0.3
14.00	NR - j50.0	29.60	0.81 + j0.
20.00	0.40 - j26.0	30.00	0.82 + j1.3
25.00	0.65 - j11.2	35.00	1.10 + j11.7
28.90	0.79 - j2.1	40.00	1.50 + j21.0

NR - No Reading

TABLE A-2 (Cont.)

TEST 24

Frequency KC	Impedance Ohms	Frequency KC	Impedance Ohms
10.00	0.23 - j86.0	33.50	0.92 - j0.30
14.00	0.30 - j55.7	33.70	0.95 + j0.
20.00	0.40 - j31.0	33.75	0.92 + j0.1
25.00	0.59 - j17.6	34.00	0.93 + j0.59
30.00	0.79 - j6.67	35.00	1.01 + j2.88
32.00	0.88 - j3.12	40.00	1.42 + j10.8

TEST 25

Frequency KC	Impedance Ohms	Frequency KC	Impedance Ohms
10.00	0.25 - j85.0	32.00	0.90 - j0.63
14.00	NR - j55.0	32.25	0.90 + j0.
20.00	0.42 - j29.5	35.00	1.02 + j5.29
25.00	0.49 - j15.6	40.00	1.58 + j13.5
30.00	0.80 - j4.66		

TEST 26

Frequency KC	Impedance Ohms	Frequency KC	Impedance Ohms
10.00	0.18 - j85.0	32.00	0.80 - j0.78
14.00	NR - j55.0	32.45	0.89 + j0.
20.00	0.41 - j29.5	35.00	1.00 + j4.85
25.00	0.58 - j15.8	40.00	1.52 + j13.4
30.00	0.77 - j5.00		

TEST 27

Frequency KC	Impedance Ohms	Frequency KC	Impedance Ohms
10.00	0.18 - j85.5	32.00	0.86 - j3.1
14.00	NR - j55.7	33.55	0.90 + j0.
20.00	0.39 - j31.0	33.60	0.91 + j0.
25.00	0.57 - j17.2	35.00	0.99 + j2.86
30.00	0.77 - j7.00	40.00	1.45 + j11.5

NR - No Reading

TABLE A-2 (Cont.)

TEST 28

Frequency KC	Impedance Ohms	Frequency KC	Impedance Ohms
10.00	0.18 - j82.0	29.40	0.79 + j0.
14.00	NR - j51.4	29.45	0.80 + j0.
20.00	0.43 - j25.5	30.00	0.81 + j1.3
25.00	0.61 - j10.4	35.00	1.07 + j12.0
29.00	0.78 - j0.86	40.00	1.53 + j21.5

TEST 29

Frequency KC	Impedance Ohms	Frequency KC	Impedance Ohms
10.00	0.20 - j87.5	29.50	0.81 + j0.
14.00	NR - j52.1	29.60	0.81 + j0.34
20.00	0.45 - j25.5	29.70	0.82 + j0.60
25.00	0.61 - j10.8	30.00	0.83 + j1.3
29.00	0.80 - j1.0	35.00	1.09 + j12.0
29.45	0.82 + j0.	40.00	1.58 + j21.8

TEST 30

Frequency KC	Impedance Ohms	Frequency KC	Impedance Ohms
10.00	0.20 - j86.5	33.60	0.93 - j0.45
14.00	NR - j56.1	33.75	0.94 - j0.1
20.00	0.40 - j31.5	33.85	0.95 + j0.0
25.00	0.58 - j18.0	35.00	1.01 + j2.0
30.00	0.79 - j7.14	40.00	1.48 + j10.5
32.00	0.88 - j3.28		

TEST 31

Frequency KC	Impedance Ohms	Frequency KC	Impedance Ohms
10.00	0.20 - j85.5	25.00	0.59 - j15.8
14.00	NR - j55.0	30.00	0.79 - j5.00
20.00	0.41 - j29.5	32.45	0.90 + j0.

TEST 32

Frequency KC	Impedance Ohms	Frequency KC	Impedance Ohms
31.95	0.89 + j0.	32.40	0.91 + j0.77
32.15	0.90 + j0.31	34.00	1.00 + j4.11
32.30	0.90 + j0.62		

NR - No Reading

TABLE A-2 (Cont.)

TEST 33

Frequency KC	Impedance Ohms	Frequency KC	Impedance Ohms
31.95	0.90 + j0.		

TEST 34

Frequency KC	Impedance Ohms	Frequency KC	Impedance Ohms
10.00	0.23 - j85.0	32.00	0.89 - j0.62
14.00	NR - j55	32.28	0.90 + j0.
20.00	0.42 - j29.5	32.45	0.91 + j0.46
25.00	0.58 - j15.8	35.00	1.03 + j5.14
30.00	0.79 - j1.67	40.00	1.52 + j13.9

TEST 35

Frequency KC	Impedance Ohms	Frequency KC	Impedance Ohms
32.00	0.88 - j0.62		
32.28	0.90 + j0.		
32.45	0.90 + j0.46		

TEST 36

Frequency KC	Impedance Ohms	Frequency KC	Impedance Ohms
10.00	0.19 - j87.0	30.50	0.95 - j0.33
14.00	NR - j55.0	30.68	0.98 + j0.
20.00	0.49 - j28.5	30.80	1.00 + j0.32
25.00	0.68 - j13.2	35.00	1.24 + j9.71
27.00	0.79 - j8.15	40.00	2.20 + j16.0
30.00	0.93 - j1.5		

TEST 39

Frequency KC	Impedance Ohms	Frequency KC	Impedance Ohms
10.00	0.22 - j85.0	28.50	0.92 + j0.70
14.00	NR - j52.1	29.00	0.97 + j2.1
20.00	0.53 - j24.5	30.00	1.02 + j4.34
25.00	0.72 - j8.40	35.00	1.32 + j16.3
28.00	0.90 - j0.54	40.00	2.17 + j24.3
28.25	0.91 + j0.		

NR - No Reading

Appendix B: PERFORMANCE RELATIONSHIPS

Short, capacitively loaded antennas of the type considered in this report are conveniently characterized by the antenna capacitance C_o and the effective height h_o. The antenna capacitance determines the input reactance (for frequencies much below resonance f_o) and, hence, the voltages which result from the current developed on the radiator. The low values of radiation resistance R_o which result from short antennas require large currents to develop appreciable quantities of radiated power. The top loading, then, is a practical necessity to maintain tolerable voltages under this situation and also, as will be shown, a vital factor in providing sufficient radiation bandwidth bw_o.

Effective Height

The effective height depends jointly on the physical length of the vertical radiator and on the current distribution. If the current distribution as a function of elevation z is I(z) and the physical height is H, then

$$h_o = \frac{1}{I_o} \int_0^H I(z)\, dz \quad . \tag{B-1}$$

Where $I_o = I(0)$, i.e., the value of the base current.

For a short, thin radiator I(z) tapers linearly from a maximum at the base to zero at the top so that

$$h_o = H/2 \text{ (Short, Thin Monopole)} \quad . \tag{B-2}$$

However, if the top loading capacitance C_o is increased sufficiently, the effective height may be made to approach the physical height.

$$\lim_{C_o \to \infty} = H \tag{B-3}$$

Practically, the effective height is considerably less than the physical height as a result of both a practical limiation on antenna capacitance and, more important, a loss in effective height resulting from currents in grounded towers and guys. As an approximation, the gross effect of the oppositely sensed (with respect to the downlead current) currents in grounded structures may be considered as altering the current distribution, I(z), and thereby reducing the effective height.

An alternate definition of effective height which lends itself to two-terminal measurements is in terms of the open-circuit base voltage V_b and the incident, vertically polarized, electric field E_i.

$$h_o = V_b/E_i \quad . \tag{B-4}$$

This definition is identical to Equation B-1 for short antennas. Equation B-4 is easier to apply experientally since it requires only two measurements, (i.e., base voltage and incident field) whereas Equation B-1 requires a knowledge of all currents on the antenna and nearby structures.

Radiation Resistance

The radiation resistance R_o is defined in terms of the antenna base current I_o and the radiated power P_o.

$$R_o = P_o/I_o^2 \text{ ohms} \quad . \tag{B-5}$$

Here P_o is the summation of the incident power over a closed surface surrounding the antenna.

For short monopole antennas, the radiation resistance is given by

$$R_o = 160\,\pi^2\,(h_o/\lambda)^2 \text{ ohms} \tag{B-6}$$

Considering Equations B-2, B-3, and B-6, it becomes apparent that top loading can increase the radiation resistance by as much as four times. This result may be obtained by integrating the total radiated power. Although this integration can theoretically be performed over any convenient surface, it is simpler to develop far-field (Fraunhofer Region) expressions for the radiation field and perform the summation of incident power essentially at infinite distance.

Base Current

Having determined the radiation resistance, the base current can be expressed in terms of the required radiated power P_o.

$$I_o = \sqrt{P_o/R_o} \text{ amps.} \tag{B-7}$$

Top Hat Voltage

Referring to the basic equivalent circuit shown in Figure B-1, the voltage at the top hat (V_t) appears across the antenna capacitance.

$$V_t = I_o/\omega C_o \text{ volts.} \tag{B-8}$$

Resonant Frequency

Since the antenna and downleads have some inductance, the antenna will have a resonant frequency f_o given by

$$f_o = \frac{1}{2\pi\sqrt{L_o C_o}} \text{ cps.} \tag{B-9}$$

Base Voltage

Using the resonant frequency, the base voltage V_b is related to the top hat voltage as

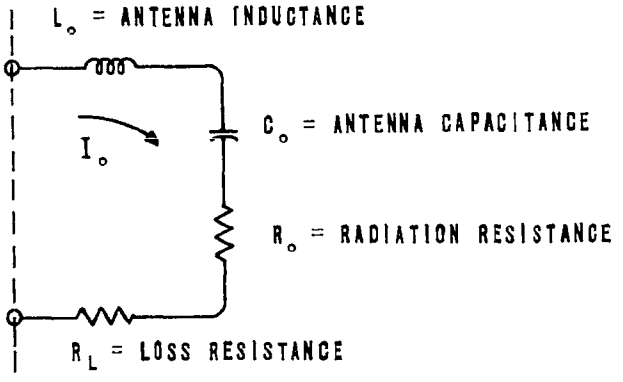

Figure B-1 BASIC EQUIVALENT CIRCUIT

$$V_b = V_t \left[1 - (f/f_o)^2\right] \text{ volts.} \qquad \text{(B-10)}$$

Thus, the base voltage is less than the top voltage for frequencies below resonance and approaches zero (i. e. limited only by the relatively small resistance) at resonance. Equations B-8 through B-10 neglect the effects of the resistance since, for short antennas, they are not significant in determining the magnitude of the input impedance.

Antenna Q

The bandwidth of the basic antenna, neglecting loss resistance R_L is derived from the antenna Q, where

$$Q = 1/\omega R_o C_o \ . \qquad \text{(B-11)}$$

Bandwidth

The half-power bandwidth (bw_o) for the undamped antenna is then given by

$$bw_o = \frac{f}{Q} = \omega R_o C_o f \text{ cps.} \qquad \text{(B-12)}$$

The actual bandwidth bw of a particular antenna is greater than the value indicated by Equation B-12. As a result of the damping effect of loss resistance R_L, where R_L is referred to the antenna circuit as shown in Figure B-1. Under this condition, the operating bandwidth is inversely proportional to the radiation efficiency η,

$$bw = \frac{bw_o}{\eta} \ . \qquad \text{(B-13)}$$

Here the radiation efficiency is given by:

$$\eta = \frac{R_o}{R_o + R_L} \ , \qquad \text{(B-14)}$$

usually expressed as a percentage.

Conductor Surface Gradient

Figure B-2 depicts a typical cylindrical conductor section whose length L is much greater than its radius r, all dimensions being much less than the wavelength λ. The relation between the displacement current density and the electric field gradient at the conductor surface will be developed in terms of measurable quantities.

Writing Maxwell's first equation,

$$\text{curl } \overline{H} = \sigma\overline{E} + \epsilon\frac{\partial\overline{E}}{\partial t} . \tag{B-15}$$

Or, for a sinusoidally time varying field,

$$\text{curl } \overline{H} = \sigma\overline{E} + j\omega\epsilon\overline{E} . \tag{B-16}$$

If we further restrict $\sigma = 0$ for application to the non-conducting space surrounding the conductor,

$$\text{curl } \overline{H} = j\omega\epsilon\overline{E} . \tag{B-17}$$

At the surface of a perfect conductor, only the normal component of the electric field is present E_ρ. For this component, which is ordinarily referred to as the gradient,

$$\text{curl}_\rho \overline{H} = j\omega\epsilon E_\rho . \tag{B-18}$$

(Note that $\overline{E}$ is the generalized vector, E_ρ being the ρ component.) Expanding,

$$\text{curl}_\rho \overline{H} = \frac{1}{\rho}\frac{\partial H_Z}{\partial \phi} - \frac{\partial H_\phi}{\partial Z} = j\omega\epsilon E_\rho . \tag{B-19}$$

This is further simplified by noting that for a long conductor $H_Z = 0$, reducing the expression to

$$\frac{\partial H_\phi}{\partial Z} = -j\omega\epsilon E_\rho . \tag{B-20}$$

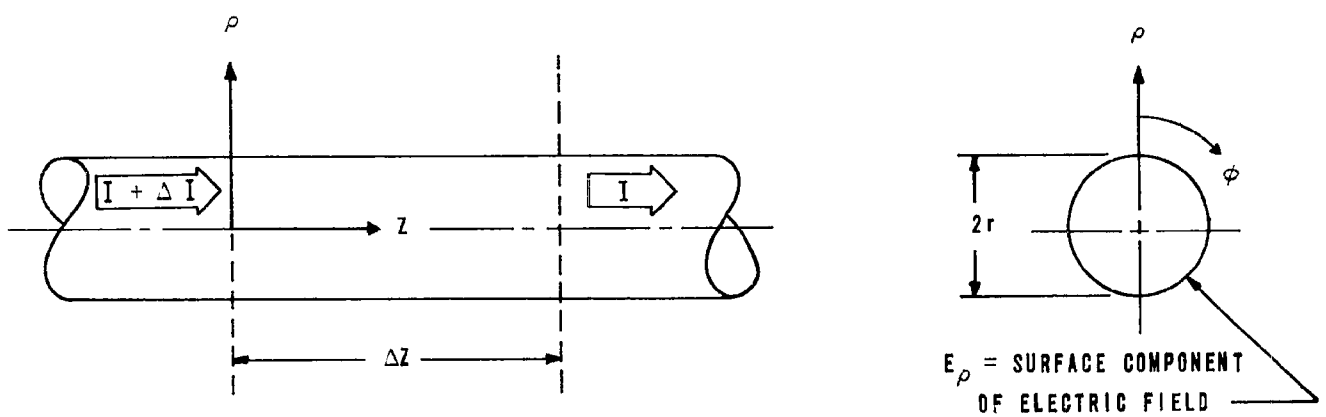

Figure B-2 INCREMENTAL SECTION OF A LONG CONDUCTOR SHOWING CYLINDRICAL CO-ORDINATE SYSTEM (ρ, ϕ, Z).

Near the surface of a long thin cylindrical conductor carrying current at a low frequency such that the radii of interest are much less than the radian length ($r << \lambda/2\pi$) the quasi-stationary field predominates and is given by

$$H_\phi = \frac{I_Z}{2\pi r} \text{ amps/meter} . \tag{B-21}$$

Inserting this relation into Equation B-20 yields

$$|E_\rho| = \frac{1}{2\pi r \omega \epsilon} \frac{\partial I_Z}{\partial Z} \text{ volts/meter.} \tag{B-22}$$

Since the magnitude of the radial field is the critical factor in corona formation, the absolute value is given in Equation B-22.

In practice, the partial derivative in Equation B-22 can be approximated by measuring the change in current (ΔI_Z) over a small but finite increment of conductor length (ΔZ). This yields a useful approximation:

$$|E_\rho| \approx \frac{1}{2\pi r \omega \epsilon} \left(\frac{\Delta I_Z}{\Delta Z}\right) \text{ volts/meter.} \tag{B-23}$$

Equation B-23 yields the conductor surface gradient on an incremental length of conductor. If a large number of similar conductors are involved, as in an antenna top hat, it is useful to be able to obtain an average value of the surface field. For this purpose, the incremental quantities ΔI_Z, ΔZ are replaced by the total base current I_o and the total length of elevated conductor L. This yields the average gradient

$$E_\rho \approx \frac{1}{2\pi r \omega \epsilon} \left(\frac{I_o}{L}\right) \text{ volts/meter.} \tag{B-24}$$

Obviously, if the incremental displacement per unit length ΔI_Z is uniform, then Equations B-23 and B-24 give identical results. In practice, however, it is not usually possible to maintain a uniform gradient, so that the value given by B-24 is a rough approximation useful only for estimating purposes.

Appendix C: ANTENNA EQUIVALENT CIRCUIT

The use of equivalent circuits simplifies some antenna problems by characterizing a physical structure involving distributed parameters by a lumped-parameter equivalent. VLF antennas of the type considered in this report are represented approximately by a simple series L-C circuit with small series resistances representing radiation and loss components. The resistance properties depend strongly upon the frequency, so that the equivalent resistance must also vary with frequency. However, the equivalent reactive components are relatively independent of frequency, so that one circuit can be used to describe the reactance properties of the antenna over the entire frequency range.

Figure C-1 (A) shows a simple or basic equivalent vlf antenna curcuit consisting of lumped inductance L_0, capacitance C_0, and resistances R_0, R_L. Except for the previously noted variation in the resistance values, this circuit is usually a close approximation for any vertical radiator whose length is short compared to a wavelength. A convenient technique for handling impedance data from such a circuit is shown in Figure C-1 (B) in which the base reactance-frequency product is plotted as a function of frequency squared. For this circuit, the input, or base, reactance-frequency product is

$$fX = 2\pi L_0 f^2 - 1 / 2\pi C_0 \qquad (C\text{-}1)$$

which is linear in f^2, with a zero-frequency intercept of $-1/2\pi C_0$ and a slope of $2\pi L_0$, as shown in Figure C-1 (B). For this circuit, the static capacitance C_0 and the resonant frequency f_0 provide two easily measured points which determine the reactance at any frequency at which the antenna current distribution is approximately linear.

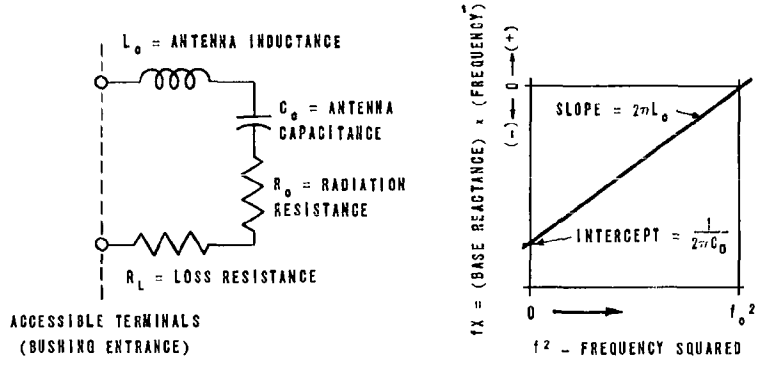

Figure C-1 BASIC EQUIVALENT CIRCUIT

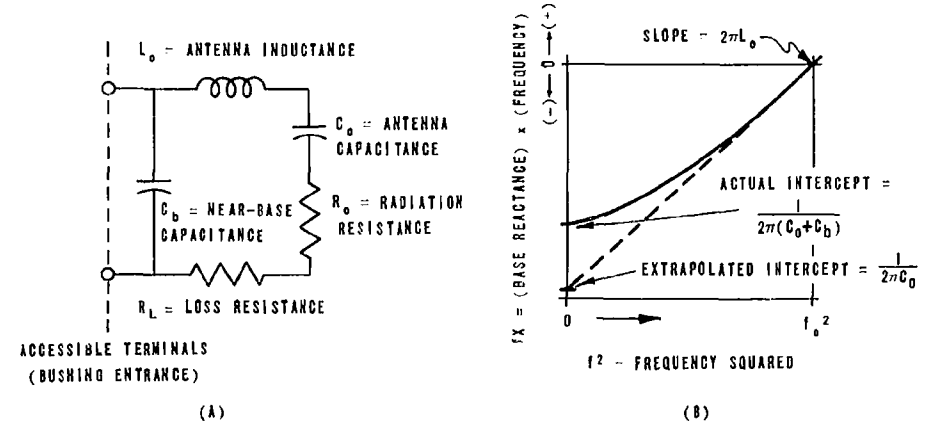

Figure C-2 REFINED EQUIVALENT CIRCUIT INCLUDING NEAR-BASE CAPACITANCE

It was found that extensive data taken from base-reactance measurements on the scale vlf antenna model described in this report showed an appreciable departure from the expected values indicated by Figure C-1 (B), particularly as the frequency approached zero. Precise measurements of the static capacitance (Section 2.2.2), and the base reactance in the operating frequency range (Section 2.2.3) revealed an apparent excess capacitance at the lower frequencies. This suggested an additional capacitance element in the equivalent circuit across the input on the input side of the antenna inductance. This additional capacitance C_b is referred to as "near-base" capacitance.

Figure C-2 (A) shows a refined equivalent circuit including a near-base capacitor. This additional capacitance is attributed to the long, horizontal busses and the insulators and support structures associated with the buswork over the Transmitter/Helix Building. For this model, the near-base capacitance is much less than the antenna, or top hat, capacitance. For this situation, the variation of reactance with frequency in the region near resonance is relatively independent of C_b. Thus, as shown in Figure C-2 (B), extrapolating from the near-resonance portion of the reactance-frequency curve should yield a zero-frequency intercept depending only on the antenna capacitance, that is $-1/2\pi C_0$. The actual intercept, however, will yield a value related to the sum of both capacitances,

$$\lim_{f \to 0} fX = -\frac{1}{2\pi (C_0 + C_b)} \qquad \text{(C-2)}$$

The above discussion describes one technique for deriving a three-element equivalent (reactance) circuit from measured data. This procedure was applied to model data and found to provide an accurate representation of the reactance variation with frequency.

In the development of the equivalent circuit, it should be noted that two minor corrections were applied to the model base-reactance data:

(a) Corrected data is referred to the bushing entrance point rather than the T/HB floor terminal. Comparing data from Tests 30 and 31 reveals an equivalent inductance of approximately 14.3 μh (full scale) for the floor-to-bushing model lead. This amounts to about 1.4 ohms at 15.5 kc.

(b) The model wire diameter was 1.4 times the scaled diameter. This increase model capacitances by approximately 2.7 percent. The corrected data reflects an appropriate reduction.

The base reactance data of Test 34 (referred to full scale) is shown in Figure C-3 to indicate the way in which the equivalent circuit values were determined. The plot of the base reactance-frequency product as a function of frequency squared shown in Figure C-3 exhibits the departure from a straight line previously noted. Specifically, the actual zero-frequency intercept indicates a static capacitance C_s of 0.1711 μf while the near-resonance extrapolation indicates only 0.1530 μf for the antenna or top hat capacitance C_o. The difference, 0.0181 μf, is attributed to near-base capacitance C_b. Correcting for the wire-diameter modeling discrepancy yields:

$C_o = 0.1490$ μf

$C_b = 0.0176$ μf

$C_s = 0.1666$ μf

The resonant frequency f_o becomes 33.8 kc after the data is referred to the bushing entrance point. Note that the wire diameter discrepancy does not change the resonant frequency due to compensating changes in inductance and capacitance.

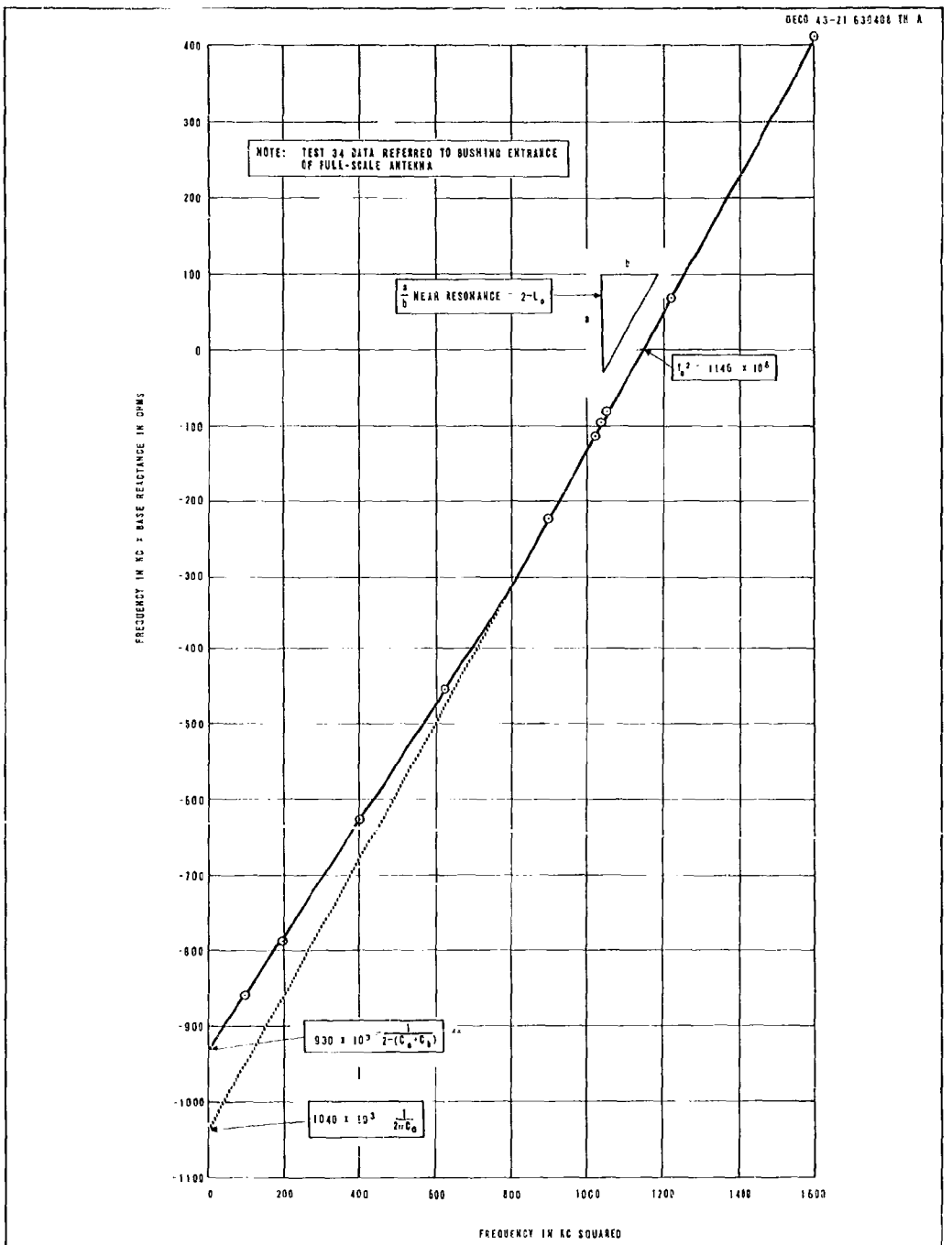

Figure C-3 DERIVATION OF EQUIVALENT CIRCUIT

The effect of the additional near-base capacitance on the performance of the antenna is not great for the values obtained. The apparent effective height becomes slightly frequency dependent because of the loading effect of the near-base capacitance. However, this will only result in a variation of about 5 percent over the frequency range of interest. Compansating changes in apparent effective height and static capacitance introduced by C_b result in the same unloaded antenna bandwidth. Other performance characteristics reflect negligible differences when computed from the circuits of Figures C-1 (A) and C-2 (A).

Appendix D: INVESTIGATION OF VLF FIELD DISTRIBUTION

The distribution of surface current density (H-field) and the distribution of vertical electric intensity (E-field) were determined in the central region of the scale model. In accordance with Navy directions, the area investigated was limited to that in the immediate vicinity of the Transmitter/Helix Building and a sector under one downlead. Figures D-1 and D-2 indicate these general areas as well as the model T/HB configuration during measurements. Within the limits of the structural variations considered in the model program, the final shape of the building and the top hat are not expected to create any significant differences in the results. While the hoist houses at the T/HB were not included at the time of modeling, any deviations of current magnitudes or directions created by their addition in actual installation are not expected to be of any primary consequence.

Figure D-1 shows the distribution of surface current density in the vicinity of the T/HB with the magnitude given in amperes per meter, normalized to a base current of 2540 amperes, with the direction of surface current indicated at each point of measurement.

In the near vicinity of the T/HB, the H-field distribution is symmetrical about the center line. Beyond the influence of the building, field symmetry is governed by the distribution of towers and guys. Near the center tower guys, 120-degree sectors of symmetry center along the center tower guy planes; in the vicinity of the intermediate towers and beyond, 60-degree sectors of symmetry center along radials passing through each intermediate tower.

In addition to the field distribution on the roof and ground mat, shown in plan view in Figure D-1, the magnitude and direction of current

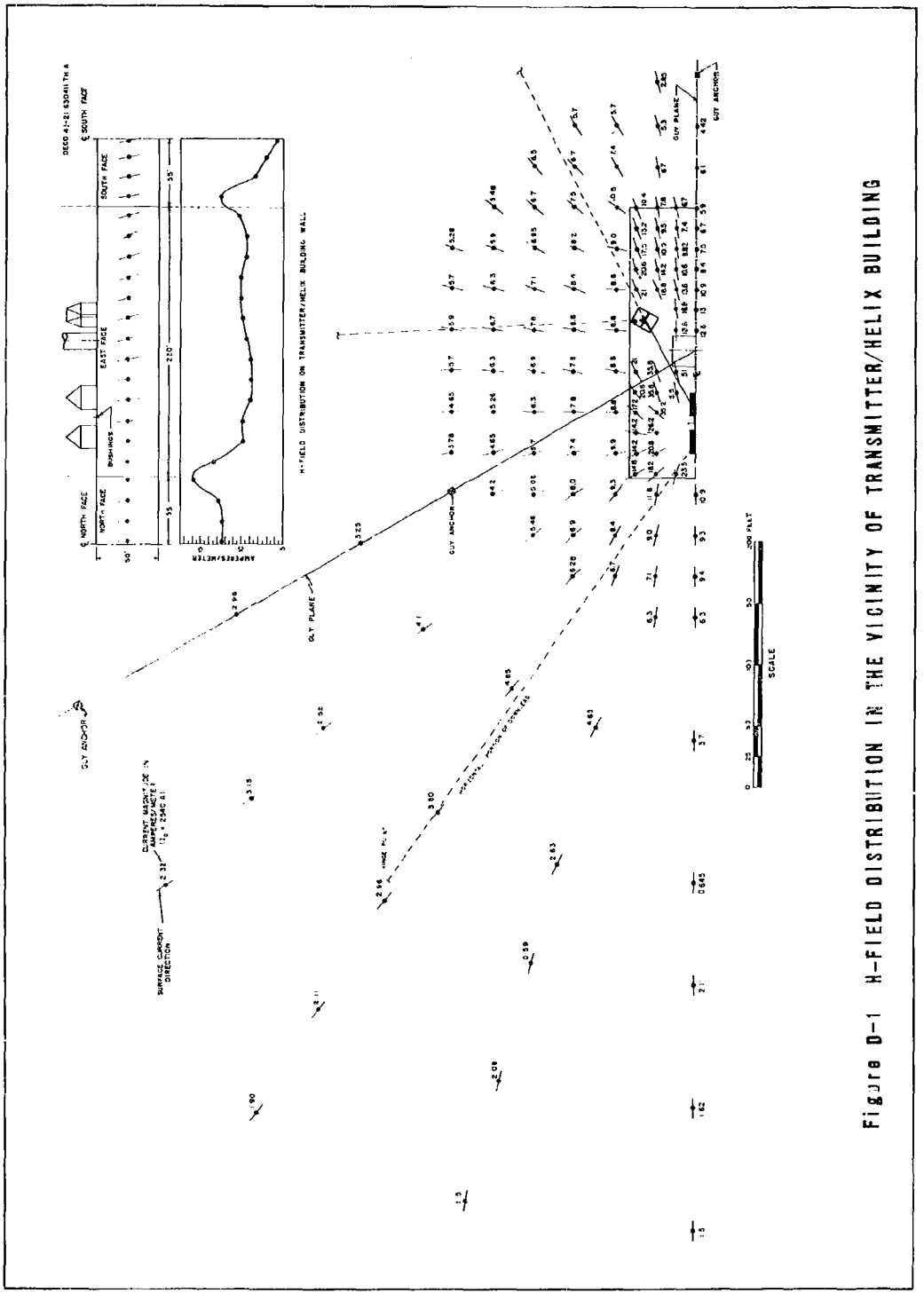

Figure D-1 H-FIELD DISTRIBUTION IN THE VICINITY OF TRANSMITTER/HELIX BUILDING

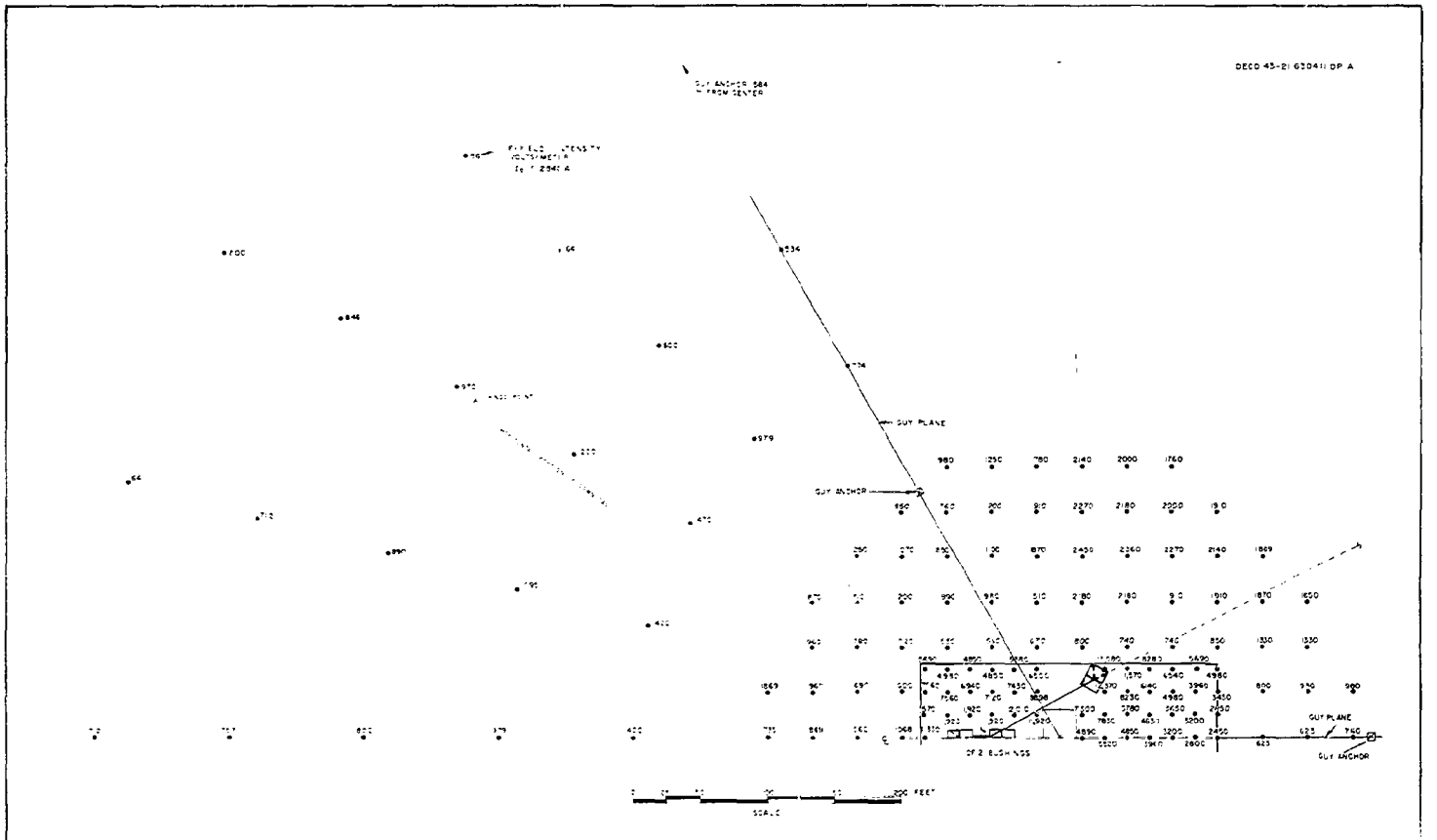

Figure D-2 E-FIELD DISTRIBUTION IN THE VICINITY OF TRANSMITTER/HELIX BUILDING

density is also shown along the center line of the T/HB exterior walls. Radio frequency currents display a tendency toward concentration in the salient areas of irregular conductors (i.e., those protruding beyond a circle of equal area). This effect is indicated in Figure D-1 by a plot of surface current density along one side and to the center line of each end of the T/HB exterior. Loss studies which guided the distribution of conductors on the T/HB and in the ground system immediately beyond were based on the measured data. In accordance with the field data, the ground system design displays a concentration of buried conductors near the building corners and some departure from true-radial directions in accordance with the measured magnitude and direction of surface current.

Figure D-2 is a plot of E-field distribution near the surface in the vicinity of the T/HB. The electric field magnitude at each point of measurement is given in volts per meter and is normal to the surface. Axes of E-field symmetry exists identical to those previously described in the H-field measurements. The values shown are normalized to full power operation at 15.5 kc.

Although measurements of E- and H-fields in typical sectors beyond the T/HB vicinity and the exploration of tower and guy resonances were originally proposed, they were deleted at the direction of cognizant Navy offices. It was felt that the similarity with the existing Cutler facility was sufficient to preclude the need for such studies.

6. SUMMARY OF PREDICTED PERFORMANCE

This report presents the results of the antenna model study which was carried out for the development of the design of the VLF PAC antenna. Beginning with an evaluation of the initial configuration (Section 5.1) this study includes the results of a continuous model program involving detailed structural revisions which occurred as part of the refined design. These revisions included changes in top hat shape, intermediate tower elevations, entrance bushings and Transmitter/Helix Building. In general, the effects of such revisions were reflected by relatively minor changes in electrical performance as derived from model measurements. Consequently, the measurement of some aspects of performance which were not considered of primary importance or were not expected to change appreciably were not repeated for the final revisions.

For comparison, Table 6-1 summarizes both the predicted full-scale basic antenna parameters and the derived operating characteristics relating to full-power (1 megawatt radiated) operation at the design frequency (15.5 kc). This data is given for (a) normal (6 panel, no wind) operation, (b) emergency (5 panel, no wind) operation, and (c) for the condition of 6 panels and maximum wind (130 mph) distortion. The normal and wind-distorted data were obtained from the final model with all pertinent revisions included. However, the emergency condition was evaluated only on the initial configuration. Since no major changes were determined in the performance for the normal condition (compare, for example, the results of Tests 22 and 34) it was considered unnecessary to repeat the emergency condition measurements.

The base reactance values shown in Table 6-1 include all corrections and are referred to the bushing entrance on the antenna. Figure 6-1 is a plot of the corrected input reactance over the entire

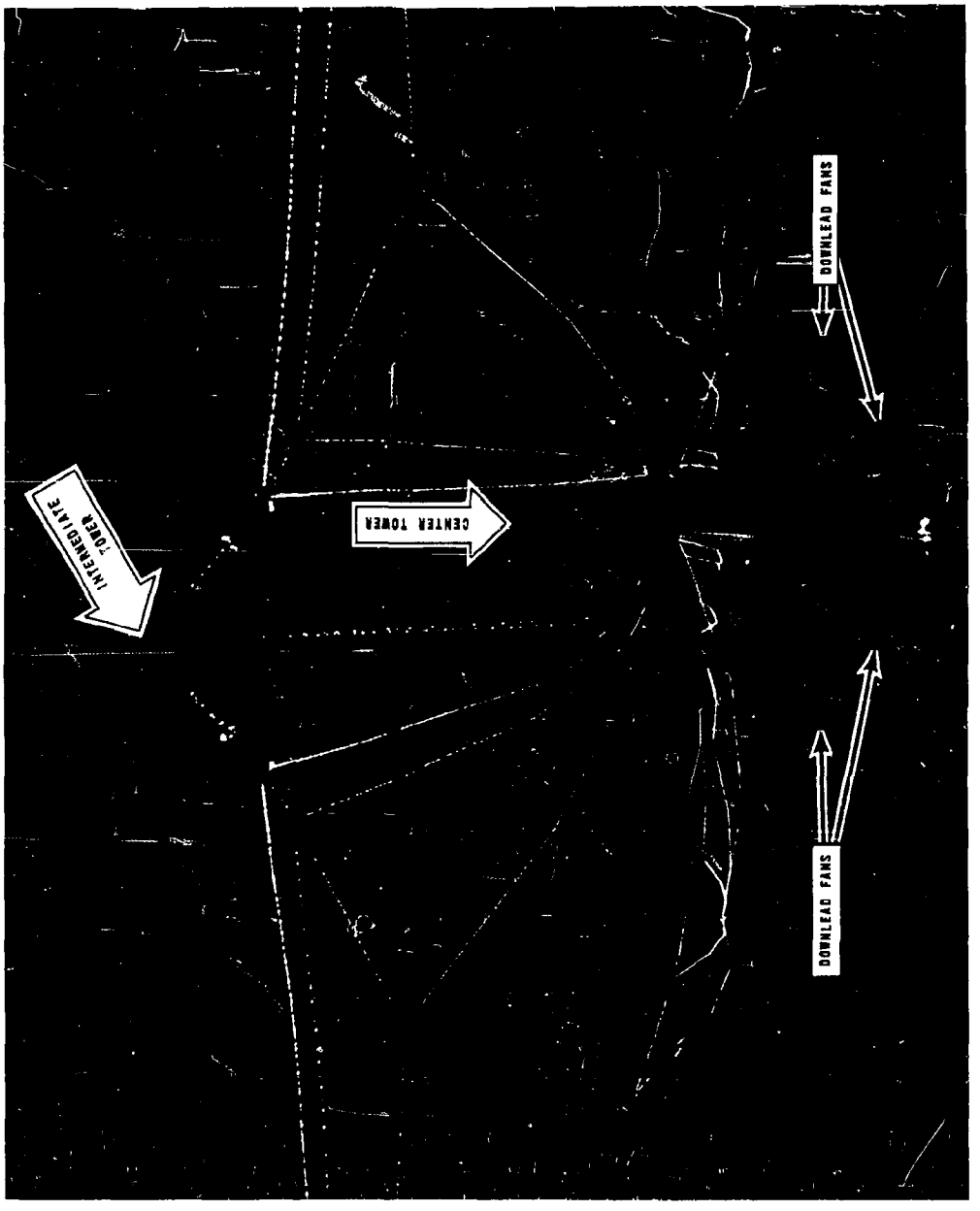

Figure E-1 ANTENNA MODEL UNDER STATIC CONDITION WITH 64 KV EXCITATION

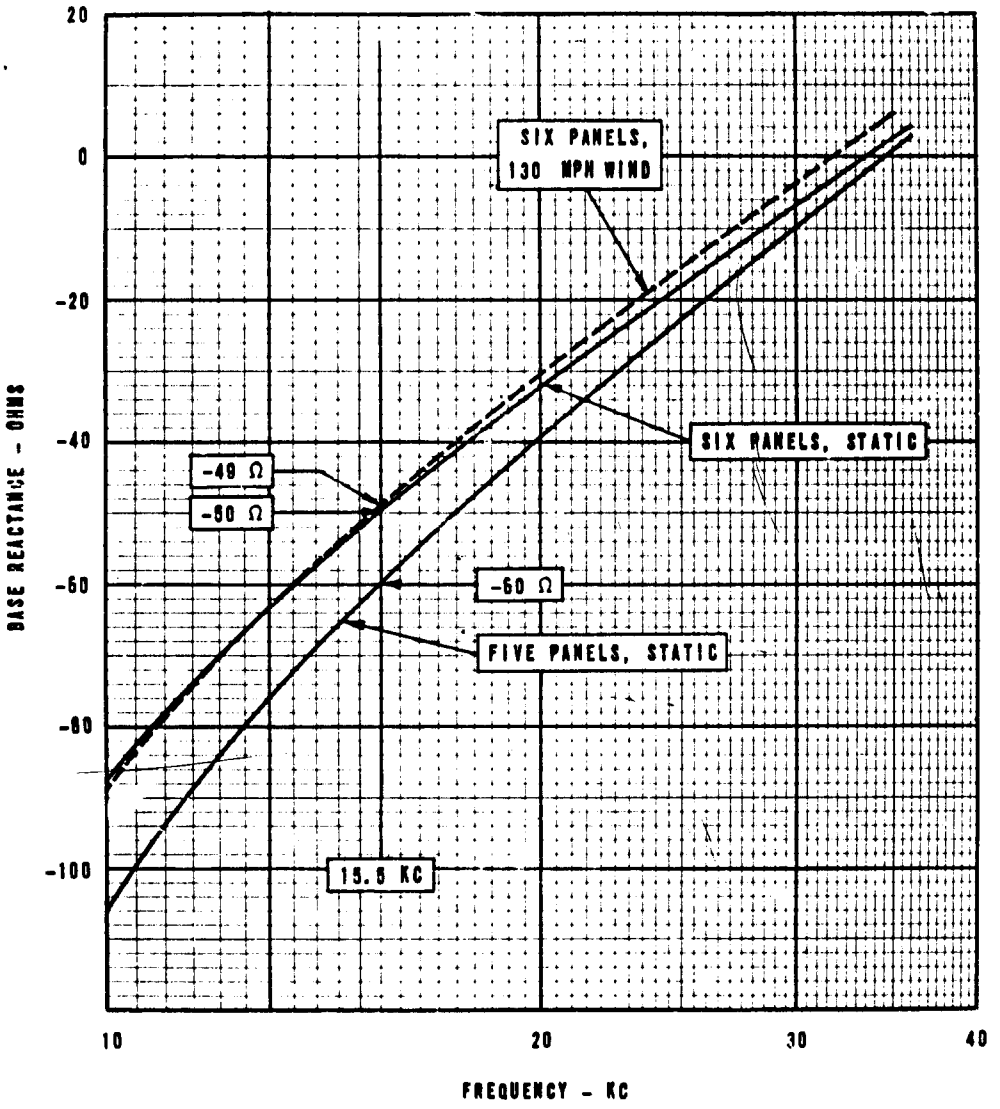

Figure 6-1 BASE REACTANCE AS A FUNCTION OF FREQUENCY

As an example of the detail obtained in this study, consider the photographs appearing in Figures E-2 and E-3. Figure E-2 shows an overall view of the model under maximum wind distortion with the observer looking toward the center tower from just beyond an outer tower of panel No. 2. (The large bright spot near the upper part of the photograph is caused by the moon.) This study was made with 30 kv excitation. Faint traces of corona are visible on the panel with brighter indications along the No. 2 panel downlead where it approaches the center tower guys to within 20 feet. Figure E-3 shows a close-up of the critical downleads (two panels are distorted identically under the wind condition studied), indicating clearly the extent of corona in this area.

Further study of the problem areas was carried out using the current distribution method to develop quantitative information relating to corona formation.

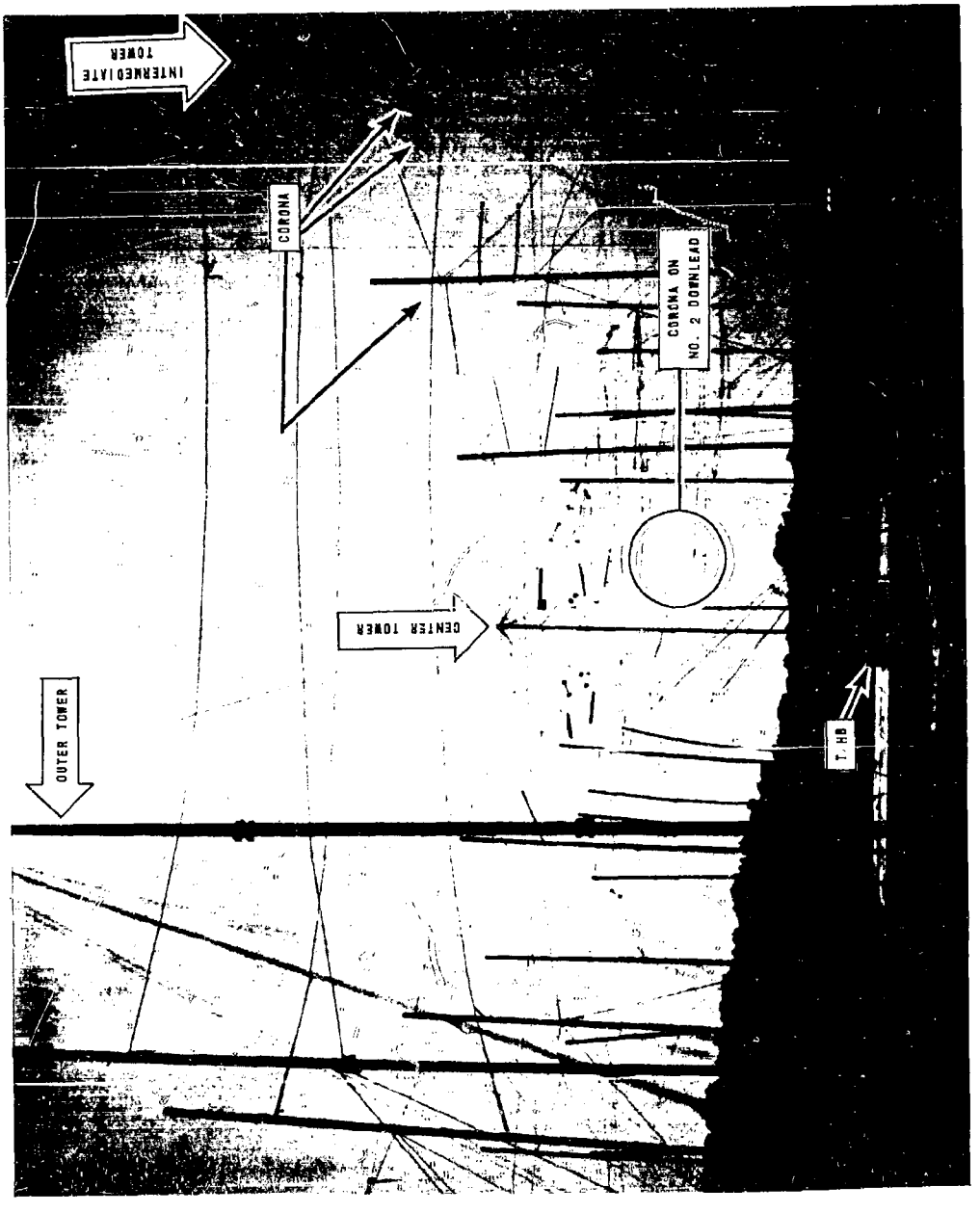

Figure E-2 ANTENNA MODEL UNDER MAXIMUM WIND DISTORTION WITH 30 KV EXCITATION

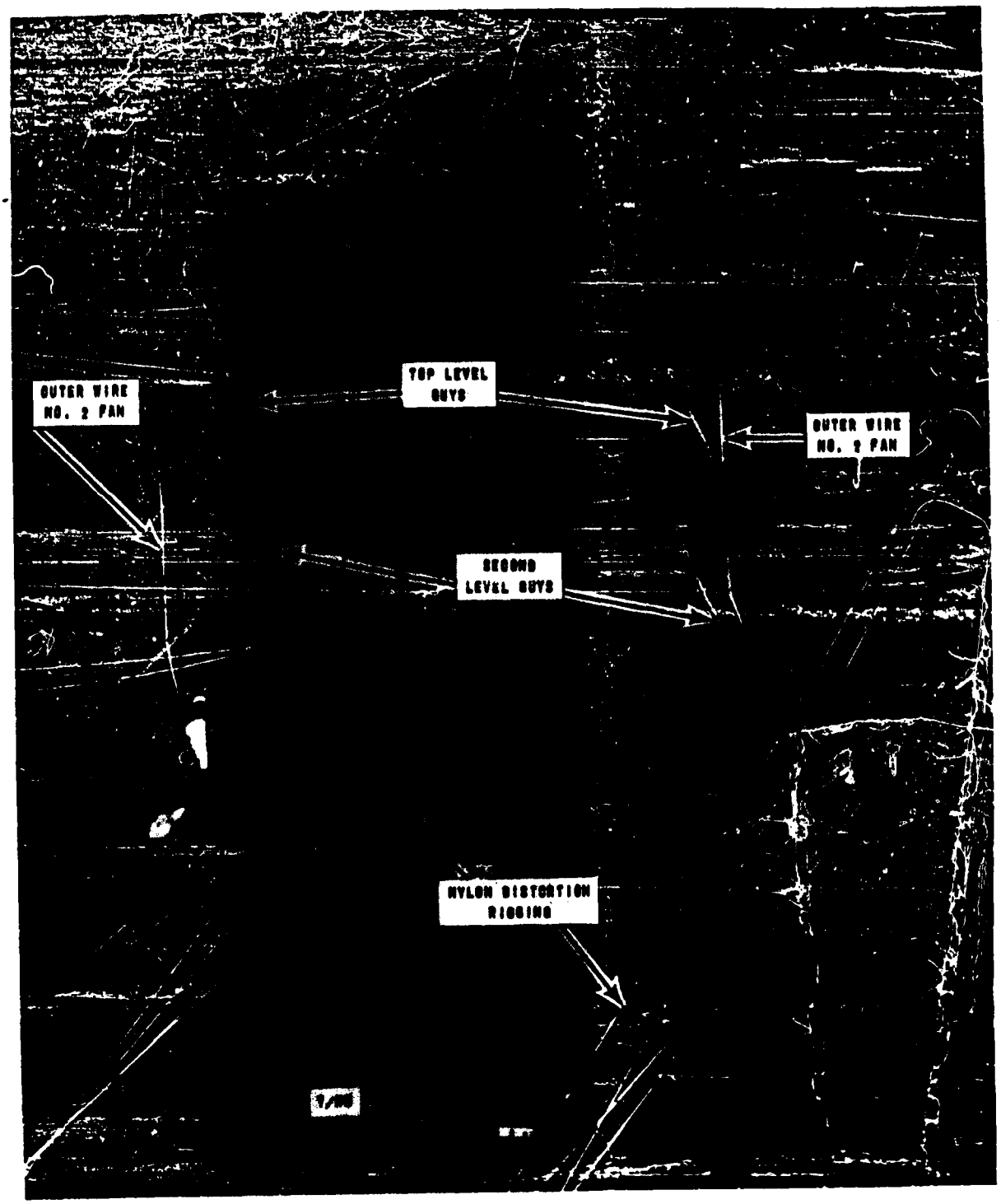

Figure E-3 No. 2 PANEL DOWNLEAD UNDER MAXIMUM WIND DISTORTION WITH 30 KV EXCITATION